

Dr. Qiang Wang
Topical Editor
Geoscientific Model Development
January 20th 2019

Manuscript reference No. GMD-2018-91

Dear Dr. Qiang Wang,

Please find attached a revised version of the manuscript, **The Brazilian Earth System Model version 2.5: Evaluation of its CMIP5 historical simulation**, which we would like to submit for publication in Geoscientific Model Development

We appreciate the opportunity to improve the manuscript.

In the following pages are our point-by-point revisions.

- Page 4, Line 10

“Ocean” has been replaced by “Oceans”

- Page 8, Line 11

“The ocean stand-alone runs for 71 years (13 years period of ocean model spin-up forced by climatological atmospheric fields plus 58 years period forced by interannually varying atmospheric fields). Then a spin-up of the fully coupled model is done for 100 years. The ocean and atmosphere states at the end of this 100 years long integration are used as the initial condition for the piControl simulation. The piControl simulation shows stable conditions after a fast adjustment over the first 13 years of simulation (figure not shown).”
has been replaced by “The ocean stand-alone runs for 71 years (13 years period of ocean model spin-up forced by climatological atmospheric fields plus 58 years period forced by interannually varying atmospheric fields). Then a spin-up of the fully coupled model is done for 100 years. The ocean and atmosphere states at the end of these 100 years long integration are used as the initial condition for the piControl simulation. The model’s versions are slightly different for 100 years spin-up and the piControl run, in the parameterizations of the land ice albedo and cloud microphysics. The Historical simulation uses as initial conditions information of the 14th year provided by the piControl simulation. The piControl simulation shows stable conditions after a fast adjustment over the first 13 years of simulation (figure not shown). Therefore, it is assumed that the Historical simulation has a spin-up of 113 years.”

- Page 12, Line 16

It has been included the following text: “The net radiation imbalance at TOA is related to significant loss of energy at TOA both from the outgoing long-wave radiation and outgoing short-wave radiation.”

- Page 14, Line 8

“ocean” has been replaced by “Ocean”

- Page 15, Line 20

“oceans” has been replaced by “Oceans”

- Page 17, Line 16

“oceans” has been replaced by “Oceans”

- Page 19, Line 12

“To evaluate how the global ocean profile evolves throughout the simulation, it is computed the depth-time Hovmöller diagrams of global mean ocean temperature and salinity departures from their respective initial conditions (Fig. 13). Here initial conditional means the value of the first year of simulation, in this case, the year 1850. The prominent warming occurs from the surface up to 400 m depth (Fig. 13a). This warming is more significant at the end of the simulation (~0.6 °C comparing with initial conditions) and is likely to be related to the global warming of the planet and consequential increasing heat flux from the atmosphere into the ocean. In deeper waters, from 1500 m up to the ocean floor, there is a weaker warming, indicating that the ocean is gaining heat mainly in the upper layers. Between 500-1500 m depth, it is observed a cooling tendency respective to initial conditions. The ocean salinity slightly increases below 1000 m depth and from 1935 the increase reaches 0.04 PSU between 1500 and 3000 m depth compared with the initial values (Fig. 13b). Above 1000 m depth there is a significant freshening of the ocean waters, with the surface waters salinity decreasing up to 0.18 PSU at the end of the simulation. Such tendency can mean that the ocean is still drifting from its initial conditions in the Historical simulation.” has been replaced by “To evaluate how the global ocean profile evolves throughout the simulation, it is computed the depth-time Hovmöller diagrams of global mean ocean salinity and temperature departures from their respective initial conditions (Fig. 13a

and 13b) for Historical simulation. Here initial conditional means the value of the first year of simulation, in this case, the year 1850. The ocean salinity slightly increases below 1000 m depth and from 1935 the increase reaches 0.04 PSU between 1500 and 3000 m depth compared with the initial values (Fig. 13a). Above 1000 m depth there is a significant freshening of the ocean waters, with the surface waters salinity decreasing up to 0.18 PSU at the end of the simulation. Concerning ocean temperature, a prominent warming occurs from the surface up to 400 m depth (Fig. 13b). This warming is more significant at the end of the simulation (~ 0.6 °C comparing with initial conditions) and is mostly caused by the ocean warming drift of the model. Fig. 13c shows the same diagram for piControl simulation (during the period in which both simulations are performed in parallel), which also presents the ocean drift. However, the ocean temperature anomalies above 600 m reaches ~ 0.6 °C in the Historical simulation whereas in the piControl it reaches ~ 0.4 °C. This difference of 0.2 °C between the two simulations is likely due to the global warming of the planet and consequential increasing heat flux from the atmosphere into the ocean (Fig. 13d). In deeper waters, from 1500 m up to the ocean floor, there is a weaker warming, indicating that the ocean is gaining heat mainly in the upper layers (Fig. 13b). Between 500-1500 m depth, it is observed a cooling tendency respective to initial conditions. Such tendency can mean that the ocean is still drifting from its initial conditions in the Historical simulation.”

- Page 20, Line 22

“The AMOC in the BESM-OA2.5 historical experiment has the typical structure described in Lumpkin and Speer (2007), with the main layers well depicted in the appropriated depths (Figure 14a).” has been replaced by “The AMOC in the BESM-OA2.5 historical experiment has the typical structure described in Lumpkin and Speer (2007), with the upper layer of the upper cell, which is the northward flux, depicted in the appropriated depth, from the surface up to ~ 1000 m (Fig. 14a). However, the upper cell is too shallow compared with the RAPID measurements (McCarthy et al., 2015). The depth of the upper cell is 2500 m in the model whereas the measurements show its

depth at ~4500 m. This shallow upper cell of the AMOC is a common feature of state-of-the-art climate models (see Menary et al., 2018). The model simulates the northward Antarctic Bottom Water in the ocean floor.”

- Page 21, Line 24

It has been included the following text: “Figure 15 shows the mean sea ice concentration simulated by BESM-OA2.5 for the end of the winter and the summer seasons for each hemisphere, over the period 1971-2000. The thick black lines represent the 15 % climatological values for the period 1971-2000 given by the 20CRv2 Reanalysis. The sea ice concentration in the Arctic winter is overestimated in the Atlantic, specifically north of the Scandinavia (Fig. 15a). However, in summer the Arctic sea ice is underestimated (Fig. 15b). In the Antarctica summer the model shows a significant underestimation of the sea ice concentration (Fig. 15c). During the Antarctica winter the model generally overestimates the extension of the sea ice concentration over all Southern Ocean (Fig. 15d). Such seasonal sea ice concentration amplitude is likely related to bias radiative net over higher latitudes that the model suffers, which during the winter in each hemisphere tend to generate higher extension of sea ice and during the summer in each hemispheres tend to enhance the sea ice melting compared with the Reanalysis.”

- Page 23, Line 4

“ocean” has been replaced by “Ocean”

- Page 23, Line 12

“15” has been replaced by “16”

- Page 23, Line 13

“15” has been replaced by “16”

- Page 23, Line 14

“15” has been replaced by “16”

- Page 23, Line 16

“16” has been replaced by “17”

- Page 23, Line 22

“ocean” has been replaced by “Ocean”

- Page 24, Line 1

“ocean” has been replaced by “Ocean”

- Page 24, Line 3

“16” has been replaced by “17”

- Page 24, Line 6

“ocean” has been replaced by “Ocean”

- Page 24, Line 21

“17” has been replaced by “18”

- Page 25, Line 3

“17” has been replaced by “18”

- Page 25, Line 7

“17” has been replaced by “18”

- Page 26, Line 8

“18” has been replaced by “19”

- Page 26, Line 13

“16” has been replaced by “18”

- Page 26, Line 16

“18” has been replaced by “19”

- Page 26, Line 17

“18” has been replaced by “19”

- Page 27, Line 9

“19” has been replaced by “20”

- Page 27, Line 21

“19” has been replaced by “20”

- Page 27, Line 23

“19” has been replaced by “20”

- Page 28, Line 19

“20” has been replaced by “21”

- Page 28, Line 20

“20” has been replaced by “21”

- Page 28, Line 23

“20” has been replaced by “21”

- Page 28, Line 23

It has been included the following text: “21”

- Page 30, Line 3

“21” has been replaced by “22”

- Page 30, Line 4

“21” has been replaced by “22”

- Page 30, Line 6

“21” has been replaced by “22”

- Page 30, Line 15

“22” has been replaced by “23”

- Page 30, Line 22

“22” has been replaced by “23”

- Page 31, Line 17

“23” has been replaced by “24”

- Page 32, Line 22

“24” has been replaced by “25”

- Page 33, Line 6

“25” has been replaced by “26”

- Page 33, Line 9

It has been included the following text: “26”

- Page 37, Line 11

It has been included the following text: “MBJ is supported by a grant funded by FAPESP (2018/06204-0).”

- Page 46, Line 24

It has been included the following text: “Menary, M. B., Kuhlbrodt, T., Ridley, J., Andrews, M. B., Dimdore-Miles, O. B., Deshayes, J. et al.: Preindustrial control simulations with HadGEM3-GC3.1 for CMIP6., *J. Adv. Model. Earth Syst.*, 10, 3049–3075, doi:<https://doi.org/10.1029/2018MS001495>, 2018.” It has been suggested by reviewer #2.

- Page 53

Figure 1 has been improved. The revised figure shows the 100 years of coupled spin-up run.

- Page 69

Figure 13 has been improved. It has been suggested by reviewer #2.

- Page 70, Line 1

“Depth-time Hovmöller diagrams of global average ocean temperature and salinity anomalies from the respective initial conditions (IC). Here the initial conditions are taken from the 1th year. The diagrams are based on annual average time series simulated by the Historical simulation over the period 1850-2005 (156 years). The thick black line represents the zero contours. Note that the vertical scales are different above and below 1000 m.” has been replaced by “Depth-time Hovmöller diagrams of global average ocean (a) salinity and (b) temperature anomalies from the respective initial conditions (IC). Here the initial conditions are taken from the 1th year for (a, b) Historical simulation, and 14th year for (c) piControl simulation. (d) presents the difference between the temperature anomalies of Historical relative to piControl. The diagrams are based on annual average time series simulated by the Historical simulation over the period 1850-2005 (156 years) and by piControl simulation over the period 14-169 years (156 years). The thick black line represents the zero contours. Note that the vertical scales are different above and below 1000 m.”

- Page 73

A new figure has been included (Figure 15). It has been suggested by reviewer #1.

- Page 73, Line 3

It has been included the following text: “Figure 15 - BESM-OA2.5 mean sea ice concentration for March (a, c) and September (b, d) for each hemisphere. The solid black lines show the 15 % mean sea ice concentration for 20CRv2 Reanalysis. The averages values are computed over the period 1971–2000 for BESM-OA2.5 and 20CRv2. The concentration is presented in percentage.”

- Page 74, Line 3

“15” has been replaced by “16”

- Page 76, Line 3

“16” has been replaced by “17”

- Page 78, Line 1

“17” has been replaced by “18”

- Page 79, Line 3

“18” has been replaced by “19”

- Page 81, Line 3

“19” has been replaced by “20”

- Page 83, Line 3

“20” has been replaced by “21”

- Page 85, Line 3

“21” has been replaced by “22”

- Page 86, Line 3

“22” has been replaced by “23”

- Page 87, Line 3

“23” has been replaced by “24”

- Page 88, Line 3

“24” has been replaced by “25”

- Page 89, Line 2

“25” has been replaced by “26”

Anonymous Referee #1

We thank the valuable comments, whose responses follow:

Major Revisions:

1.1 The CMIP6 historical experiment forcing is released a longtime ago, and the BESM model is targeted at the CMIP6 project, why do not run the BESM with CMIP6 forcing data?

Reply:

The present study uses data from a simulation forced following the CMIP5 protocol with the objective of evaluating the model version implemented for the CMIP5 project. Presently, our group is working on an updated version of the BESM model to be used for CMIP6.

1.2 Moreover, the GHG forcing is only one aspect of the historical forcing, what is the consideration to ignore other forcing? It is unfair to compare the GHG-historical simulation to the real-world observation, how to clarify the role of other forcing (e.g. aerosols)?

Reply:

We agree with your observations. To compare with real-world it is desirable that the historical simulation is forced with observed aerosols concentration and land use changes jointly with GHG forcing. However, in the process of developing a full ESM, comparing the current version of the model (without the effects of aerosols and land use change, for example) with observations is the only possibility at hand. Many centers have evaluated their models piControl simulation against observed and/or Reanalysis (e.g. Swapna et al., 2015 and Menary et al., 2018). We consider that evaluating ours Historical simulation against reanalysis, in this context, is less of a problem than contrasting the piControl run.

2. The model suffers a large TOA energy imbalance (about -4 W m^{-2}) and surface imbalance (about 1.2 W m^{-2}) from the beginning of historical simulation (e.g. 1850-1900). The authors should discuss the possible reason and causing of the energy bias. Is the imbalance due to the non-conservation in the AGCM or coupling process?

Reply:

The AGCM stand-alone run shows a net radiation at TOA of 0.25 W m^{-2} during 20 years of simulation (Fig. 1a). Such radiative imbalance is within the range simulated by different atmospheric models. However, in the coupled simulation, the net radiation imbalance at TOA is amplified up to -4 W m^{-2} (Fig. 1b). The reason for such imbalance is related to higher loss of energy at TOA both from the outgoing long-wave radiation (OLR) and outgoing short-wave radiation (OSR), compared with AGCM stand-alone simulation (Fig. 1c and 1d). In Fig. 1c and 1d, the solid lines represent the coupled model and the dashed lines represent the AGCM. The higher loss of energy through outgoing long-wave radiation is due to the warm SST bias that BESM-OA2.5 suffers (Fig. 10c, manuscript). The higher loss of energy through the outgoing short-wave radiation is potentially due to enhanced cloud formation in the coupled model run.

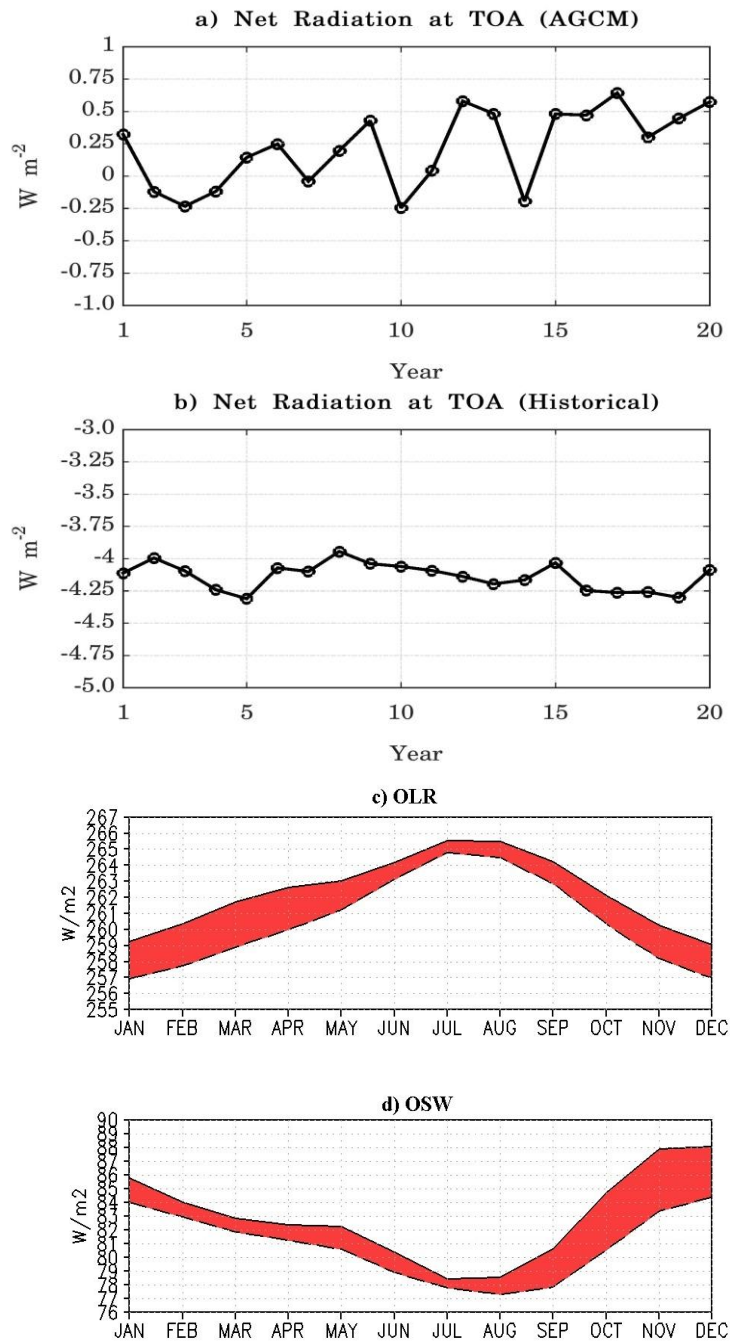


Figure 1 – Net of the radiation of TOA simulated by (a) stand-alone AGCM for 20 years and (b) BESM-OA2.5 Historical for the first 20 years (1850-1870). (c) and (d) are outgoing long-wave radiation and outgoing short-wave radiation, respectively. In (c) and (d) the solid lines represent the coupled model and the dashed lines represent the AGCM. Units are in $W m^{-2}$.

This information has been included in the revised manuscript (Page 12, Lines L16-L18).

3.1 Figure 2 shows the 2-m air temperature is less response to the GHG forcing in BESM during 1850s-1960s, while it isn't the case for any CMIP5 model. Any explanation for this unique feature?

Reply:

The net radiation at TOA has a mean value of -4.20 W m^{-2} and the net ocean/atmosphere heat flux has a mean value of 1.16 W m^{-2} in the first 50 years (Fig. 3, manuscript). Throughout the simulation, the net radiation at TOA becomes less negative due to the increasing CO_2 on the atmosphere and consequential increasing atmospheric heat content. Part of this heat is transferred into the ocean as indicated by the increasing positive net heat flux into the ocean. Negative values of net radiation flux at TOA means that the atmosphere is losing heat to the outer space during the simulation, which is likely the reason for the weak air temperature response to the GHG forcing observed in the Historical simulation (Fig. 2; manuscript).

3.2 The simulated SST is much warmer than the ERSST v4 during the evaluation period (Fig. 10), how is the land surface temperature?

Reply:

The land surface temperature bias for BESM-OA2.5 Historical simulation is generally negative over desert and semi-arid regions (Fig. 2). Such negative bias is noticed in the Arabian Desert, but also in the Sahara, Kalahari, Gobi, Polar Arctic, Patagonia, Sonoran and Australian deserts. The negative bias is also present in the Brazilian semi-arid region. Conversely, over the most vegetated regions the model presents positive bias, as the Amazon, tropical Africa, North America and Europe. Such biases are likely caused by drier air simulated by the model over desert regions, which tends to enhance the latent heat flux from the land surface over desert areas and causing higher cooling effect compared with Reanalysis, particularly during the night. Conversely, in forest regions the excess of air moisture constrains the loss of latent heat flux from the land surface. This enhances the land surface temperature compared with the Reanalysis.

Land surface skin temperature bias

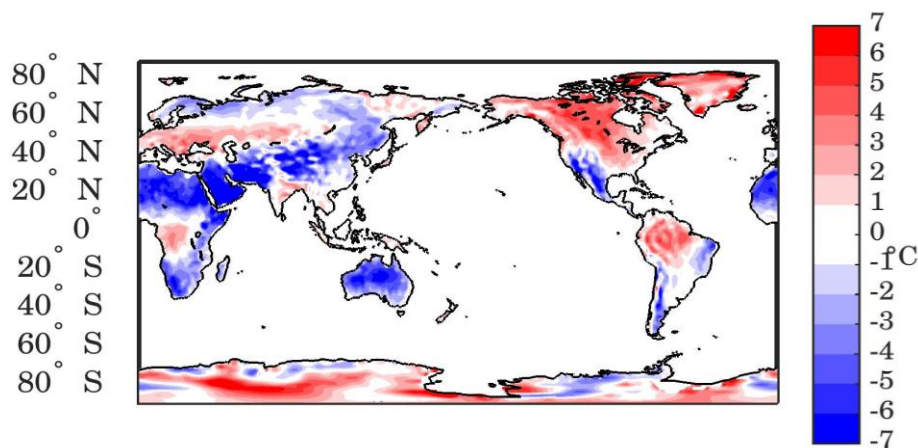


Figure 2 - Spatial map of annual mean land surface skin temperature bias of BESM-OA2.5 relative to ERA-Interim. The averages values are computed over the periods 1971–2000 (BESM-OA2.5) and 1979–2008 (ERA-Interim). Units are in °C.

3.3 How is the sea ice simulation under such a warm climate, please provide the figure of sea ice performance?

Reply:

Figure 3 shows the mean sea ice concentration simulated by BESM-OA2.5 for the end of the winter and the summer seasons for each hemisphere, over the period 1971-2000. The thick black lines represent the 15 % climatological values for the period 1971-2000 given by the 20CRv2 Reanalysis. The sea ice concentration in the Arctic winter is overestimated in the Atlantic, specifically north of the Scandinavia (Fig. 3a). However, in summer the Arctic sea ice is underestimated (Fig. 3b). In the Antarctica summer the model shows a significant underestimation of the sea ice concentration (Fig. 3c). During the Antarctica winter the model generally overestimates the extension of the sea ice concentration over all Southern Ocean (Fig. 3d). Such seasonal sea ice concentration amplitude is likely related to bias radiative net over higher latitudes that the model suffers, which during the winter in each hemisphere tend to generate higher extension of sea ice and during the summer in each hemispheres tend to enhance the sea ice melting compared with the Reanalysis.

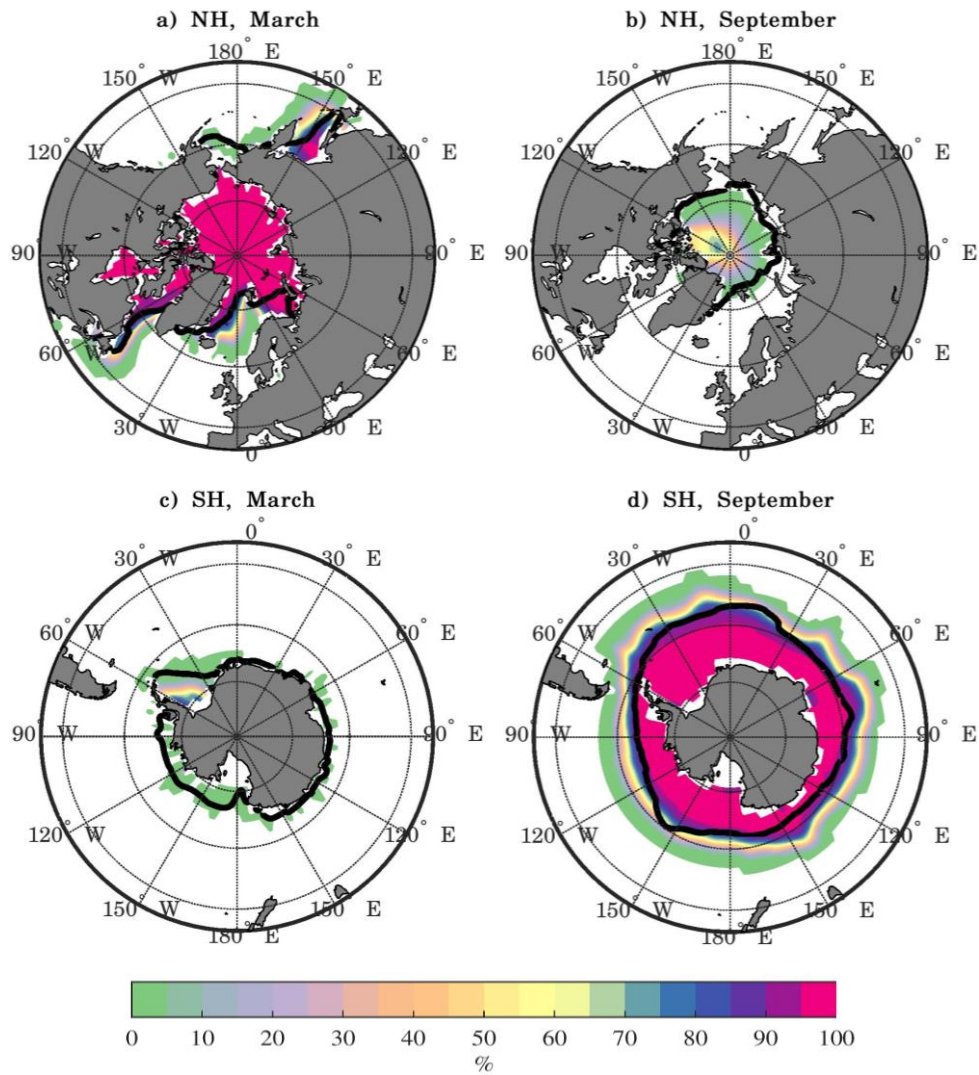


Figure 3 - BESM-OA2.5 mean sea ice concentration for March (a, c) and September (b, d) for each hemisphere. The solid black lines show the 15 % mean sea ice concentration for 20CRv2 reanalysis. The averages values are computed over the period 1971–2000 for BESM-OA2.5 and 20CRv2. The concentration is presented in percentage.

This topic has been included in the revised manuscript (Pages 21-22, Lines L24-L12).
 The figure has also been included in the revised manuscript (Page 73).

3.4 It is also necessary to clarify whether the 1.5K SST warming affect the model climate variability or not.

Reply:

Some important climate variabilities are reasonable well simulated by the model, as NAO, AMM, AMOC, PSA or PNA. Therefore, it is not clear whether the general warm bias that the model suffers has a profound impact on the climate variability simulated by the model. However, we have analyzed the global spatial standard deviation of variables that are influenced by SST, as precipitation, outgoing long-wave radiation (OLR), sea level pressure (SLP) and surface air temperature (SAT).

The global standard deviation of monthly precipitation anomalies simulated by BESM-OA2.5 over the period 1971-2000 is compared with GPCP standard deviation over the period 1979-2010 (Fig. 4). The largest precipitation variability is found in the west equatorial Pacific (Fig 4a). BESM-OA2.5, besides simulating a comparable standard deviation in the west equatorial Pacific, presents spurious large precipitation variability over the Indian Ocean (Fig 4b). The same pattern is observed in the OLR, which indicates an enhanced convection over the Indian Ocean (Fig 5). It is not clear the reasons for such phenomenon, but the Indian Ocean warm bias can enhance the convection in this region. The tropical Atlantic is other region that shows significant differences between the model and Reanalysis. BESM-OA2.5 has a strong variability over the tropical South Atlantic. Global SLP anomalies standard deviation shows no significant difference between the model and Reanalysis (Fig 6). The pattern is reasonably captured, particularly the higher variability over the Aleutian Islands, Iceland and Amundsen Sea (60-70 °S; 90 °W). In the case of SAT, the model generally presents lower SAT anomalies variability, although the pattern is captured by the model (Fig. 7). Thus, the standard deviation of precipitation, OLR, SLP and SAT anomalies do not show significant difference from the Reanalysis, besides the Indian Ocean region, as has been discussed above.

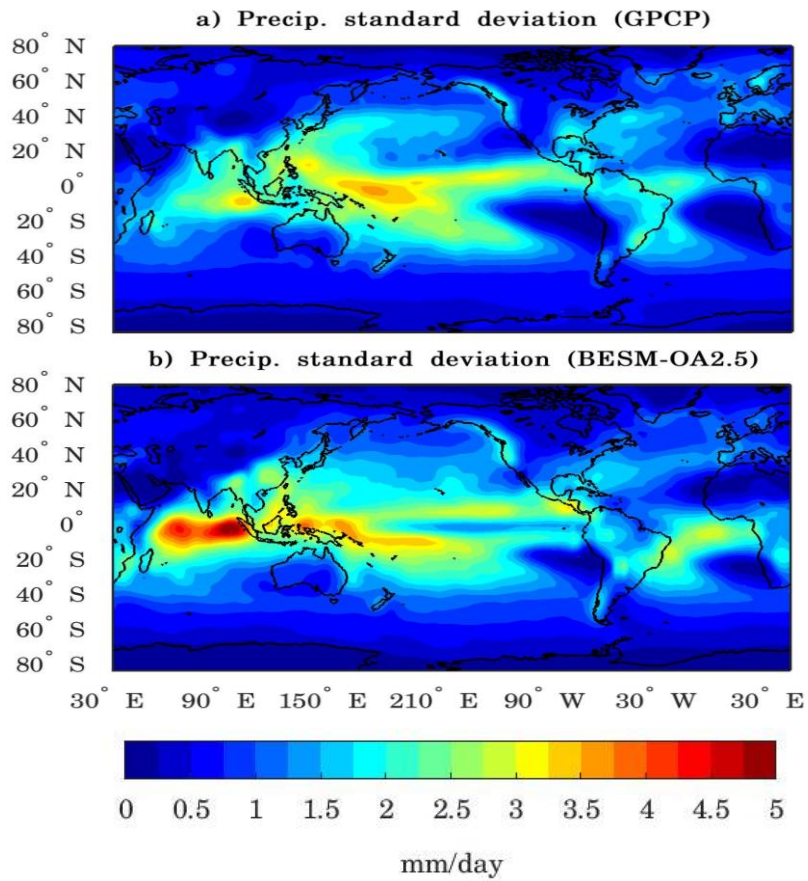


Figure 4 – Standard deviation of monthly precipitation anomalies for (a) GPCP and (b) BESM-OA2.5. The standard deviation values are computed over the periods 1971–2000 (BESM-OA2.5) and 1979–2010 (GPCP). Units are in mm/day.

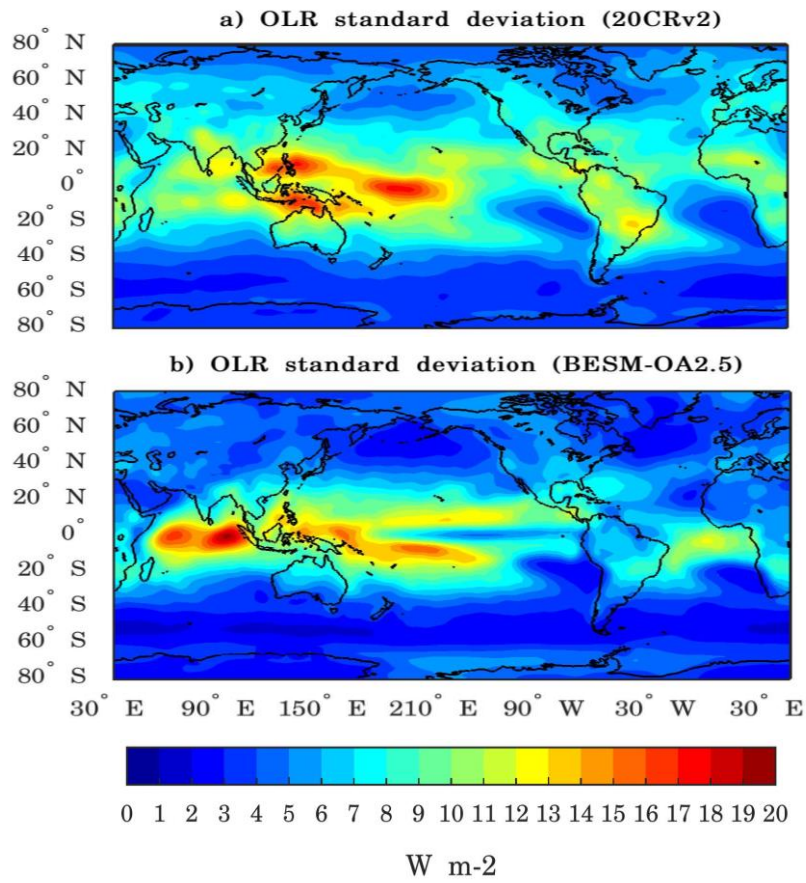


Figure 5 – Standard deviation of monthly OLR anomalies for (a) 20CRv2 and (b) BESM-OA2.5. The standard deviation values are computed over the period 1971–2000. Units are in $W m^{-2}$.

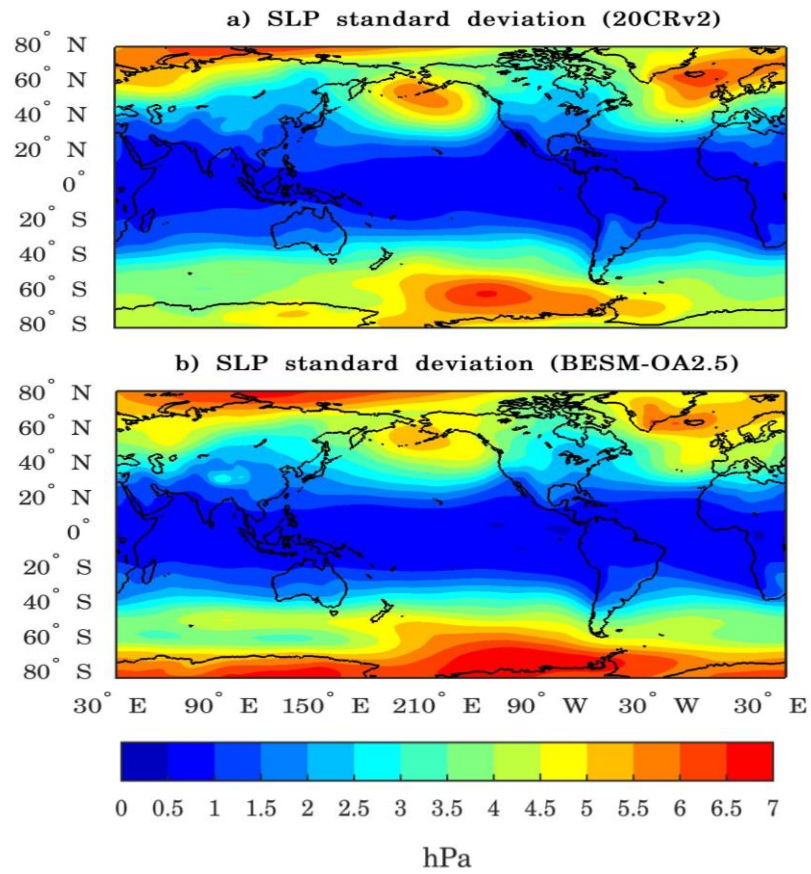


Figure 6 – Standard deviation of monthly SLP anomalies for (a) 20CRv2 and (b) BESM-OA2.5. The standard deviation values are computed over the period 1971–2000. Units are in hPa.

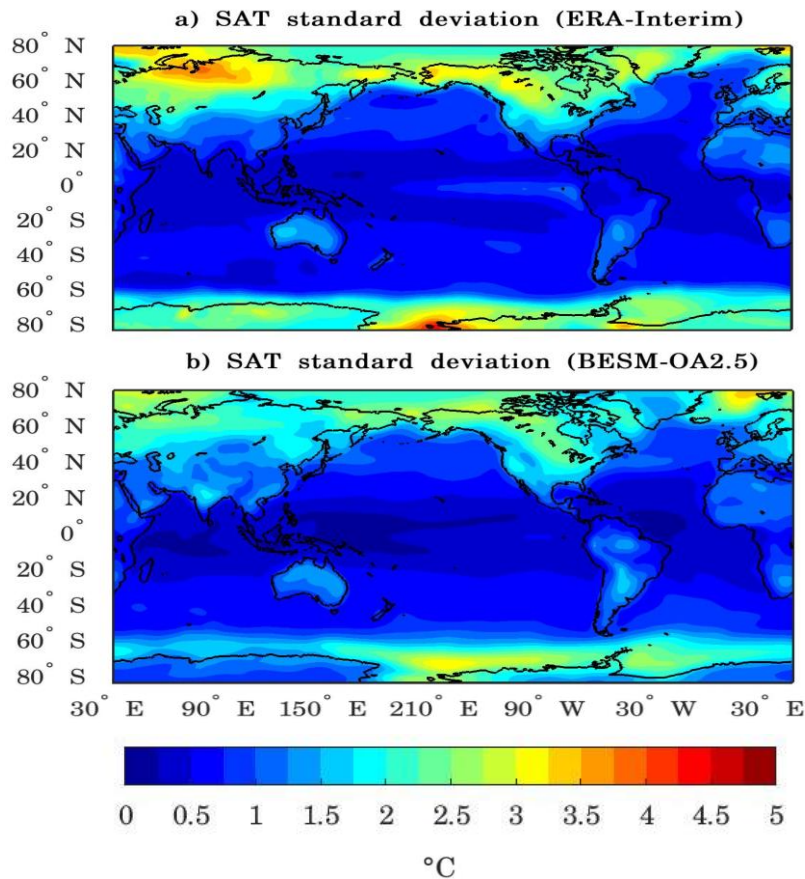


Figure 7 – Standard deviation of monthly SAT anomalies for (a) ERA-Interim and (b) BESM-OA2.5. The standard deviation values are computed over the period 1971–2000. Units are in $^{\circ}\text{C}$.

4. As point out by reviewer 2, the coupled model spin-up period is very short. It is unclear, from the manuscript, whether the decadal variability is affected by model spin-up or not. Is the weakening of AMOC strength (Fig. 14) due to the model adjustment?

Reply:

The AMOC negative linear trend observed in Historical simulation is likely linked to the model's drifting throughout simulation. Such conclusion is also reinforced by the depth-time Hovmöller diagrams of global mean ocean temperature and salinity departures from their respective initial conditions simulated by the Historical run is shown in Fig. 8. Here initial conditional means the value of the first year of simulation, in this case, the year 1850. The prominent warming occurs from the surface up to 400 m depth (Fig. 8a). This warming is more significant at the end of the simulation ($\sim 0.6\text{ }^{\circ}\text{C}$ comparing with initial conditions) and is likely to be related to the

global warming of the planet and consequential increasing heat flux from the atmosphere into the ocean. In deeper waters, from 1500 m up to the ocean floor, there is a weaker warming, indicating that the ocean is gaining heat mainly in the upper layers. Between 500-1500 m depth, it is observed a cooling tendency respective to initial conditions. The ocean salinity slightly increases below 1000 m depth and from the year 1935 the increase reaches 0.04 PSU between 1500 and 3000 m depth compared with the initial values (Fig. 8b). Above 1000 m depth there is a significant freshening of the ocean waters, with the surface waters salinity decreasing up to 0.18 PSU at the end of the simulation. Such tendency can mean that the ocean is still drifting from its initial conditions in the Historical simulation. Similar drift of the model is also observed in the piControl simulation for global average ocean temperature and salinity anomalies from the respective initial conditions.

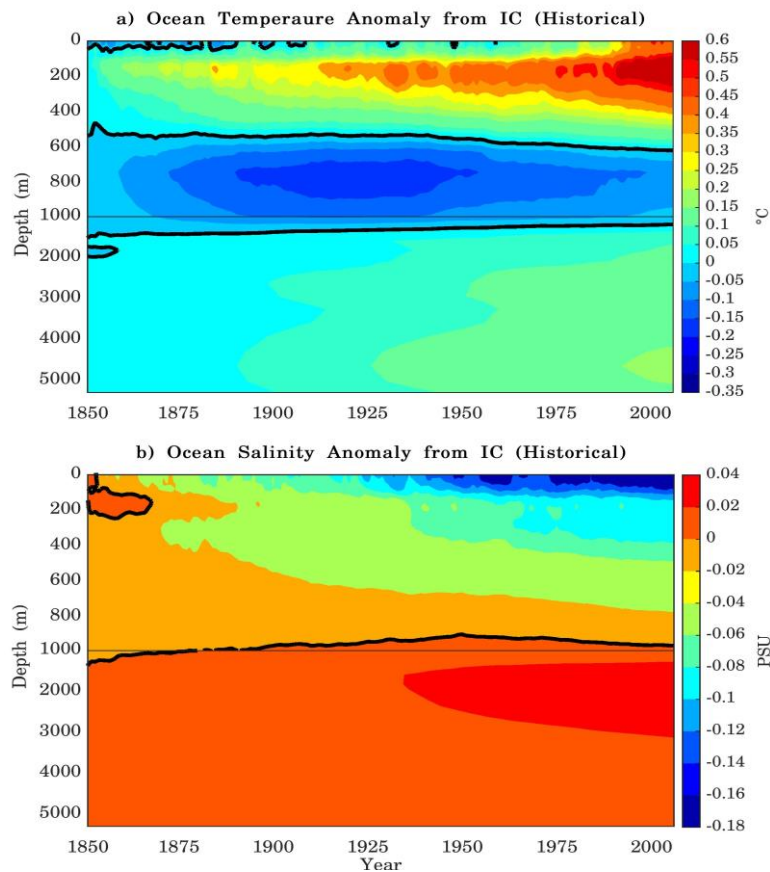


Figure 8 - Depth-time Hovmöller diagrams of global average ocean temperature and salinity anomalies from the respective initial conditions (IC). Here the initial conditions are taken from the 1th year (1850). The diagrams are based on annual average time series simulated by the Historical simulation over the period 1850-2005 (156 years). The thick black line represents the zero contours. Note that the vertical scales are different above and below 1000 m.

5. Some experience on coupled model tuning would be desirable.

Reply:

Since all simulations of the BESM-OA2.5 have already been performed, this suggestion will be taken into account on future simulations performed with the new version.

Bibliography

Swapna, P., Roxy, M. K., Aparna, K., Kulkarni, K., Prajeesh, A. G., Ashok, K., ... & Goswami, B. N. (2015). The IITM earth system model: transformation of a seasonal prediction model to a long-term climate model. *Bulletin of the American Meteorological Society*, 96(8), 1351-1367.

Menary, M. B., Kuhlbrodt, T., Ridley, J., Andrews, M. B., Dimdore-Miles, O. B., Deshayes, J., et al. (2018). Preindustrial control simulations with HadGEM3-GC3.1 for CMIP6. *Journal of Advances in Modeling Earth Systems*, 10. <https://doi.org/10.1029/2018MS001495>

Anonymous Referee #2

We thank the valuable comments, whose responses follow:

Minor Revisions:

1. The authors have responded to the reviewer's comment at length and explained in detail the spin-up procedure and the problem of model drift. Some of the new information has entered the revised manuscript, but some important issues are still missing in the main text, or is misleading.

The issue of model drift is still somewhat “put under the carpet”. The authors state that the surface quantities assume a stable state after 13 years in the PiControl run and suggest that drift is therefore no issue. However, the more than 1 W/m^2 excess heat that the ocean receives over the entire simulation leads to strong heat uptake. The authors have shown that to the reviewer in their response (Fig 2). However, comparing this figure with the Hovmueller plot in the main text (Figure 13 revised version) suggest that a considerable part of that warming is simply drift and not, as the authors claim in the text, a response to global warming.

Since the historical and PiControl runs have been run in parallel, a solution would be to include the control run figure. Another possibility would be to discuss the model drift in terms of an integrated quantity, e. g. heat content or steric (thermohaline) sea-level change, where the “real” changes in the historical run is estimated after the control run drift is subtracted.

Reply:

We agree with your observation. The ocean temperature anomalies above 600 m reaches $\sim 0.6 \text{ }^\circ\text{C}$ in the Historical simulation whereas in the piControl it reaches $\sim 0.4 \text{ }^\circ\text{C}$. This difference of $0.2 \text{ }^\circ\text{C}$ between the two simulations is likely due to the global warming. Therefore, there is a contribution of the ocean drift and a smaller contribution of the global warming of the ocean temperature increase in the Historical simulation. To properly provide this information we have included a figure showing the differential heating (Historical minus piControl). The improved text has been included in the revised manuscript (Pages 19, Lines L12). The figure has also been improved in the revised manuscript (Page 69).

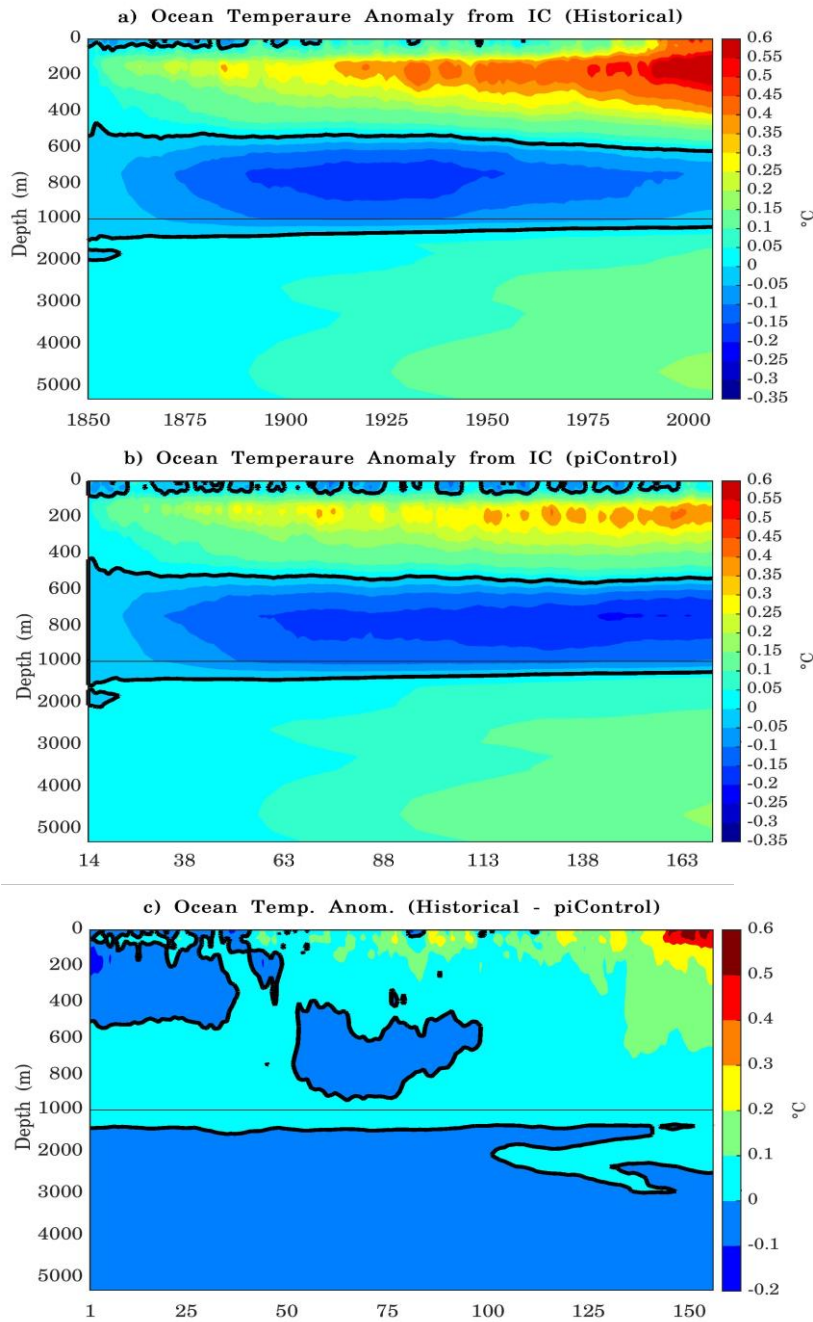


Figure 1 – Depth-time Hovmöller diagrams of global average ocean temperature anomalies for (a) Historical and (b) piControl simulations from the respective initial conditions (IC), and (c) the difference between Historical and piControl simulations. In the case of the Historical simulation, the initial conditions are taken from the 1th year. In the case of the piControl the initial conditions are taken from the 14th year, therefore after the 13 initial years of the adjustment. The diagrams are based on annual average time series. The thick black line represents the zero contours. Note that the vertical scales are different above and below 1000 m.

2. I am also still confused by the description of the spin-up procedure. In the authors' response it is explained that there has been a 100-year spin up (with a slightly different version of the coupled model) "as initial conditions for the piControl". I don't understand, why this is not mentioned in the main text and in the schematic and there is just talk of a 13 year spin-up. Was that done in addition to the 100 years?

Reply:

We agree with the reviewer's concern. A new figure has been included, depicting the complete spin-up process. Yes, the 13 years spin-up is additional to the 100 years spin-up, with slight differences between the atmospheric model's versions. To explain the spin-up process accurately, the experiments design figure has been improved (Figure 1 revised manuscript; Page 53) and the following text has been included on the experiments design topic in the revised manuscript (Page 8, Lines L11-L20):

"The ocean stand-alone runs for 71 years (13 years period of ocean model spin-up forced by climatological atmospheric fields plus 58 years period forced by interannually varying atmospheric fields). Then a spin-up of the fully coupled model is done for 100 years. The ocean and atmosphere states at the end of these 100 years long integration are used as the initial condition for the piControl simulation. The atmospheric model's versions are slightly different for 100 years spin-up and the piControl run, in the parameterizations of the land ice albedo and cloud microphysics. The Historical simulation uses as initial conditions information of the 14th year provided by the piControl simulation. The piControl simulation shows stable conditions after a fast adjustment over the first 13 years of simulation (figure not shown). Therefore, it is assumed that the Historical simulation has a spin-up of 113 years"

3 Page 7, lns 3ff: How is river runoff and transfer to the ocean treated?

Reply:

River runoff is treated as a time invariant inflow on a spatially fixed grid along the continental margins, to mass balance ocean precipitation minus evaporation over the ocean area. This is a standard feature of the ocean model configuration as distributed by GFDL.

4. Page 20, lns 3ff: “appropriate depth”: Not sure if that is true, e.g. the zero crossing in the North Atlantic is below 2500 m. (Compare for example, with the recent paper by Menary et al.: <https://agupubs.onlinelibrary.wiley.com/doi/abs/10.1029/2018MS001495>).

Reply:

Thank you for this comment. We agree that a more precise description is necessary. The following improved text has been included in the revised manuscript (Page 20, Line L22):

“The AMOC in the BESM-OA2.5 historical experiment has the typical structure described in Lumpkin and Speer (2007), with the upper layer of the upper cell, which is the northward flux, depicted in the appropriated depth, from the surface up to ~1000 m (Fig. 14a). However, the upper cell simulated by BESM is too shallow compared with the RAPID measurements (McCarthy et al., 2015). The depth of the upper cell is 2500 m in the model whereas the measurements show its depth at ~4500 m. This shallow upper cell of the AMOC is a common feature of state-of-the-art climate models (see Menary et al., 2018). The model simulates the northward Antarctic Bottom Water in the ocean floor.”

1 **The Brazilian Earth System Model version 2.5: Evaluation of**
2 **its CMIP5 historical simulation**

3
4
5 **Sandro F. Veiga¹, Paulo Nobre², Emanuel Giarolla³, Vinicius Capistrano⁴, Manoel**
6 **Baptista Jr.², AndréL. Marquez², Silvio Nilo Figueroa², JoséPaulo Bonatti², Paulo**
7 **Kubota², Carlos A. Nobre⁵**

8
9 ¹Earth System Science Center-CCST, National Institute for Space Research (INPE), S ão
10 Jos édos Campos 12227-010, S ão Paulo, Brazil

11 ²Center for Weather Forecasting and Climate Studies-CPTEC, National Institute for
12 Space Research (INPE), Cachoeira Paulista 12630-000, S ão Paulo, Brazil

13 ³Center for Weather Forecasting and Climate Studies-CPTEC, National Institute for
14 Space Research (INPE), S ão Jos édos Campos 12227-010, S ão Paulo, Brazil

15 ⁴Amazonas State University (UEA), Manaus 69005-010, Amazonas, Brazil

16 ⁵CN Research, S ão Jos édos Campos 12544-590, S ão Paulo, Brazil

17
18 *Correspondence to:* Sandro F. Veiga (sandro.veiga@inpe.br)

1 **Abstract**

2

3 The performance of the coupled ocean-atmosphere component of the Brazilian Earth
4 System Model version 2.5 (BESM-OA2.5) simulating the historical period 1850-2005 is
5 evaluated. Following climate model validation procedure, in which the atmospheric and
6 oceanic main variabilities are evaluated against observation and Reanalysis datasets, the
7 evaluation particularly focuses the mean climate state and the most important large-
8 scale climate variability patterns simulated in the historical run, which is forced by
9 observed greenhouse gas concentration. The most significant upgrades in the model's
10 components are also presented briefly. BESM-OA2.5 is able to reproduce the most
11 important large-scale variabilities, particularly over the Atlantic (e.g. the North Atlantic
12 Oscillation, the Atlantic Meridional Mode and the Atlantic Meridional Overturning
13 Circulation) and the extratropical modes that occur in both hemispheres. The model's
14 ability in simulating large-scale variabilities indicates its usefulness for seasonal climate
15 prediction and climate change studies.

16

1 **1. Introduction**

2 Climate Models and their recent extension to become Earth System Models, by
3 the inclusion of biogeochemical cycles, are key tools to investigate climate phenomena
4 which greatly influence human societies (e.g. von Storch, 2010; Flato, 2011). Since
5 2008 the Brazilian climate community has been engaged in setting up the Brazilian
6 Earth System Model (BESM; Nobre et al., 2013; Giarolla et al., 2015); a major
7 scientific task which has been carried out by Brazilian scientific institutions invoking
8 the critical need to address reliable future climate projections and their potential
9 impacts, particularly over South America. The primary objective encompassed in this
10 effort is to build up the scientific expertise capable to develop and maintain a state-of-
11 the-art Earth System Model. Such an achievement would represent a significant step
12 forward in establishing a scientific tool which can be used in different arrays of research
13 activities. The importance of such undertaking lies in the understanding of the physics
14 of the Earth system to produce and confer credibility to studies of impacts of climate
15 change in different areas of great importance; such as food and water security, tropical
16 ecosystems, natural disasters, and so on. One of the primordial aims of the BESM
17 project is to participate in the Coupled Model Intercomparison Project's sixth phase
18 (CMIP6; Meehl et al., 2014).

19 The Brazilian Earth System Model (BESM) has been set up at the Brazilian
20 National Institute for Space Research (INPE). At present, it consists of a land-ocean-
21 atmosphere coupled model, in which the coupling is done through the Flexible
22 Modeling System (FMS) coupler, developed at the Geophysical Fluid Dynamics
23 Laboratory (GFDL) of the National Oceanic and Atmospheric Administration (NOAA).

1 The inclusion of aerosols (as read-in fields) and atmospheric chemistry components are
2 in the phase of implementation and tests. Currently, work has been done on activate the
3 biogeochemical model (TOPAZ) within the MOM5 in order to simulate biogeochemical
4 cycles in future simulations.

5 The previous version of BESM (BESM-OA2.3) was firstly evaluated in Nobre et
6 al. (2013). This version showed a significant bias on precipitation in the tropical region,
7 with a deficient representation of precipitation in the Amazon region. In order to
8 improve these aspects, studies were conducted to ameliorate cloud parameterizations
9 over the tropics, which improved the precipitation over the same region and the
10 representation of Convergence Zones over both the Atlantic and Pacific Oceans basins
11 (Bottino and Nobre, 2018). Main changes of the current version relate to BESM's
12 atmospheric model, with modifications in the surface wind field and its
13 parameterizations, described in Capistrano et al. (2018). The updated version presented
14 in this manuscript is BESM-OA2.5.

15 From the operational point of view, BESM-OA2.3 is already being used for
16 extended weather forecast (10-30 days) to seasonal climate prediction (three months), as
17 well as for producing global climate change scenarios (Nobre et al., 2013) and to
18 provide atmospheric and oceanic boundary conditions to regional climate models for
19 dynamical downscaling of climate change scenarios (Chou et al., 2014).

20 This overview paper describes the most important developments and
21 improvements in the model components, presenting the simulation of recent past mean
22 climate conditions and major large-scale climate phenomena. In section 2 the BESM-
23 OA2.5 components and experimental design are briefly described; section 3 presents the

1 methodology and the observed data used to evaluate the model; section 4 presents the
2 evaluation of the historical simulation, in which are evaluated the most important
3 atmospheric and oceanic variables regarding to their climatological fields and the
4 prominent large-scale phenomena of the climate system; finally, section 5 presents the
5 summary.

6 **2 Model Description and Simulation Experiment Design**

7 **2.1 BESM-OA2.5**

8 The atmospheric component of BESM-OA2.5 is the Brazilian Global
9 Atmospheric Model (BAM; Figueroa et al., 2016) developed at Center for Weather
10 Forecasting and Climate Studies (CPTEC/INPE). It is a primitive equation model with
11 spectral representation with triangular truncation at the wave number 62, corresponding
12 to a grid resolution of approximately $1.875^\circ \times 1.875^\circ$; and 28 sigma levels in the
13 vertical, with uneven increment between the levels, i.e. T62L28 resolution. As
14 mentioned before, it is in the atmospheric component which resides the main
15 differences between BESM-OA2.5 and BESM-OA2.3 (Nobre et al., 2013). The new
16 version shows a key improvement in the energy balance at the top of the atmosphere, by
17 reducing the mean global bias from -20 W m^{-2} in version BESM-OA2.3 to -4 W m^{-2} in
18 the current version (Capistrano et al. 2018). Version 2.5 of BESM incorporates the
19 formulation presented in Jiménez et al. (2012) for the representation of the wind,
20 humidity and temperature in the surface layer. The model runs without flux correction
21 or adjustment. The physics parameterizations for the continental processes are based on
22 the Simplified Simple Biosphere Model (SSiB) land surface model (Xue et al., 1991), in

1 shortwave radiation Clirad scheme (Tarasova et al. 2007; Chou and Suarez 1999), in
2 longwave radiation Harshvardhan scheme (Harshvardhan et al., 1987), in Cloud
3 microphysics Ferrier scheme (Ferrier et al. 2002), in the turbulence level 2 module
4 (Mellor and Yamada, 1982), in the gravity wave module (Anthes, 1977), in the deep
5 convection module (Arakawa and Schubert, 1974; Grell and Dévényi, 2002), and in the
6 shallow convection module (Tiedtke, 1983). More details can be found in Figueroa et
7 al. (2016) and in Capistrano et al. (2018).

8 The oceanic component of BESM-OA2.5 is the Modular Ocean Model version
9 4p1 (MOM4p1; Griffies, 2009) developed at GFDL, which includes the Sea Ice
10 Simulator (SIS) built-in ice model (Winton, 2000). There are no changes in the physics
11 parameterizations from those used in BESM-OA2.3. The horizontal grid resolution in
12 the zonal direction is 1° and in the meridional direction it varies uniformly from $1/4^\circ$
13 between 10°S and 10°N to 1° of resolution at 45° and to 2° of resolution at 90° , in both
14 hemispheres. The vertical resolution has 50 levels with approximately 10 m resolution
15 in the upper 220 m, increasing gradually to about 370 m resolution at deeper levels. The
16 oceanic model spin-up was done in a manner similar to that of Nobre et al. (2013) and
17 Giarolla et al. (2015), in which is begin the spin-up run from rest, and the T-S structure
18 of the oceans of Levitus (1982). The initial stage of the ocean model spin-up was done
19 over a 13 years period, forced by climatological atmospheric fields (winds, solar
20 radiation, air temperature and humidity, and precipitation). It was then integrated by an
21 additional 58 years period, forced by interannually varying atmospheric fields from
22 Large and Yeager (2009), while the river discharges and the sea ice variables were kept
23 at their respective monthly mean climatological values. The forced ocean model run

1 was used to save the oceanic dynamical and thermodynamical structures in order to be
2 used in the initialization of future coupled model experiments.

3 The atmospheric and oceanic models are coupled via the Flexible Modeling
4 System (FMS) coupler, which was also developed at GFDL and incorporated in
5 MOM4p1. The atmospheric model receives SST and ocean albedo from the ocean and
6 sea ice models at hourly time steps. On the other hand, the oceanic model receives
7 information about freshwater (liquid and solid precipitation), momentum fluxes (winds
8 at 10 m), specific humidity, heat, vertical diffusion of velocity components and surface
9 pressure, all also at hourly time steps. Wind stress fields are computed within MOM4p1
10 using Monin-Obukhov scheme (Obukhov, 1971). In coupled simulations, the ocean
11 temperature and salinity restoration options are turned off.

12 **2.2 Experiments design**

13 A set of numerical experiments were carried out with the coupled ocean-
14 atmosphere version of BESM-OA2.5, following the CMIP5 experiment design protocol
15 (Taylor et al., 2012), and shown schematically in Figure 1. Out of those experiments
16 listed below, only the Historical simulation is evaluated in this paper:

- 17 ● Historical: the simulation runs over the period 1850–2005 (156 years), forced by
18 atmospheric equivalent CO₂ observed historical concentration (greenhouse gas
19 only) over this period, based on CMIP5 protocol.
- 20 ● piControl: it runs for 1140 years, forced by invariant pre-industrial atmospheric
21 CO₂ concentration level (280 ppmv).
- 22 ● Abrupt 4×CO₂: it runs for 1000 years, consisting of an abrupt quadruplication of

1 the atmospheric CO₂ concentration level from the piControl simulation.

- 2 ● RCP4.5: it runs over the period 2006–2105 (100 years), forced by the time series
3 of greenhouse gases level projected by the Representative Concentration
4 Pathways 4.5 (RCP4.5), based on CMIP5 protocol. This simulation continues
5 the historical simulation throughout the 21th century, reaching the radiative
6 atmospheric forcing of 4.5 W m⁻² in 2100.
- 7 ● RCP8.5: same as the RCP4.5 simulation, but forced by the time series of
8 greenhouse gases level projected by the Representative Concentration Pathways
9 8.5 (RCP8.5), based on CMIP5 protocol; i.e., reaching the radiative atmospheric
10 forcing of 8.5 W m⁻² in 2100.

11 The ocean stand-alone runs for 71 years (13 years period of ocean model spin-up forced by
12 climatological atmospheric fields plus 58 years period forced by interannually varying
13 atmospheric fields). Then a spin-up of the fully coupled model is done for 100 years. The ocean
14 and atmosphere states at the end of this 100 years long integration are used as the initial
15 condition for the piControl simulation. The model's versions are slightly different for 100 years
16 spin-up and the piControl run, in the parameterizations of the land ice albedo and cloud
17 microphysics. The Historical simulation uses as initial conditions information of the 14th year
18 provided by the piControl simulation. The piControl simulation shows stable conditions after a
19 fast adjustment over the first 13 years of simulation (figure not shown). Therefore, it is assumed
20 that the Historical simulation has a spin-up of 113 years. ~~The ocean stand-alone runs for 71~~
21 ~~years (13 years period of ocean model spin-up forced by climatological atmospheric~~
22 ~~fields plus 58 years period forced by interannually varying atmospheric fields). Then a~~
23 ~~spin-up of the fully coupled model is done for 100 years. The ocean and atmosphere~~
24 ~~states at the end of this 100 years long integration are used as the initial condition for~~
25 ~~the piControl simulation. The piControl simulation shows stable conditions after a fast~~

~~adjustment over the first 13 years of simulation (figure not shown).~~ The analysis of the piControl and 4×CO₂ simulations are described in Capistrano et al. (2018) and Nobre et al. (2018, in preparation). Capistrano et al. (2018) estimates that BESM-OA2.5 has an equilibrium climate sensitivity of 2.96 °C for the abrupt 4×CO₂ experiment. This value is within the range from 2.07 to 4.74 °C that has been computed for 25 CMIP5 models and close to the ensemble averaged value (3.30 °C).

3. Methods and Data

To evaluate the outputs of the BESM-OA2.5 historical simulation, comparisons are done against observed datasets and Reanalysis products. The atmospheric fields are from the Twentieth-Century Reanalysis dataset version 2 (20CRv2; Compo et al., 2011) with a global horizontal resolution of 2° × 2° and 24 vertical levels (https://www.esrl.noaa.gov/psd/data/gridded/data.20thC_ReanV2.html); the precipitation dataset is obtained from Global Precipitation Climatology Project version 2.2 Combined Precipitation Dataset (GPCP; Adler et al., 2003; Huffman et al., 2009) with global horizontal resolution of 2.5° × 2.5° (<http://rda.ucar.edu/datasets/ds728.2/#!/description>) and from the CPC Merged Analysis of Precipitation (CMAP; Xie and Arkin, 1997) with global horizontal resolution of 2.5° × 2.5° (<https://www.esrl.noaa.gov/psd/data/gridded/data.cmap.html>); for comparison of the global average air surface temperature, it is used the Hadley Centre-Climate Research Unit Temperature Anomalies version 4 (HadCRUT4, Morice et al., 2012), globally averaged air temperature anomaly at 2 meters time series (<https://crudata.uea.ac.uk/cru/data/temperature/>); the cloud cover is compared to data from The International Satellite Cloud Climatology Project (ISCCP D2; Rossow and

1 Schiffer, 1999) with global horizontal resolution of $2.5^{\circ} \times 2.5^{\circ}$
2 (<https://isccp.giss.nasa.gov/products/onlineData.html>); finally, for Sea Surface
3 Temperature (SST) comparisons it is used the Extended Reconstructed Sea Surface
4 Temperature version 4 (ERSSTv4, Huang et al., 2015) available on a $2^{\circ} \times 2^{\circ}$ grids
5 resolution (<https://www.esrl.noaa.gov/psd/data/gridded/data.noaa.ersst.v4.html>).

6 To identify the main modes of climate variability, all analyses presented in the
7 paper are done using detrended data sets anomalies. Detrended data sets are obtained by
8 removing the linear trend based on a least squares regression. Analysis using monthly
9 data sets, the annual cycle was removed by subtracting climatological monthly means
10 from the respective individual month. Prior to performing the analysis, the model's data
11 sets were interpolated to the grid resolution of the respective observation or Reanalysis
12 data sets used for comparison.

13 The Empirical Orthogonal Function analysis (EOF; Hannachi et al., 2007) is
14 used to analyze the capacity of the model in simulating major modes of climate
15 variability and compare them with observations. Prior to performing the EOF
16 calculations, the data were weighted by the square root of the cosine of latitude. The
17 results of the EOF maps are shown as the original data anomalies regressed onto the
18 normalized Principal Component (PC) time series, i.e. by the standard deviation.

19 In this paper, in order to evaluate the periodicity of the phenomena, it is applied
20 the power spectrum technique based on Fourier Analysis on the normalized time series,
21 in which the normalization is done by their long-term monthly standard deviation.

22 To have a better insight of BESM-OA2.5 performance of the global average

1 near-surface air temperature and on the average SST along both equatorial Pacific and
2 Atlantic, a comparison with 11 CMIP5 models is carried out. Since BESM-OA2.5
3 historical simulation is forced only by observed CO₂ equivalent concentration, for the
4 comparison it is chosen the historical simulation forced only by greenhouse gas
5 (historical GHG) shown in Table 1.

6 **4. Results**

7 **4.24.1 Mean Climate State**

8 In this section, the most important atmospheric and oceanic variables are
9 evaluated regarding their climatological fields, either globally or over regions in which
10 their representation are key elements of the climate system.

11 **4.1.1 Mean Surface Air Temperature**

12 The evolution of global surface air temperature throughout the industrial era is a
13 key element to analyze the long-term model behavior while being forced by the
14 observed conditions. The HadCRUT4 observation and BESM-OA2.5 time series of the
15 globally averaged air temperature anomaly at 2 meters are shown in Figure 2. The time
16 series are annual mean anomalies relative to the period 1850–1879. BESM-OA2.5
17 simulation of the global average surface air temperature evolution follows closely the
18 observed time series. However, since BESM-OA2.5 does not have the representation of
19 aerosols and consequently its cooling effects, the rate surface air warming should be
20 higher similarly to the remaining models (the grey shadow in Figure 2). In order to
21 compare BESM-OA2.5 with the selected CMIP5 models, the grey shadow represents
22 the spread of the minimum and the maximum values of anomalies at each year among

1 the 11 models (Table 1). In this comparison, it is used the historical GHG simulation, in
2 which the models are only forced by well-mixed greenhouse gases (mainly carbon
3 dioxide, methane, and nitrous oxides), without the cooling resulting from the direct and
4 indirect effects of aerosols, volcanos and effects of the land use change. Thus, the
5 CMIP5 models show a warmer tendency compared with the observations (see Jones et
6 al., 2013 for more details). Although BESM-OA2.5 has the same forcing conditions it
7 does not show the warming tendency of remaining models. With exception of GFDL-
8 ESM2M (1861–2005) and HadGEM2-ES (1860–2005), all the remaining CMIP5
9 models span their simulations throughout the period 1850–2005 and their respective
10 anomalies are from the period 1850–1879. For GFDL-ESM2M and HadGEM2-ES, the
11 anomalies are computed relative to the periods 1861–1890 and 1860–1889,
12 respectively.

13 The net radiation at the top of atmosphere (TOA) has a negative bias and net of
14 the ocean/atmosphere heat flux has a positive bias (Fig. 3). The net radiation at TOA
15 has a mean value of -4.20 W m^{-2} and the net ocean/atmosphere heat flux has a mean
16 value of 1.16 W m^{-2} in the first 50 years. The net radiation imbalance at TOA is related
17 to significant loss of energy at TOA both from the outgoing long-wave radiation and
18 outgoing short-wave radiation. Throughout the simulation the net radiation at TOA
19 becomes less negative due to the increasing CO_2 on the atmosphere and consequential
20 increasing atmospheric heat content. Part of this heat is transferred into the ocean as
21 positive net of the ocean/atmosphere heat flux increasing indicates. The negative net
22 radiation at TOA and the positive ocean/atmosphere heat flux are likely the reason for
23 the weak warming observed in the Historical simulation (Fig. 2), since the atmosphere

1 is losing heat to the outer space and into ocean during the simulation.

2 **4.1.2 Mean Precipitation**

3 One of the key points in evaluating a Climate Model is to gauge its ability to
4 simulate the hydrological cycle due to its importance to the energy balance of the
5 climate system. Figure 4 shows the spatial distribution of annual mean precipitation for
6 (a) BESM-OA2.5, (b) GPCP dataset, and the spatial distribution of annual mean
7 precipitation bias (c) for BESM-OA2.5 relative to the GPCP dataset and (d) for BESM-
8 OA2.5 relative to the CMAP dataset. The spatial annual mean precipitation are averaged
9 values over the periods 1971–2000 and 1979–2008, for BESM-OA2.5, and GPCP and
10 CMAP datasets, respectively. The global model's mean biases are similar for GPCP
11 (0.3 mm day^{-1}) and CMAP (0.4 mm day^{-1}). In the case of the global model's rmse
12 biases, they are also similar for GPCP (1.4 mm day^{-1}) and CMAP (1.5 mm day^{-1}).
13 BESM-OA2.5 is able to reproduce global observed patterns of precipitation and
14 indicates a slight improvement in the global mean precipitation simulation compared
15 with the previous version (BESM-OA2.3). The spatial average biases are 0.3 mm day^{-1}
16 and 0.5 mm day^{-1} , and the rmse are 1.4 mm day^{-1} and 1.7 mm day^{-1} for BESM-OA2.5
17 and BESM-OA2.3, respectively. The improvements are particularly seen in the Pacific
18 and Atlantic Ocean areas, where BESM-OA2.5 reduces the positive bias that extends to
19 subtropical southeast Pacific and both north and south Atlantic subtropics observed in
20 BESM-OA2.3 (see Fig. 6a of Nobre et al., 2013). Despite these improvements, BESM-
21 OA2.5 still generates a strong negative bias over the Amazon region. This is a particular
22 concern since an important aim is related to the model for future climate projections in
23 the region. Based on the progress observed from BESM-OA2.3 to BESM-OA2.5, work

1 on cloud parametrizations that can improve the precipitation over the Amazon is still
2 carried out. Nevertheless, some state-of-the-art models show deficiencies in generating
3 precipitation over the Amazon region. This is the case of the IITM-ESM (Fig. 5;
4 Swapna et al., 2018), although the bias is more confined to the north of the Amazon and
5 NESM that has a more distributed bias over the region (Fig. 9; Cao et al., 2018). The
6 Indian subcontinent region also has a significant negative bias and strong positive bias
7 appears over the Indian Ocean and in the South Pacific Convergence Zone (SPCZ).
8 Such strong positive bias over the Indian Ocean (near the African coast) is also
9 identified in different versions of CCSM model (Fig. 5; Gent et al., 2011).

10 In order to draw an associated global atmospheric circulation associated with the
11 deficient precipitation over both the Amazon and Indian regions, it is computed the
12 global anomalies of the velocity potential and the divergence of the wind at 200 hPa
13 pressure level, and shown in Figure 5. The velocity potential and divergent wind
14 anomalies are averaged over the period 1971–2000 for BESM-OA2.5 outputs (Fig. 5a),
15 Reanalysis (Fig. 5b) and the difference BESM-OA2.5 minus Reanalysis (Fig. 5c, 5d and
16 5e). Figure 5c shows anomalous convergence over the Amazonian and Indian regions,
17 resulting of the model's deficient capacity for creating convection and consequently in
18 generating precipitation. Figures 5d and 5e show the velocity potential and wind
19 divergence separated by seasons. For the Amazonian rainfall season, which occurs
20 during MAM, it is possible to observe anomalous convergence at high levels of the
21 atmosphere (Fig 5d). The equivalent result is observed for the Indian region for the JJA
22 season (Fig. 5e).

23 Figure 6 shows zonally averaged precipitation during the four seasons. For this

1 comparison, results of BESM-OA2.3 used in Nobre et al. (2013) are also shown. Both
2 versions are able to reproduce the maximum peaks of precipitation in both tropical and
3 subtropical regions. BESM-OA2.5 shows a negative bias from around 40° latitude
4 poleward in both hemispheres. In the seasons DJF, JJA and SON, BESM-OA2.5 has a
5 positive bias on the peak of maximum precipitation corresponding to the ITCZ. In
6 MAM season the model still fails to perform the interhemispheric transition of the
7 ITCZ. However, the JJA season shows that BESM-OA2.5 is able to do the transition
8 completely, whilst BESM-OA2.3 shows a double ITCZ in JJA and SON seasons. The
9 double ITCZ problem is one of the most significant biases that persist in climate models
10 (e.g. Hwang and Frierson, 2013; Li and Xie, 2014; Tian, 2015). With the exception of
11 the MAM season, BESM-OA2.5 shows identical zonal precipitation to the observations,
12 although with a generally positive bias. It should be noted that BESM-OA2.5 has a
13 rapid precipitation decline at high latitudes. The model shows peaks of precipitation at
14 the mid-latitudes related to the storm tracks and less precipitation at the subtropics
15 compared to the GPCP dataset.

16 Figure 7 shows the general characteristics of cloudiness over the globe simulated
17 by the model. In particular, Figure 7a shows that the model underestimates cloudiness in
18 most part of the globe, with significant exceptions of the high latitudes in the boreal
19 hemisphere and in the southern subequatorial regions of the Pacific and Atlantic
20 | Oceans when compared to observations. Globally, BESM-OA2.5 has a cloudiness
21 negative bias of -13.9 % with a root-mean-square-error of 19.9 %. The periods used are
22 1971–2000 and 1984–2009 for BESM-OA2.5 and ISCCP, respectively. The model fails
23 to generate clouds in the high latitudes of the austral hemisphere, as can be observed in

1 Figure 7b, where the percentage of cloud cover is negligible. The reason for such lack
2 of simulated cloudiness in this region is not clear yet. However, through the Figure 7b it
3 is possible to see the meridional variation of cloud cover simulated by the model is
4 similar to the observation.

5 **4.1.3 Zonal Atmospheric Mean State**

6 Figures 8 and 9 present the analysis of the zonally averaged vertical profiles of
7 air temperature and zonal wind for all seasons simulated by BESM-OA2.5 and the
8 respective bias relative to the 20CRv2 Reanalysis dataset, in which all data are time
9 averaged over the period 1971–2000. BESM-OA2.5 has a large positive air temperature
10 bias that appears above 250 hPa height (Fig. 8) in subpolar and polar regions in all
11 seasons. This result indicates that the model warms abnormally in the tropopause and
12 the lower stratosphere in polar regions. The warm bias is stronger in DJF and MAM
13 seasons over the northern polar region, reaching a maximum bias of 20 °C in the DJF
14 season. Such a bias is a matter of concern since other models, despite present strong
15 bias in the Polar Regions, does not show such a strong bias. BNU-ESM presents
16 positive biases up to 10 °C in the austral hemisphere during the season JJA (Fig. 3a; Ji et
17 al., 2014) and NorESM1-M presents negative biases (~ -10 °C) during the seasons DJF
18 and JJA (Fig. 9; Bentsen et al., 2013). In the lower and middle troposphere, the model
19 shows a negative temperature bias, which is stronger in the lower troposphere over the
20 polar region in the respective winter-spring seasons in both hemispheres, i.e. DJF and
21 MAM over the North Pole, and JJA and SON over the South Pole. This negative bias
22 reaches its maximum of -10 °C over the South Pole in SON. This negative bias over the
23 troposphere has already been reported to occur in many CMIP5 models (see Charlton-

1 Perez et al., 2013; Tian et al., 2013).

2 Concerning to the zonal wind, BESM-OA2.5 simulates a much weaker wind
3 speed at the tropopause and stratosphere over the boreal hemisphere, mainly in the DJF
4 season, which has a maximum negative bias of -26 m s^{-1} at 50–30 hPa (Fig. 9a). This
5 bias is out of the range (-10 m s^{-1} to 10 m s^{-1}) that some models presents, as NorESM1-
6 M (Fig. 10; Bentsen et al., 2013) or NESMv3 (Fig. 10d; Cao et al., 2018). The
7 tropospheric jets and their seasonal migration are reasonably well simulated, although
8 the eastward wind is stronger at subtropics with the maximum positive bias of 12 m s^{-1}
9 occurring at 300–100 hPa in the MAM season.

10 **4.1.4 Ocean Mean State**

11 The global distribution and the range values of the sea surface temperature
12 (SST) are important characteristics of the mean climate state. Figure 10 shows the
13 spatial map of the annual mean SST for (a) BESM-OA2.5, (b) ERSSTv4 and (c) the
14 bias for BESM-OA2.5 relative to the ERSSTv4 dataset. BESM-OA2.5 has a warm SST
15 bias which spreads throughout all oceans, contrasting with the negative biases which
16 most of the CMIP5 models show over the North Pacific and North Atlantic Oeceans
17 (see Wang et al., 2014). However, the extreme values found in the south of Greenland
18 and in the North Pacific, where it reaches $\sim 6 \text{ }^{\circ}\text{C}$, is well within the range of biases
19 reported by other models, as NorESM1-M (Fig. 12b; Bentsen et al., 2013) or IITM-
20 ESM (Fig. 3; Swapna et al., 2018). Such warm bias does not appear in the tropical and
21 subtropical regions in the BESM-OA2.3 simulation (Fig. 5a of Nobre et al., 2013),
22 where there are cold SST biases. The spatial average biases are $1.5 \text{ }^{\circ}\text{C}$ and $0.9 \text{ }^{\circ}\text{C}$, and
23 the rmse are $1.9 \text{ }^{\circ}\text{C}$ and $2.1 \text{ }^{\circ}\text{C}$ for BESM-OA2.5 and BESM-OA2.3, respectively. A

1 notable feature of BESM-OA2.5 is its strong warm SST bias in the North Pacific and in
2 the Californian coast, and south of Greenland. The model still overestimates SSTs in the
3 major eastern coastal upwelling regions. Such a feature is a systematic error observed in
4 different state-of-the-art models, in which the causes can be related to a simulation of a
5 weaker than observed alongshore winds which leads to an underrepresentation of
6 upwelling and alongshore currents (e.g. Humboldt, California and Benguela Currents),
7 and/or the under predicted effects of shortwave radiation due to deficient simulation of
8 stratocumulus clouds over cold waters (see Richter, 2015). Nevertheless, the bias is
9 negligible over the north equatorial Pacific and in large parts of tropical western
10 Atlantic.

11 Figure 11a shows the mean SST along equatorial Pacific for BESM-OA2.5 and
12 ERSSTv4, averaged over the period 1971–2000. The equatorial region is defined over
13 the region between the latitudes 2°S and 2°N . The model simulates a warmer mean
14 SST over the western and extreme eastern parts of the equatorial Pacific Ocean. This
15 positive bias is most notable in the western part, where it is about $1.5\text{--}2^{\circ}\text{C}$ warmer than
16 observations and is warmer than the CMIP5 models (shown by the shaded grey area in
17 Figure 11a). But for the extreme eastern part of the basin, the model has a lower bias
18 compared with the CMIP5 models. For most of the central Pacific Ocean, the model has
19 a very good representation of the SST, with a RMSE of 0.14°C between 160°E and
20 120°W . The annual cycle of the equatorial Pacific SST anomalies for BESM-OA2.5
21 and ERSSTv4 are shown in figure 11b and c, respectively. BESM-OA2.5 simulates
22 reasonably well the marked annual cycle which occurs on the eastern Pacific, although
23 the negative SST anomalies between July and December are up to 1°C colder than
24 observations. The propagation of the SST anomaly patterns from the eastern to the

1 western part of the Pacific Ocean that occurs throughout the year is not well captured by
2 the model. BESM-OA2.5 shows an annual cycle in the western part of the Pacific
3 Ocean, where observations show a semiannual pattern of SST anomalies. The same
4 methodology is used for the tropical Atlantic. Figure 12a shows that in the Atlantic
5 basin there is a significant bias of ~ 3 °C in the eastern part of the basin. This bias starts
6 in the central Atlantic and it is higher than the CMIP5 models (shown by the shaded
7 grey area in Figure 12a). However, it should be noted that the CMIP5 models also have
8 a warm bias in the eastern part of the tropical Atlantic, which is a problem discussed in
9 previous studies (e.g. Richter et al., 2014 and references therein). Although this warm
10 bias, the tropical Atlantic seasonal SST variation is well simulated by BESM-OA2.5 in
11 particular on the eastern side of the basin, as it can be seen in Figures 12b and c.

12 To evaluate how the global ocean profile evolves throughout the simulation, it is
13 computed the depth-time Hovmöller diagrams of global mean ocean salinity
14 ~~temperature~~ and temperature salinity departures from their respective initial conditions
15 (Fig. 13a and 13b) for Historical simulation. Here initial conditional means the value of
16 the first year of simulation, in this case, the year 1850. The ocean salinity slightly
17 increases below 1000 m depth and from 1935 the increase reaches 0.04 PSU between
18 1500 and 3000 m depth compared with the initial values (Fig. 13a**b**). Above 1000 m
19 depth there is a significant freshening of the ocean waters, with the surface waters
20 salinity decreasing up to 0.18 PSU at the end of the simulation. Concerning ocean
21 temperature, a~~The~~ prominent warming occurs from the surface up to 400 m depth (Fig.
22 13b**a**). This warming is more significant at the end of the simulation (~ 0.6 °C comparing
23 with initial conditions) and is mostly caused by the ocean warming drift of the model.
24 Fig. 13c**b** shows the same diagram for piControl simulation (during the period in which

1 both simulations are performed in parallel), which also presents the ocean drift.
2 However, the ocean temperature anomalies above 600 m reaches ~0.6 °C in the
3 Historical simulation whereas in the piControl it reaches ~0.4 °C. This difference of 0.2
4 °C between the two simulations is likely due to the global warming of the planet and
5 consequential increasing heat flux from the atmosphere into the ocean (Fig. 13d). ~~is~~
6 ~~likely to be related to the global warming of the planet and consequential increasing~~
7 ~~heat flux from the atmosphere into the ocean.~~ In deeper waters, from 1500 m up to the
8 ocean floor, there is a weaker warming, indicating that the ocean is gaining heat mainly
9 in the upper layers (Fig. 13b). Between 500-1500 m depth, it is observed a cooling
10 tendency respective to initial conditions. ~~The ocean salinity slightly increases below~~
11 ~~1000 m depth and from 1935 the increase reaches 0.04 PSU between 1500 and 3000 m~~
12 ~~depth compared with the initial values (Fig. 13b). Above 1000 m depth there is a~~
13 ~~significant freshening of the ocean waters, with the surface waters salinity decreasing up~~
14 ~~to 0.18 PSU at the end of the simulation.~~ Such tendency can mean that the ocean is still
15 drifting from its initial conditions in the Historical simulation.

16 The meridional overturning circulation (MOC) plays an important role in
17 transporting heat from the tropics to higher latitudes of both hemispheres. This is
18 particularly important in the North Atlantic, where the Atlantic Meridional Overturning
19 Circulation (AMOC) has a profound impact on the climate of the surrounding
20 continents (see Buckley and Marshall, 2015). ~~The AMOC in the BESM-OA2.5~~
21 ~~historical experiment has the typical structure described in Lumpkin and Speer (2007),~~
22 ~~with the main layers well depicted in the appropriated depths (Figure 14a).~~ The AMOC
23 in the BESM-OA2.5 historical experiment has the typical structure described in Lumpkin and
24 Speer (2007), with the upper layer of the upper cell, which is the northward flux, depicted in the

1 appropriated depth, from the surface up to ~1000 m (Fig. 14a). However, the upper cell
2 simulated by BESM-OA2.5 is too shallow compared with the RAPID measurements (McCarthy
3 et al., 2015). The depth of the upper cell is 2500 m in the model whereas the measurements
4 show its depth at ~4500 m. This shallow upper cell of the AMOC is a common feature of state-
5 of-the-art climate models (see Menary et al., 2018). The model simulates the northward
6 Antarctic Bottom Water in the ocean floor. The annual mean maximum AMOC strength
7 simulated by BESM-OA2.5 is about 15 Sv ($1 \text{ Sv} \equiv 10^6 \text{ m}^3 \text{ s}^{-1}$) between 25 °N and 30 °N
8 at about 850 m depth (see Figure 14a). This maximum value is within the 17.2 ± 4.6 Sv
9 mean strength (with a 10 day filtered root mean square variability of 4.6 Sv) observed
10 by the project RAPID at 26.5 °N (McCarthy et al., 2015). It is also in the range of
11 maximum volume transport strength simulated by the state-of-the-art models of the
12 CMIP5 (Weaver et al., 2012; Cheng et al., 2013). Figure 14b shows the maximum
13 annual mean AMOC strength time series for the historical period at the 30 °N. For
14 comparison, Figure 14c plots the AMOC maximum volume transport strength measured
15 by the Rapid project over the period April/2004 to October/2015
16 (http://www.rapid.ac.uk/rapidmoc/rapid_data/datadl.php).

17 Averaging the maximum AMOC strength over the first and the last 30 years of
18 the time series, i.e. over the periods 1850–1879 and 1976–2005 respectively, the result
19 shows a decrease of 11.2 %, from 16.9 Sv to 15.1 Sv in each period, respectively.
20 Modeling results indicate that the AMOC has a multidecadal cycle, however the power
21 spectrum of its strength time series do not show a multidecadal oscillation (not shown).
22 The standard deviation of the detrended maximum AMOC strength time series is 1.4
23 Sv.

24 Figure 15 shows the mean sea ice concentration simulated by BESM-OA2.5 for

1 the end of the winter and the summer seasons for each hemisphere, over the period
2 1971-2000. The thick black lines represent the 15 % climatological values for the period
3 1971-2000 given by the 20CRv2 Reanalysis. The sea ice concentration in the Arctic
4 winter is overestimated in the Atlantic, specifically north of the Scandinavia (Fig. 15a).
5 However, in summer the Arctic sea ice is underestimated (Fig. 15b). In the Antarctica
6 summer the model shows a significant underestimation of the sea ice concentration (Fig.
7 15c). During the Antarctica winter the model generally overestimates the extension of
8 the sea ice concentration over all Southern Ocean (Fig. 15d). Such seasonal sea ice
9 concentration amplitude is likely related to bias radiative net over higher latitudes that
10 the model suffers, which during the winter in each hemisphere tend to generate higher
11 extension of sea ice and during the summer in each hemispheres tend to enhance the sea
12 ice melting compared with the Reanalysis.

14 **4.2 Climate Variability**

15 In this section, we evaluate the most prominent global climate variability
16 patterns. This allows us to infer the ability of the model in simulating atmospheric
17 internal and ocean-atmosphere coupled variabilities in the climate system correctly.

18 **4.2.1 Tropical Variability**

19 **4.2.1.1 El Niño-Southern Oscillation**

20 The El Niño-Southern Oscillation (ENSO) in the equatorial Pacific Ocean is one
21 of the most prominent climate variability phenomena at interannual time scales
22 (Dijkstra, 2006), with strong impacts on regions surrounding the Indian and Pacific

1 Oceans and regions that are influenced by its teleconnections (see McPhaden et al.,
2 2006 and references therein). There are many methods to evaluate the ENSO variability.
3 In the present study, it is applied the EOF to detrended monthly SST anomalies over the
4 tropical Pacific Ocean (30° S–30° N; 240°–70° W) for the period 1950–2005 for both
5 BESM-OA2.5 simulations and ERSSTv4 data. Figures 15a and b show the leading EOF
6 patterns associated with the El Niño/La Niña variability. The model simulates the El
7 Niño/La Niña variability deficiently, with lower amplitude of SST variability and the
8 center of maxima variability confined to the eastward part of the basin. The model's
9 leading EOF explains 17.9 % of the total variance, substantially less than the 45 %
10 explained by observations. The lower amplitude of the simulated El Niño/La Niña can
11 be verified in the power spectrum of the leading Principal Component (PC) shown in
12 Figure 165. Even though the simulation shows two significant peaks between 2–4 years
13 cycle (Fig. 165c), which is within the range of the period cycle given by the leading PC
14 of observations (3–7 years cycle; figure 165d), the amplitude of the simulated variance
15 is lower than that of observations.

16 Figure 176 shows the spatial correlation between detrended monthly anomalies
17 of the Niño-3 index (defined inside the black rectangle area, bounded by 5° S–5° N,
18 90°–150° W) and detrended monthly anomalies of global SST computed for BESM-
19 OA2.5 and ERSSTv4 over the period 1900–2005. The model has not a strong
20 correlation at grid points inside the Niño-3 area, which is a signal that the El Niño/La
21 Niña spatial pattern is weakly simulated. The horseshoe pattern of negative correlation
22 observed in the Pacific Ocean is also weakly simulated by the model, particularly in
23 the westward equatorial part. The positive correlation of observed SST over the Indian

Ocean and Niño-3 index is absent in the model's simulation. It is worth mentioning that the model simulates the observed correlation pattern of SST anomalies over the Atlantic Ocean with Niño-3 index, although it is not so robust (Figure 176).

4.2.1.2 Atlantic Meridional Mode

The leading modes of coupled ocean-atmosphere variability over the Tropical Atlantic Ocean are the zonal mode, also referred as equatorial mode (Zebiak, 1993; Lutz et al., 2015), and the meridional mode, also referred as the interhemispheric mode (Nobre and Shukla, 1996). The first is an ENSO-like phenomenon that emerges in the Gulf of Guinea mainly in the boreal summer and has a strong impact on West African precipitation (Zebiak, 1993; Lutz et al., 2015). The second is characterized by a cross-equatorial SST gradient associated with a meridional wind stress toward the warmer SST anomalies. The maxima amplitude of the meridional mode occurs during the boreal spring, influencing the precipitation in Northeast Brazil and West Africa (Nobre and Shukla, 1996; Chang et al., 1997; Chiang and Vimont, 2004). The Atlantic Meridional Mode (AMM) has an interannual and decadal temporal scale of variability and is a result of a thermodynamic coupling between the wind speed, the sea surface evaporation induced by the wind stress, and the SST, mechanism known as Wind-Evaporation-SST feedback (WES feedback, Xie and Philander, 1994; Chang et al., 1997; Xie, 1999). To evaluate the AMM simulations, a joint EOF of SST and wind stress (Taux and Tauy) fields analysis is computed, as such a variability is the response of a coupled ocean-atmospheric system. Figure 187 shows the AMM simulated by BESM-OA2.5, and obtained by observed data. The AMM pattern simulated by the model is similar to obtained from observations, regardless of the weaker gradient pole at

1 the South Atlantic. Nevertheless, the explained variance by the model is very close to
2 the observed one, being respectively, 10.7 % and 11.8 %. The patterns shown in Figure
3 | 187 are defined as a positive phase of the AMM, with the inter-hemisphere cross-
4 equatorial wind from south to north, and with corresponding negative SST anomalies
5 over the southern pole and positive SST anomalies over the northern pole (the negative
6 phase of AMM is the reverse pattern). Over the second half of the 20th century, the
7 | AMM shows a predominant decadal periodicity of 11–13 years. Figures 187c and d
8 show the power spectrum of the PC of the AMM patterns simulated by the model and
9 from the observation, respectively. It is possible to see that the pattern simulated by
10 BESM-OA2.5 shows, similarly to the observed one, a predominant periodicity at
11 decadal timescales.

12 **4.2.1.3 South Atlantic Convergence Zone**

13 The South Atlantic Convergence Zone (SACZ) is characterized by an intense
14 NW-SE oriented cloud band that extends from the Amazon Basin to the South Atlantic
15 subtropics, mainly during austral summer (Nogués-Paegle and Mo, 1997; Carvalho et
16 al., 2004; de Oliveira Vieira et al., 2013). The formation of the SACZ has a strong
17 influence on the precipitation over southeast South America and is considered, together
18 with the convection activity over the Amazon Basin, the main component of the South
19 American Monsoon System (Jones and Carvalho, 2002). The southern part of the SACZ
20 usually lies over cooler SST (Grimm, 2003; Robertson and Mechoso, 2000). Chaves
21 and Nobre (2004) suggests that the formation of SACZ over the ocean tend to block the
22 solar radiation by clouds, cooling the SST beneath. AGCM are not able to simulate the
23 precipitation over cooler SST caused by SACZ (Marengo et al., 2003; Nobre et al.,

2006; Nobre et al., 2012), since such models tend to increase the precipitation over warmer SST, as an hydrostatic response. Nobre et al. (2012) has shown that coupled AOGCMs are able to simulate the SACZ formation over colder SST anomalies, as this class of models englobes the atmosphere-ocean surface thermodynamic coupling. Following Nobre et al. (2012), a correlation between seasonal precipitation and SST anomalies for the austral summer (DJF) over the tropical South Atlantic (40° S–10° N; 70° W–20° E) over the period 1979–2010 for observations and for the period 1971–2002 for the model, so 32 years are used. Figure 198 shows the rainfall-SST anomaly correlation maps for both BESM-OA2.5 and observations. BESM-OA2.5 are able to simulate an inverse correlation between precipitation and SST in the southeast of Brazil (near 20 °S), suggesting the capacity of simulating precipitation over cooler SST, a feature related to the formation of SACZ (that tends to cooler the SST). Its noteworthy in Figure 196 that BESM-OA2.5 is capable to generate both positive and negative SSTA-rainfall correlations over the equatorial Atlantic (positive, thermally direct driven circulation over the equatorial region and negative, thermally indirect driven atmospheric circulation over the SW tropical Atlantic, Figure 198a), a feature also present in the observation correlation map of Figure 198b.

4.2.1.4 Madden-Julian Oscillation

The Madden-Julian Oscillation (MJO) is the prominent intraseasonal variability (30-90 days) over the eastern Indian and western Pacific tropical regions and consists on events of deep convection coupled to atmospheric circulation that packed propagate together through the equatorial region eastward (Madden and Julian, 1971, Madden and Julian, 1972; Zhang, 2005). The influence of MJO events with large-scale phenomena

1 has been reported, as in the case of the evolution of ENSO (e.g. Takayabu et al., 1999),
2 formation of tropical cyclones (e.g. Liebmann et al., 1994) or in the North Atlantic
3 Oscillation (e.g. Lin et al., 2009). To evaluate the MJO simulated by the model it is
4 performed the wavenumber-frequency power spectrum analysis for tropical (10°S–10°
5 N) averaged daily outgoing long-wave radiation (OLR) and daily zonal wind
6 component at 850 hPa pressure level (U850), for the boreal winter (Nov–Apr) over the
7 period 1971–2000. To compute and plot the wavenumber-frequency power spectrum it
8 is used the MJO Simulation Diagnostic package (details in Waliser et al., 2009).

9 | Fig. 2019a and Fig. 2019b show the wavenumber-frequency power spectrum for
10 | OLR for BESM-OA2.5 and 20CRv2, respectively. Although BESM-OA2.5 presents an
11 | eastward propagating disturbance with wavenumber 1, it is characterized by lower
12 | frequency (> 80 days) compared to the maxima peak within 30–80 days frequency band
13 | shown by the 20CRv2, despite it spreads over lower frequencies than 80 days. This
14 | observed peak has more energy for wavenumber 2. A westward propagating disturbance
15 | (negative frequencies) with weaker energy than the eastward propagating counterpart
16 | appears in 20CRv2, with a peak for wavenumber 2. Similarly, BESM-OA2.5 also
17 | shows a westward propagating disturbance with weaker energy for wavenumber 1–3.
18 | The wavenumber-frequency power spectrum for U850 in 20CRv2 shows an eastward
19 | propagating disturbance which peaks at the 30–80 days frequency band with
20 | wavenumber 1 (Fig. 2019d). In the case of BESM-OA2.5 there is an eastward
21 | propagation with a periodicity slightly higher than 80 days for wavenumber 1 but this
22 | disturbance spreads over different frequencies out of the 30–80 days frequency band
23 | (Fig. 2019c). It also presents a westward propagating disturbance that is absent in the
24 | Reanalysis. BESM-OA2.5 poorly simulates the MJO and underestimates its amplitude.

1 However, MJO has been highlighted as a phenomenon that climate models struggle to
2 simulate in a proper way, especially by underestimate OLR and representing a coherent
3 eastward propagation (Kim et al., 2009; Ahn et al., 2017).

4 **4.2.2 Extratropical Variability**

5 **4.2.2.1 North Atlantic Oscillation**

6 The North Atlantic Oscillation (NAO) is a major atmospheric variability pattern
7 occurring in the North Atlantic, which is characterized by the oscillation of the
8 difference on the sea level pressure (SLP) between Iceland and Portugal (Wanner et al.,
9 2001; Hurrell et al., 2003). NAO has a great impact in the Euro-Atlantic region (Hurrell
10 et al., 2003; Hurrell and Deser, 2009), with the notable work of Namias (1972) relating
11 droughts over the Northeast Brazil to NAO variations. Recent studies also show its
12 teleconnections to the East Asia (e.g. Yu and Zhou, 2004; Wu et al., 2012). The NAO's
13 influence on a rapid climate change in the Northern Hemisphere has been highlighted in
14 (Delworth et al., 2016), which increases the importance of its correct simulation. Since
15 NAO's largest amplitude of variation occurs mainly during the boreal winter, the
16 analysis here is centered on this season. The period used to perform the analyses is
17 1950–2005. The leading EOF of the SLP averaged for boreal winter season (DJF) in the
18 Euro-Atlantic region shows that the NAO is well simulated by BESM-OA2.5 (Fig.
19 | 210a), simulating the NAO dipole centers and their amplitudes very similar to the
20 | observed pattern (Fig. 210b). The variances explained by the leading EOF are also
21 | similar, 50.2 % and 44 % for BESM-OA2.5 and Reanalysis, respectively. The spectral
22 | analysis of the leading PCs shows that BESM-OA2.5 captures the ~2.5 years cycle on
23 | the time variability but fails to capture the ~8 years cycle (Fig. 210c and 21d). It is

1 interesting to note that BESM-OA2.5 simulates a NAO spatial pattern, without
2 capturing its low-frequency variability. By analyzing the NAO variability, we consider
3 that it is not necessary to analyze the Northern Annular Mode (NAM), since both are
4 manifestation of same mode of variability (Hurrell and Deser, 2009).

5 **4.2.1.2 Pacific-North America Pattern**

6 Jointly, the NAO and the Pacific-North American pattern (PNA) are the
7 dominant atmospheric internal modes over the boreal hemisphere. The PNA is
8 characterized by four centers of high pressure anomalies in the North Pacific and North
9 America, respectively; over Hawaii, to the south of the Aleutian Islands, in the
10 intermountain region of North America, and in the Gulf Coast region of the U.S.A.,
11 representing the centers of action of a stationary wave train extending from the tropical
12 Pacific into North America (Wallace and Gutzler, 1981). It exerts a significant influence
13 on surface temperature and precipitation over North America (Leathers et al., 1991).
14 Some studies have shown that, although the PNA is an internal atmospheric variability
15 phenomena, it is influenced by other climate variabilities, as the ENSO and the Pacific
16 Decadal Oscillation (PDO) (see Straus and Shukla, 2002; Yu and Zwiers, 2007).

17 Similar to NAO, the PNA has its largest variation of amplitude during the boreal
18 winter; therefore, the present analysis is performed for this season. Following Wallace
19 and Gutzler (1981), we construct one-point correlation maps for BESM-OA2.5 and
20 20CRv2 Reanalysis in order to evaluate the capacity of the model to reproduce the PNA
21 pattern. The one-point correlation maps correlate 500 hPa geopotential height at the
22 reference point (45 °N, 165 °W) with all the other grid points of the map domain (0°–80°
23 N; 240°–70° W). The time series used to perform the correlations are averaged boreal

1 winter seasonal (DJF) dataset over the period 1950–2005. The time series are departed
2 from their long-term mean and normalized at each grid point prior the correlation
3 computation. Figure 22+ shows the one-point correlation maps for BESM-OA2.5 (Fig.
4 22+a) and 20CRv2 (Fig. 2+b). In this figure, it is possible to check the four centers of
5 action simulated by the model, which shows a stronger correlation between the four
6 high pressure centers when compared with reanalysis correlation maps in Figure 22+b.

7 **4.2.1.2 Pacific-South America Patterns**

8 The second and third EOF of 500 hPa geopotential height over the Southern
9 Hemisphere (20°–90° S) present a notable resemblance to the Pacific-South America
10 (PSA) teleconnection pattern (Mo and Peagle, 2001). PSA patterns are stationary
11 Rossby wave trains extending from central Pacific to Argentina, in which the PSA1
12 (EOF2) is a response to ENSO and the PSA2 (EOF3) is associated to the quasi-biennial
13 component of ENSO (Karoly, 1989; Mo and Peagle, 2001). These patterns have a
14 significant impact on rainfall anomalies over South America (Mo and Peagle, 2001).
15 Figure 23+ shows the PSA patterns both simulated by BESM-OA2.5 and from
16 Reanalysis. As the explained variance of EOF2 and EOF3 are close, the EOFs seem to
17 degenerate for both Reanalysis and model simulation. In order to relax the orthogonality
18 constraint, it is performed a rotated EOF (REOF) retaining the first 10 modes. The
19 REOF2 and REOF3 resemble the EOF2 and EOF3 respectively, implying that they are
20 independent modes. The PSA pattern is well simulated by BESM-OA2.5, although the
21 model changes the order of the EOF patterns. BESM-OA2.5 shows an anomaly south of
22 South Africa (Fig. 23+c) that does not appear in the Reanalysis (Fig. 23+b). PSA
23 patterns have significant interannual and decadal variabilities (Zhang et al., 2016). PSA

1 patterns simulated by BESM-OA2.5 have only significant variability in the interannual
2 scale, with absent decadal variability (figure not shown).

3 **4.2.1.4 Southern Annular Mode**

4 The Southern Annular Mode (SAM) is the dominant atmospheric variability in
5 the Southern Hemisphere, occurring in the extra-tropics and in the high latitudes
6 (Kidson,1988). It is also referred to as Antarctic Oscillation (AAO; Gong and Wang,
7 1999). SAM variability is characterized by anomalies variation in the polar low-
8 pressure and in the surrounded zonally high-pressure belt. It can be captured through the
9 first EOF applied to different atmospheric variables, as the sea level pressure, different
10 geopotential height levels or the surface air temperature (Kidson, 1988; Rogers and van
11 Loon, 1982; Thompson and Wallace, 2000). To evaluate the capacity of BESM-OA2.5
12 to simulate this atmospheric mode of variability, EOF analysis is applied to the monthly
13 mean 500 hPa geopotential height field from 20 °S to 90 °S, over the period 1950–2005,
14 for both model and Reanalysis. The SAM pattern simulated by BESM-OA2.5 resembles
15 very well the observed pattern, with the mid-latitude 500 hPa geopotential height
16 variation centers depicted in the same longitudes as observations, but with differences in
17 the amplitude values (Fig. 243). However, the explained variance is higher compared
18 with observation. The explained variances of BESM-OA2.5 and 20CRv2 are 34.1 %
19 and 21.0 %, respectively. The SAM is a quasi-decadal mode of variability (see Yuan
20 and Yonekura, 2011), however the BESM-OA2.5 power spectrum reveals a SAM with
21 a markedly interannual variability, without the peak between 8 and 16 years as obtained
22 in the Reanalysis (figure not shown).

23

1 **4.2.1.5 Pacific Decadal Oscillation**

2 Observed SST anomalies over the North Pacific have shown an oscillatory
3 pattern in the central and western parts in relation to the tropical part and along the
4 North American west coast. This oscillatory shift of SST anomalies with interdecadal
5 periodicity was termed Pacific Decadal Oscillation (PDO) and it is defined as the
6 leading EOF of the monthly SST anomalies over North Pacific (Mantua et al., 1997).
7 The positive phase of PDO is defined when negative SST anomalies predominate over
8 the central and western parts of North Pacific, and positive SST anomalies predominate
9 over the Tropical Pacific and along the North American west coast; being the negative
10 phase the reverse pattern. Many studies have connected the PDO with variations on
11 precipitation regimes in different regions around the world, as South China monsoon
12 (e.g. Wu and Mao, 2016), Indian monsoon (e.g. Krishnamurthy and Krishnamurthy,
13 2016) and together with ENSO in the precipitation regime in North America (see Hu
14 and Huang, 2009). There are different mechanisms that modulate PDO, in which one of
15 them is the response of the Northern Pacific SST to the ENSO variability via the
16 “atmospheric bridge” (for a detailed review, see Newman et al., 2016).

17 Following the definition (Mantua et al., 1997), the spatial pattern of PDO is
18 obtained by regressing the SST anomalies onto the leading normalized PC time series,
19 shown in Figure 24 which in this case is showing the positive phase of the PDO. The
20 EOF is applied to monthly SST anomalies over North Pacific (20°–60° N; 240°–110°
21 W) over the period 1900–2005. BESM-OA2.5 is not capable of reproducing this pattern
22 | by the leading EOF. The PDO pattern only appears on the second EOF (Fig. 254a), with
23 the explained variance of 14.0 % against 20.5 % of observations. Although the EOF2

1 resembles the PDO mode, the tropical part has a weaker variation than the observation.
2 The reason of incapacity of the model in reproducing the PDO as the leading mode of
3 variability is probably due to the model's simulation of weaker ENSO variability, both
4 in spatial and temporal scales. These deficiencies may impact the mechanisms that
5 reproduce the PDO, mainly via the "atmospheric bridge" as referred earlier. Figures
6 | [265a](#) and [26b](#) show the normalized PC2 and PC1 time series of BESM-OA2.5 and
7 | ERSSTv4, respectively. It is possible to note that both time series present a
8 | multidecadal periodicity, but in different time scales as it is confirmed by the power
9 | spectrum (Fig. [265c](#) and [26d](#)). The power spectrum shows that both time series present
10 | interannual periodicity (~5-6 years), with BESM-OA2.5 multidecadal variability
11 | strongest spectrum around 15 years, a higher frequency compared with observation (~22
12 | and ~40-45 years).

13 **5. Summary**

14 The capacity of Earth System Models to project a future climate under the
15 conditions given by future scenarios of atmospheric greenhouse gas concentrations can
16 be assessed by how accurate these models are able to reproduce observed climate
17 features. Therefore, the evaluation of how these models perform for the historical period
18 when there are observations to compare with model's calculations represents a key part
19 of the Earth System modelling. In this study, BESM-OA2.5 historical simulation is
20 evaluated for the period 1850–2005 following the CMIP5 protocol (Taylor et al., 2012)
21 with focus on simulations of its mean climate and key large-scale modes of climate
22 variability.

1 BESM-OA2.5 is an updated version of BESM-OA2.3 (Nobre et al. 2013;
2 Giarolla et al. 2015) regarding the atmospheric model, which consists in the new
3 Brazilian Global Atmospheric Model (BAM; Figueroa et al., 2016). This new version
4 allowed to alleviate a mean global bias of energy balance at the top of the atmosphere of
5 -20 W m^{-2} to -4 W m^{-2} . Moreover, systematic errors were reduced in wind, humidity and
6 temperature in the surface layer over oceanic regions by the inclusion formulations
7 presented by Jiménez et al. (2012).

8 The analysis of the mean climate shows that the model is able to simulate the
9 general mean climate state. Nevertheless, some significant biases appear at the
10 simulation, as a double ITCZ over the Pacific and Atlantic Oceans, some notable
11 regional biases in the precipitation field (e.g., over the Amazon and Indian regions) and
12 in the SST field (e.g., south of Greenland). Yet, the model has shown an improvement
13 in simulating the ITCZ and a reduction in the global precipitation RMSE compared with
14 BESM-OA version 2.3. BESM-OA2.5 shows an almost globally positive SST bias,
15 which did not occur in version 2.3, however the SST RMSE was slightly reduced in the
16 newer version of the model.

17 The most relevant climate patterns on interannual to decadal time scales
18 simulated by BESM-OA2.5 are compared with the ones obtained from observations and
19 Reanalysis. Over the Pacific, the ENSO is simulated with lower amplitude of variability
20 than the observations and such weak ENSO seems to impact other Pacific variability
21 patterns such as the PDO. Conversely, the major phenomena on the Atlantic basin are
22 well represented in BESM-OA2.5 simulations. This is the case for the Tropical Atlantic
23 mode of interhemispheric variability (AMM) that is very well simulated by the model in

1 term of the spatial pattern and temporal variability. It is worth to note that this mode is
2 considered poorly simulated by the models used in the Intergovernmental Panel on
3 Climate Change (IPCC) fifth assessment report (AR5) (Flato et al., 2013). It is also
4 relevant to highlight BESM-OA2.5 ability to represent the enhanced rainfall over cooler
5 waters over the SW Tropical Atlantic, associated with the South Atlantic Convergence
6 Zone (SACZ). The capacity of the model in simulating the AMM and SACZ is an
7 important result since one of the main aims is the representation of modes that directly
8 impacts the precipitation over South America. The AMOC reproduced by BESM-
9 OA2.5 has the meridional overturning structure comparable with the ensemble AMOC
10 simulated by the CMIP5's models. BESM's maximum AMOC strength average value is
11 slighter lower than the average value that has been observed by the project RAPID, but
12 well within the range of mean square root variability that is observed. Although the
13 averaged maximum strength AMOC simulated by the CMIP5 models is within the
14 mean range square root variability that is observed, most models tend to simulate strong
15 AMOC, with a maximum strength above 20 Sv, and out of the range (Zhang and Wang,
16 2013). The NAO atmospheric variability, which is well simulated by the CMIP5 models
17 (Ning and Bradley, 2016) is also very well simulated by BESM-OA2.5. In the extra-
18 tropics, BESM-OA2.5 is capable to reproduce fairly well majors variabilities in both
19 Hemispheres, as the PNA, PSA, and the SAM teleconnections patterns, comparable to
20 CMIP5 models that reproduce the PNA (Ning and Bradley, 2016) and the SAM (Zheng
21 et al. 2013).

22 Similarly to Nobre et al. (2013), this study aims to evaluate the BESM-OA2.5
23 by comparing the most important features of the climate system simulated by the model

1 with observations and Reanalysis. The next version of the model (BESM-OA2.8) is
2 already under development. In this new version, the MOM4p1 ocean model has been
3 replaced by the MOM5. Regarding the atmospheric model, new developments have
4 been carried out to improve BAM's capacity, being the most important the inclusion of
5 a scheme of humidity in the planetary boundary layer, a new dynamic core and new
6 cloud cover scheme (Figuroa et al., 2016). This new version of BESM carries the
7 challenges of improving the simulation of the precipitation, in particular to alleviate the
8 deficit over the Amazon. The ENSO is the large-scale phenomenon that will receive a
9 scrutiny in order to understand the reasons for a weak variability. The other feature of
10 the model is the weaker warming under the CO₂ equivalent only forcing, relative to
11 other CMIP5 that do not consider the direct and indirect effects of atmospheric aerosols.
12 Assuming that BESM-OA2.5 should respond consistently with CMIP5 models, it would
13 underestimate the warming observed in the last decades. However, models can respond
14 in different ways to external forcing, therefore, in the near future, the aim is to carry out
15 a numerical experiment in which the model is forced with observed estimate of aerosol
16 concentration (as read-in field) in order to address to what extension BESM is impacted.
17 In the future, a study comparing the versions 2.5 and 2.8 of the BESM-OA is aimed in
18 order to fully report the advances of the modeling work developed in the last couple
19 years. Such a study will give a broader perspective of the technical challenges overcome
20 throughout this project and assess the improvements achieved in each version of the
21 model in simulating the climate system.

22

23

1 **Code and data availability**

2 The BESM-OA2.5 source code is freely available after signature of a license agreement.

3 Please contact Paulo Nobre to obtain the source code and data of BESM-OA2.5.

4

5 **Competing interests**

6 There are no competing interests of which the authors are aware.

7

8 **Acknowledgements**

9 This research was partially funded by FAPESP (2009/50528-6), FAPESP (2008/57719-
10 9) and by the National Institute of S&T for Climate Change (CNPq ~~573797/2008-0~~).
11 SFV is supported by a Ph.D. grant funded by CAPES. [MBJ is supported by a grant](#)
12 [funded by FAPESP \(2018/06204-0\)](#). The authors would like to acknowledge Rede
13 CLIMA, FAPESP and INPE for the use of its supercomputer facility, which made this
14 work possible. Twentieth Century Reanalysis Project data sets (20CRv2) are provided
15 by the U.S. Department of Energy, Office of Science Innovative and Novel
16 Computational Impact on Theory and Experiment (DOE INCITE) program, and Office
17 of Biological and Environmental Research (BER), and by the National Oceanic and
18 Atmospheric Administration Climate Program Office. The GPCP combined
19 precipitation data sets were developed and computed by the NASA/Goddard Space
20 Flight Center's Mesoscale Atmospheric Processes Laboratory. The HadCRUT4 data

1 sets are provided by the Met Office Hadley Centre and the University of East
2 Anglia/Climatic Research Unit. The ISCCP D2 data sets are provided through the
3 International Satellite Cloud Climatology Project, maintained by the ISCCP research
4 group at the NASA/Goddard Institute for Space Studies. The Extended Reconstructed
5 Sea Surface Temperature (ERSSTv4) is provided by the NOAA/OAR/ESRL/PSD. Data
6 from the RAPID-WATCH MOC monitoring project are funded by the Natural
7 Environment Research Council. The authors acknowledge the World Climate Research
8 Programme's Working Group on Coupled Modelling, which is responsible for CMIP,
9 and we thank the climate modeling groups (listed in Table 1 of this paper) for producing
10 and making available their model output. For CMIP the U.S. Department of Energy's
11 Program for Climate Model Diagnosis and Intercomparison provides coordinating
12 support and led development of software infrastructure in partnership with the Global
13 Organization for Earth System Science Portals. This work is part of the Ph.D. thesis of
14 SFV under the guidance of CN and PN.

15

1 **References**

- 2 Adler, R. F., Huffman, G. J., Chang, A., Ferraro, R., Xie, P.-P., Janowiak, J., Rudolf, B.,
3 Schneider, U., Curtis, S., Bolvin, D., Gruber, A., Susskind, J., Arkin, P. and
4 Nelkin, E.: The Version-2 Global Precipitation Climatology Project (GPCP)
5 Monthly Precipitation Analysis (1979–Present), *J. Hydrometeorol.*, 4(6), 1147–
6 1167, doi:10.1175/1525-7541(2003)004<1147:TVGPCP>2.0.CO;2, 2003.
- 7 Anthes, R. A.: A Cumulus Parameterization Scheme Utilizing a One-Dimensional
8 Cloud Model, *Mon. Weather Rev.*, 105(3), 270–286, doi:10.1175/1520-
9 0493(1977)105<0270:ACPSUA>2.0.CO;2, 1977.
- 10 Ahn, M. S., Kim, D., Sperber, K. R., Kang, I. S., Maloney, E., Waliser, D. and Hendon,
11 H.: MJO simulation in CMIP5 climate models: MJO skill metrics and process-
12 oriented diagnosis, *Clim. Dyn.*, 49(11–12), 4023–4045, doi:10.1007/s00382-
13 017-3558-4, 2017.
- 14 Arakawa, A. and Schubert, W. H.: Interaction of a Cumulus Cloud Ensemble with the
15 Large-Scale Environment, Part I, *J. Atmos. Sci.*, 31(3), 674–701,
16 doi:10.1175/1520-0469(1974)031<0674:IOACCE>2.0.CO;2, 1974.
- 17 Bentsen, M., Bethke, I., Debernard, J. B., Iversen, T., Kirkevåg, A., Seland, Ø., Drange,
18 H., Roelandt, C., Seierstad, I. A., Hoose, C. and Kristjánsson, J. E.: The
19 Norwegian Earth System Model, NorESM1-M – Part 1: Description and basic
20 evaluation of the physical climate, *Geosci. Model Dev.*, 6(3), 687–720,
21 doi:10.5194/gmd-6-687-2013, 2013.
- 22 Bottino, M. J., and Nobre, P.: Impacts of cloud cover schemes on the Atlantic climate in
23 the Brazilian Earth System Model – BESM-OA2.3. (Submitted to *Climate*
24 *Dynamics*).
- 25 Buckley, M. W. and Marshall, J.: Observations, inferences, and mechanisms of the
26 Atlantic Meridional Overturning Circulation: A review, *Rev. Geophys.*, 54, 5–
27 63, doi:10.1002/2015RG000493.Received, 2015.

- 1 Cao, J., Wang, B., Yang, Y.-M., Ma, L., Li, J., Sun, B., Bao, Y., He, J., Zhou, X. and
2 Wu, L.: The NUIST Earth System Model (NESM) version3: description and
3 preliminary evaluation, *Geosci. Model Dev.*, 11(7), 2975–2993,
4 doi:10.5194/gmd-11-2975-2018, 2018.
- 5
- 6 Capistrano, V. B., Nobre, P., Tedeschi, R., Silva, J., Bottino, M., da Silva Jr., M. B.,
7 Menezes Neto, O. L., Figueroa, S. N., Bonatti, J. P., Kubota, P. Y., Reyes
8 Fernandez, J. P., Giarolla, E., Vial, J., and Nobre, C. A.: Overview of climate
9 change in the BESM-OA2.5 climate model, *Geosci. Model Dev. Discuss.*,
10 <https://doi.org/10.5194/gmd-2018-209>, in review, 2018.
- 11 Carvalho, L. M. V, Jones, C. and Liebmann, B.: The South Atlantic convergence zone:
12 Intensity, form, persistence, and relationships with intraseasonal to interannual
13 activity and extreme rainfall, *J. Clim.*, 17(1), 88–108, doi:10.1175/1520-
14 0442(2004)017<0088:TSACZI>2.0.CO;2, 2004.
- 15 Chang, P., Ki, L. and Li, H.: A decadal climate variation in the tropical Atlantic Ocean
16 from thermodynamic air-sea interactions, *Nature*, 385(6), 516–518,
17 1997.
- 18 Charlton-Perez, A. J., Baldwin, M. P., Birner, T., Black, R. X., Butler, A. H., Calvo, N.,
19 Davis, N. A., Gerber, E. P., Gillett, N., Hardiman, S., Kim, J., Krüger, K., Lee,
20 Y. Y., Manzini, E., McDaniel, B. A., Polvani, L., Reichler, T., Shaw, T. A.,
21 Sigmond, M., Son, S. W., Toohey, M., Wilcox, L., Yoden, S., Christiansen, B.,
22 Lott, F., Shindell, D., Yukimoto, S. and Watanabe, S.: On the lack of
23 stratospheric dynamical variability in low-top versions of the CMIP5 models, *J.*
24 *Geophys. Res. Atmos.*, 118(6), 2494–2505, doi:10.1002/jgrd.50125, 2013.
- 25 Chaves, R. R. and Nobre, P.: Interactions between sea surface temperature over the
26 South Atlantic Ocean and the South Atlantic Convergence Zone, *Geophys. Res.*
27 *Lett.*, 31(3), 1–4, doi:10.1029/2003GL018647, 2004.

28

- 1 Cheng, W., Chiang, J. C. H. and Zhang, D.: Atlantic meridional overturning circulation
2 (AMOC) in CMIP5 Models: RCP and historical simulations, *J. Clim.*, 26(18),
3 7187–7197, doi:10.1175/JCLI-D-12-00496.1, 2013.
- 4 Chiang, J. C. H. and Vimont, D. J.: Analogous Pacific and Atlantic Meridional Modes
5 of Tropical Atmosphere – Ocean Variability, *J. Clim.*, 17, 4143–4158,
6 doi:10.1175/JCLI4953.1, 2004.
- 7 Chou, M.-D. and Suarez, M. J.: A solar radiation parameterization (CLIRAD-SW) for
8 atmospheric studies. NASA Tech. Memo NASA/TM-1999-104606, 40 pp.,
9 1999.
- 10 Chou, S. C., Lyra, A., Mourão, C., Dereczynski, C., Pilotto, I., Gomes, J., Bustamante,
11 J., Tavares, P., Silva, A., Rodrigues, D., Campos, D., Chagas, D., Sueiro, G.,
12 Siqueira, G., Nobre, P. and Marengo, J.: Evaluation of the Eta Simulations
13 Nested in Three Global Climate Models, *Am. J. Clim. Chang.*, 3(5), 438–454,
14 doi:10.4236/ajcc.2014.35039, 2014.
- 15 Compo, G. P., Whitaker, J. S., Sardeshmukh, P. D., Matsui, N., Allan, R. J., Yin, X.,
16 Gleason, B. E., Vose, R. S., Rutledge, G., Bessemoulin, P., BroNnimann, S.,
17 Brunet, M., Crouthamel, R. I., Grant, A. N., Groisman, P. Y., Jones, P. D., Kruk,
18 M. C., Kruger, A. C., Marshall, G. J., Maugeri, M., Mok, H. Y., Nordli, O.,
19 Ross, T. F., Trigo, R. M., Wang, X. L., Woodruff, S. D. and Worley, S. J.: The
20 Twentieth Century Reanalysis Project, *Q. J. R. Meteorol. Soc.*, 137(654), 1–28,
21 doi:10.1002/qj.776, 2011.
- 22 Delworth, T. L. and Mann, M. E.: Observed and simulated multidecadal variability in
23 the Northern Hemisphere, *Clim. Dyn.*, 16(9), 661–676,
24 doi:10.1007/s003820000075, 2000.
- 25 Delworth, T. L., Zeng, F., Vecchi, G. A., Yang, X., Zhang, L. and Zhang, R.: The North
26 Atlantic Oscillation as a driver of rapid climate change in the Northern
27 Hemisphere, *Nat. Geosci.*, 9(7), 509–512, doi:10.1038/ngeo2738, 2016.

- 1 Dijkstra, H. A.: The ENSO phenomenon: theory and mechanisms, *Adv. Geosci.*, 6, 3–
2 15, doi:10.5194/adgeo-6-3-2006, 2006.
- 3 Enfield, D. B., Mestas-Nuñez, A. M. and Trimble, P. J.: The Atlantic multidecadal
4 oscillation and its relation to rainfall and river flows in the continental U.S.,
5 *Geophys. Res. Lett.*, 28(10), 2077–2080, doi:10.1029/2000GL012745, 2001.
- 6 Ferrier, B. S., Jin, Y., Lin, Y., Black, T., Rogers, E. and DiMego, G.: Implementation of
7 a 527 new grid-scale cloud and precipitation scheme in the NCEP Eta model.
8 *Amer. Meteor. Soc.*, 280–283, 2002.
- 9 Figueroa, S. N., Bonatti, J. P., Kubota, P. Y., Grell, G. A., Morrison, H., Barros, S. R.
10 M., Fernandez, J. P. R., Ramirez, E., Capistrano, V. B., Alvim, D. S., Enor é D.
11 P., Diniz, F. L. R., Barbosa, H. M. J., Mendes, C. L. and Panetta, J.: The
12 Brazilian Global Atmospheric Model (BAM): Performance for Tropical Rainfall
13 Forecasting and Sensitivity to Convective Scheme and Horizontal Resolution,
14 *Weather Forecast.*, 31(5), 1547–1572, doi:10.1175/WAF-D-16-0062.1, 2016.
- 15 Flato, G. M.: Earth system models: An overview, *Wiley Interdiscip. Rev. Clim. Chang.*,
16 2(6), 783–800, doi:10.1002/wcc.148, 2011.
- 17 Flato, G., J. Marotzke, B. Abiodun, P. Braconnot, S.C. Chou, W. Collins, P. Cox, F.
18 Driouech, S. Emori, V. Eyring, C. Forest, P. Gleckler, E. Guilyardi, C. Jakob, V.
19 Kattsov, C. Reason and M. Rummukainen, 2013: Evaluation of Climate Models.
20 In: *Climate Change 2013: The Physical Science Basis. Contribution of Working*
21 *Group I to the Fifth Assessment Report of the Intergovernmental Panel on*
22 *Climate Change* [Stocker, T.F., D. Qin, G.-K. Plattner, M. Tignor, S.K. Allen, J.
23 Boschung, A. Nauels, Y. Xia, V. Bex and P.M. Midgley (eds.)]. Cambridge
24 University Press, Cambridge, United Kingdom and New York, NY, USA.
- 25 Gent, P. R., Danabasoglu, G., Donner, L. J., Holland, M. M., Hunke, E. C., Jayne, S. R.,
26 Lawrence, D. M., Neale, R. B., Rasch, P. J., Vertenstein, M., Worley, P. H.,
27 Yang, Z.-L., Zhang, M.: The Community Climate System Model Version 4, *J.*
28 *Clim.*, 24(19), 4973–4991, doi:10.1175/2011JCLI4083.1, 2011.

- 1 Giarolla, E., Siqueira, L. S. P., Bottino, M. J., Malagutti, M., Capistrano, V. B. and
2 Nobre, P.: Equatorial Atlantic Ocean dynamics in a coupled ocean atmosphere
3 model simulation, *Ocean Dyn.*, 65(6), 831–843, doi:10.1007/s10236-015-0836-
4 8, 2015.
- 5 Gong, D. and Wang, S.: Definition of Antarctic Oscillation Index, *Geophys. Res. Lett.*,
6 26(4), 459–462, doi:10.1029/1999GL900003, 1999. Grell, G. and Dévényi, D.
7 A.: A generalized approach to parameterizing convection combining ensemble
8 and data assimilation techniques, *Geophys. Res. Lett.*, 29(14), 10–13,
9 doi:10.1029/2002GL015311, 2002.
- 10 Griffies, S. M.: Elements of MOM4p1. NOAA/Geophysical Fluid Dynamics Laboratory
11 Ocean Group Tech. Rep. 6, 444 pp., 2009.
- 12 Grimm, A. M.: The El Niño impact on the summer monsoon in Brazil: Regional
13 processes versus remote influences, *J. Clim.*, 16(2), 263–280, doi:10.1175/1520-
14 0442(2003)016<0263:TENIOT>2.0.CO;2, 2003.
- 15 Harshvardhan, Davies, R., Randall, D. A. and Corsetti, T. G.: A fast radiation
16 parameterization for atmospheric circulation models, *J. Geophys. Res.*, 92(D1),
17 1009–1016, doi:10.1029/JD092iD01p01009, 1987.
- 18 Hu, Z. Z. and Huang, B.: Interferential impact of ENSO and PDO on dry and wet
19 conditions in the U.S. great plains, *J. Clim.*, 22(22), 6047–6065,
20 doi:10.1175/2009JCLI2798.1, 2009.
- 21 Huang, B., Banzon, V. F., Freeman, E., Lawrimore, J., Liu, W., Peterson, T. C., Smith,
22 T. M., Thorne, P. W., Woodruff, S. D. and Zhang, H. M.: Extended
23 reconstructed sea surface temperature version 4 (ERSST.v4). Part I: Upgrades
24 and intercomparisons, *J. Clim.*, 28(3), 911–930, doi:10.1175/JCLI-D-14-
25 00006.1, 2015.
- 26 Huffman, G. J., Adler, R. F., Bolvin, D. T. and Gu, G.: Improving the global
27 precipitation record: GPCP Version 2.1, *Geophys. Res. Lett.*, 36(17), L17808,
28 doi:10.1029/2009GL040000, 2009.

- 1 Hurrell, J. W. and Deser, C.: North Atlantic climate variability: The role of the North
2 Atlantic Oscillation, *J. Mar. Syst.*, 78(1), 28–41,
3 doi:10.1016/j.jmarsys.2008.11.026, 2009.
- 4 Hurrell, J. W., Kushnir, Y., Otterson, G. and Visbeck, M.: An Overview of the North
5 Atlantic Oscillation, *North Atl. Oscil. Clim. Significance Environ. Impact*, 134,
6 263, doi:10.1029/GM134, 2003.
- 7 Hwang, Y.-T. and Frierson, D. M. W.: Link between the double-Intertropical
8 Convergence Zone problem and cloud biases over the Southern Ocean., *Proc.*
9 *Natl. Acad. Sci. U. S. A.*, 110(13), 4935–40, doi:10.1073/pnas.1213302110,
10 2013.
- 11 Ji, D., Wang, L., Feng, J., Wu, Q., Cheng, H., Zhang, Q., Yang, J., Dong, W., Dai, Y.,
12 Gong, D., Zhang, R. H., Wang, X., Liu, J., Moore, J. C., Chen, D. and Zhou, M.:
13 Description and basic evaluation of Beijing Normal University Earth System
14 Model (BNU-ESM) version 1, *Geosci. Model Dev.*, 7(5), 2039–2064,
15 doi:10.5194/gmd-7-2039-2014, 2014.
- 16 Jiménez, P. A., Dudhia, J., González-Rouco, J. F., Navarro, J., Montávez, J. P. and
17 García-Bustamante, E.: A Revised Scheme for the WRF Surface Layer
18 Formulation, *Mon. Weather Rev.*, 140(3), 898–918, doi:10.1175/MWR-D-11-
19 00056.1, 2012.
- 20 Jones, C. and Carvalho, L. M. V: Active and break phases in the South American
21 monsoon system, *J. Clim.*, 15(8), 905–914, doi:10.1175/1520-
22 0442(2002)015<0905:AABPIT>2.0.CO;2, 2002.
- 23 Karoly, D. J.: Southern Hemisphere Circulation Features Associated with El-Nino-
24 Southern Oscillation Events, *J. Clim.*, 2, 1239–1252, doi: 10.1175/1520-
25 0442(1989)002<1239:SHCFAW>2.0.CO;2., 1989.
- 26 Kidson, J. W.: Interannual Variations in the Southern Hemisphere Circulation, *J. Clim.*,
27 1(12), 939–953, doi:10.1175/1520-0442(1988)001<1177:IVITSH>2.0.CO;2,
28 1988.

- 1 Kim, D., Sperber, K., Stern, W., Waliser, D., Kang, I. S., Maloney, E., Wang, W.,
2 Weickmann, K., Benedict, J., Khairoutdinov, M., Lee, M. I., Neale, R., Suarez,
3 M., Thayer-Calder, K. and Zhang, G.: Application of MJO simulation
4 diagnostics to climate models, *J. Clim.*, 22(23), 6413–6436,
5 doi:10.1175/2009JCLI3063.1, 2009.
- 6 Krishnamurthy, L. and Krishnamurthy, V.: Indian monsoon' s relation with the decadal
7 part of PDO in observations and NCAR CCSM4, *Int. J. Climatol.*,
8 doi:10.1002/joc.4815, 2016.
- 9 Large, W. G. and Yeager, S. G.: The global climatology of an interannually varying air
10 - Sea flux data set, *Clim. Dyn.*, 33(2–3), 341–364, doi:10.1007/s00382-008-
11 0441-3, 2009.
- 12 Leathers, D. J., Yarnal, B., Palecki, M. A., Leathers, D. J., Yarnal, B. and Palecki, M.
13 A.: The Pacific/North American Teleconnection Pattern and United States
14 Climate. Part I: Regional Temperature and Precipitation Associations, *J. Clim.*,
15 4(5), 517–528, doi:10.1175/1520-0442(1991)004<0517:TPATPA>2.0.CO;2,
16 1991.
- 17 Levitus, S.: Climatological Atlas of the World Ocean. NOAA Prof. Paper 13, 173 pp.
18 and 17 microfich, 1982.
- 19 Li, G. and Xie, S. P.: Tropical biases in CMIP5 multimodel ensemble: The excessive
20 equatorial pacific cold tongue and double ITCZ problems, *J. Clim.*, 27(4), 1765–
21 1780, doi:10.1175/JCLI-D-13-00337.1, 2014.
- 22 Liebmann, B., Hendon, H. H. and Glick, J. D.: The Relationship Between Tropical
23 Cyclones of the Western Pacific and Indian Oceans and the Madden-Julian
24 Oscillation, *J. Meteorol. Soc. Japan. Ser. II*, 72(3), 401–412,
25 doi:10.2151/jmsj1965.72.3_401, 1994.
- 26 Lin, H., Brunet, G. and Derome, J.: An observed connection between the North Atlantic
27 oscillation and the Madden-Julian oscillation, *J. Clim.*, 22(2), 364–380,
28 doi:10.1175/2008JCLI2515.1, 2009.

- 1 Lu, R., Dong, B. and Ding, H.: Impact of the Atlantic Multidecadal Oscillation on the
2 Asian summer monsoon, *Geophys. Res. Lett.*, 33, L24701, doi(24), 101029/
3 doi:10.1029/2006GL027655, 2006.
- 4 Lumpkin, R. and Speer, K.: Global Ocean Meridional Overturning, *J. Phys. Oceanogr.*,
5 37(10), 2550–2562, doi:10.1175/JPO3130.1, 2007.
- 6 Lutz, K., Jacobeit, J. and Rathmann, J.: Atlantic warm and cold water events and impact
7 on African west coast precipitation, *Int. J. Climatol.*, 35(1), 128–141,
8 doi:10.1002/joc.3969, 2015.
- 9 Madden, R. A. and Julian, P. R.: Detection of a 40–50 Day Oscillation in the Zonal
10 Wind in the Tropical Pacific, *J. Atmos. Sci.*, 28(5), 702–708, doi:10.1175/1520-
11 0469(1971)028<0702:DOADOI>2.0.CO;2, 1971.
- 12 Madden, R. A. and Julian, P. R.: Description of Global-Scale Circulation Cells in the
13 Tropics with a 40–50 Day Period, *J. Atmos. Sci.*, 29(6), 1109–1123,
14 doi:10.1175/1520-0469(1972)029<1109:DOGSCC>2.0.CO;2, 1972.
- 15 Mantua, N. J., Hare, S. R., Zhang, Y., Wallace, J. M. and Francis, R. C.: A Pacific
16 Interdecadal Climate Oscillation with Impacts on Salmon Production, *Bull. Am.*
17 *Meteorol. Soc.*, 78(6), 1069–1079, doi:10.1175/1520-
18 0477(1997)078<1069:APICOW>2.0.CO;2, 1997.
- 19 Marengo, J. A., Calvalcanti, I. F. A., Satyamurty, P., Trosnikov, I., Nobre, C. A.,
20 Bonatti, J. P., Camargo, H., Sampaio, G., Sanches, M. B., Manzi, A. O., Castro,
21 C. A. C., D’Almeida, C., Pezzi, L. P. and Candido, L.: Assessment of regional
22 seasonal rainfall predictability using the CPTEC/COLA atmospheric GCM,
23 *Clim. Dyn.*, 21(5–6), 459–475, doi:10.1007/s00382-003-0346-0, 2003.
- 24 [Menary, M. B., Kuhlbrodt, T., Ridley, J., Andrews, M. B., Dimdore-Miles, O. B.,](#)
25 [Deshayes, J. et al.: Preindustrial control simulations with HadGEM3-GC3.1 for](#)
26 [CMIP6., J. Adv. Model. Earth Syst., 10, 3049–3075,](#)
27 [doi:https://doi.org/10.1029/2018MS001495, 2018.](https://doi.org/10.1029/2018MS001495)

- 1 | McCarthy, G. D., Smeed, D. A., Johns, W. E., Frajka-Williams, E., Moat, B. I., Rayner,
2 | D., Baringer, M. O., Meinen, C. S., Collins, J. and Bryden, H. L.: Measuring the
3 | Atlantic Meridional Overturning Circulation at 26 N, *Prog. Oceanogr.*, 130, 91–
4 | 111, doi:10.1016/j.pocean.2014.10.006, 2015.
- 5 | McPhaden, M. J., Zebiak, S. E. and Glantz, M. H.: ENSO as an integrating concept in
6 | earth science, *Science*, 314(5806), 1740–1745, doi:10.1126/science.1132588,
7 | 2006.
- 8 | Meehl, G. A., Moss, R., Taylor, K. E., Eyring, V., Stouffer, R. J., Bony, S. and Stevens,
9 | B.: Climate model intercomparisons: Preparing for the next phase, *Eos*, 95(9),
10 | 77–78, doi:10.1002/2014EO090001, 2014.
- 11 | Mellor, G. L. and Yamada, T.: Development of a turbulence closure model for
12 | geophysical fluid problems, *Rev. Geophys.*, 20(4), 851–875,
13 | doi:10.1029/RG020i004p00851, 1982.
- 14 | Mo, K. C. and Peagle, J. N.: The Pacific-South American modes and their downstream
15 | effects, *Int. J. Climatol*, 21(10), 1211–1229, doi:10.1002/joc.685, 2001.
- 16 | Morice, C. P., Kennedy, J. J., Rayner, N. A. and Jones, P. D.: Quantifying uncertainties
17 | in global and regional temperature change using an ensemble of observational
18 | estimates: The HadCRUT4 data set, *J. Geophys. Res. Atmos.*, 117(8), 1–22,
19 | doi:10.1029/2011JD017187, 2012.
- 20 | Newman, M., Alexander, M. A., Ault, T. R., Cobb, K. M., Deser, C., Di Lorenzo, E.,
21 | Mantua, N. J., Miller, A. J., Minobe, S., Nakamura, H., Schneider, N., Vimont,
22 | D. J., Phillips, A. S., Scott, J. D. and Smith, C. A.: The Pacific decadal
23 | oscillation, revisited, *J. Clim.*, 29(12), 4399–4427, doi:10.1175/JCLI-D-15-
24 | 0508.1, 2016.
- 25 | Ning, L. and Bradley, R. S.: NAO and PNA influences on winter temperature and
26 | precipitation over the eastern United States in CMIP5 GCMs, *Clim. Dyn.*, 46(3–
27 | 4), 1257–1276, doi:10.1007/s00382-015-2643-9, 2016.

- 1 Nobre, P., Shukla, J.: Variation of Sea surface Temperature, Wind Stress, and Rainfall
2 over the Tropical Atlantic and South America, *J. Clim.*, 9, 2464–2479,
3 doi:[http://dx.doi.org/10.1175/1520-0442\(1996\)009<2464:VOSSTW>2.0.CO;2](http://dx.doi.org/10.1175/1520-0442(1996)009<2464:VOSSTW>2.0.CO;2),
4 1996.
- 5 Nobre, P., Marengo, J. A., Cavalcanti, I. F. A., Obregon, G., Barros, V., Camilloni, I.,
6 Campos, N. and Ferreira, A. G.: Seasonal-to-decadal predictability and
7 prediction of South American climate, *J. Clim.*, 19(23), 5988–6004,
8 doi:10.1175/JCLI3946.1, 2006.
- 9 Nobre, P., De Almeida, R. A., Malagutti, M. and Giarolla, E.: Coupled ocean-
10 atmosphere variations over the South Atlantic Ocean, *J. Clim.*, 25(18), 6349–
11 6358, doi:10.1175/JCLI-D-11-00444.1, 2012.
- 12 Nobre, P., Siqueira, L. S. P., De Almeida, R. A. F., Malagutti, M., Giarolla, E., Castel ã
13 O, G. P., Bottino, M. J., Kubota, P., Figueroa, S. N., Costa, M. C., Baptista, M.,
14 Irber, L. and Marcondes, G. G.: Climate simulation and change in the brazilian
15 climate model, *J. Clim.*, 26(17), 6716–6732, doi:10.1175/JCLI-D-12-00580.1,
16 2013.
- 17 Nogués-Paegle, J. and Mo, K. C.: Alternating Wet and Dry Conditions over South
18 America during Summer, *Mon. Weather Rev.*, 125, 279–291, doi:10.1175/1520-
19 0493(1997)125<0279:AWADCO>2.0.CO;2, 1997.
- 20 Obukhov, A. M.: Turbulence in an atmosphere with a non-uniform temperature,
21 *Boundary-Layer Meteorol.*, 2(1), 7–29, doi:10.1007/BF00718085, 1971.
- 22 de Oliveira Vieira, S., Satyamurty, P. and Andreoli, R. V.: On the South Atlantic
23 Convergence Zone affecting southern Amazonia in austral summer, *Atmos. Sci.*
24 *Lett.*, 14(1), 1–6, doi:10.1002/asl2.401, 2013.
- 25 Palmer, T. N., Doblas-Reyes, F. J., Weisheimer, A. and Rodwell, M. J.: Toward
26 seamless prediction: Calibration of climate change projections using seasonal
27 forecasts, *Bull. Am. Meteorol. Soc.*, 89(4), 459–470, doi:10.1175/BAMS-89-4-
28 459, 2008.

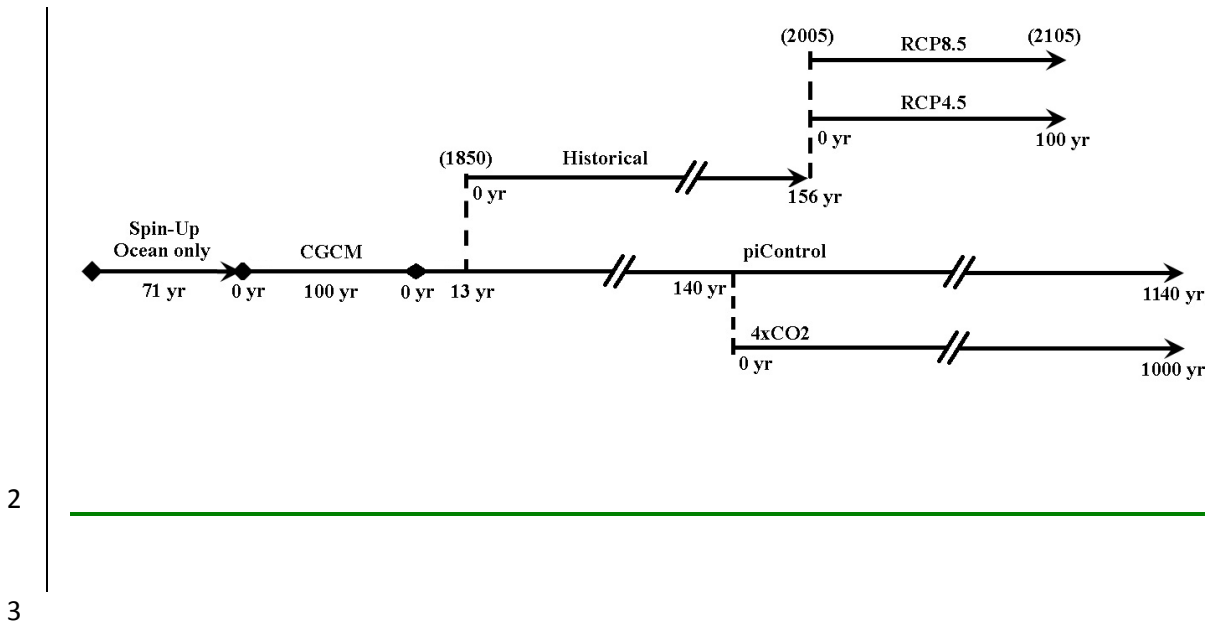
- 1 Richter, I.: Climate model biases in the eastern tropical oceans: Causes, impacts and
2 ways forward, *Wiley Interdiscip. Rev. Clim. Chang.*, 6(3), 345–358,
3 doi:10.1002/wcc.338, 2015.
- 4 Richter, I., Xie, S. P., Behera, S. K., Doi, T. and Masumoto, Y.: Equatorial Atlantic
5 variability and its relation to mean state biases in CMIP5, *Clim. Dyn.*, 42(1–2),
6 171–188, doi:10.1007/s00382-012-1624-5, 2014.
- 7 Robertson, A. and Mechoso, C.: Interannual and interdecadal variability of the South
8 Atlantic Convergence Zone, *Mon. Weather Rev.*, 128(8), 2947–2957,
9 doi:10.1175/1520-0493(2000)128<2947:IAIVOT>2.0.CO;2, 2000.
- 10 Rogers, J. C. and van Loon, H.: Spatial Variability of Sea Level Pressure and 500 mb
11 Height Anomalies over the Southern Hemisphere, *Mon. Weather Rev.*, 110(10),
12 1375–1392, doi:10.1175/1520-0493(1982)110<1375:SVOSLP>2.0.CO;2, 1982.
- 13 Rossow, W. B. and Schiffer, R. a: Advances in Understanding Clouds from ISCCP,
14 *Bull. Amer. Meteor. Soc.*, 80(11), 2261–2287, doi:10.1175/1520-
15 0477(1999)080<2261:AIUCFI>2.0.CO;2, 1999.
- 16 von Storch, H.: Climate models and modeling: an editorial essay, *Wiley Interdiscip.*
17 *Rev. Clim. Chang.*, 1(3), 305–310, doi:10.1002/wcc.12, 2010.
- 18 Straus, D. M. and Shukla, J.: Does ENSO force the PNA?, *J. Clim.*, 15(17), 2340–2358,
19 doi:10.1175/1520-0442(2002)015<2340:DEFTP>2.0.CO;2, 2002.
- 20 Sutton, R. T. and Hodson, D. L. R.: Atlantic Ocean Forcing of North American and
21 European Summer Climate, *Science*, 309(5731), 115–118,
22 doi:10.1126/science.1109496, 2005.
- 23 Swapna, P., Krishnan, R., Sandeep, N., Prajeesh, A. G., Ayantika, D. C., Manmeet, S.
24 and Vellore, R.: Long-Term Climate Simulations Using the IITM Earth System
25 Model (IITM-ESMv2) With Focus on the South Asian Monsoon, *J. Adv. Model.*
26 *Earth Syst.*, 10(5), 1127–1149, doi:10.1029/2017MS001262, 2018.
- 27 Takayabu, Y. N., Iguchi, T., Kachi, M., Shibata, A. and Kanzawa, H.: Abrupt

- 1 termination of the 1997-98 El Nino in response to a Madden-Julian oscillation,
2 Nature, 402(6759), 279–282, doi:10.1038/46254, 1999.
- 3 Tarasova, T. A., Barbosa, H. M. J. and Figueroa, S. N.: In- corporation of new solar
4 radiation scheme into CPTECGCM. Instituto Nacional de Pesquisas Espaciais
5 Tech. Rep. INPE- 14052-NTE/371, 44 pp. [Available online at [http://mtc-m15.
6 sid.inpe.br/col/sid.inpe.br/iris%401915/2006/01.16.10.40/doc/publicacao.pdf](http://mtc-m15.sid.inpe.br/col/sid.inpe.br/iris%401915/2006/01.16.10.40/doc/publicacao.pdf),
7 2006.
- 8 Tian, B.: Spread of model climate sensitivity linked to double-Intertropical
9 Convergence Zone bias, Geophys. Res. Lett., 42(10), 4133–4141,
10 doi:10.1002/2015GL064119, 2015.
- 11 Tian, B., Fetzer, E. J., Kahn, B. H., Teixeira, J., Manning, E. and Hearty, T.: Evaluating
12 CMIP5 models using AIRS tropospheric air temperature and specific humidity
13 climatology, J. Geophys. Res. Atmos., 118(1), 114–134,
14 doi:10.1029/2012JD018607, 2013.
- 15 Tiedtke, M.: The sensitivity of the time-mean large-scale flow to cumulus convection in
16 the ECMWF model. Proc. Work-shop on Convection in Large-Scale Models,
17 Reading, United Kingdom, ECMWF, 297–316, 1983.
- 18
- 19 Waliser, D., Sperber, K., Hendon, H., Kim, D., Maloney, E., Wheeler, M., Weickmann,
20 K., Zhang, C., Donner, L., Gottschalck, J., Higgins, W., Kang, I. S., Legler, D.,
21 Moncrieff, M., Schubert, S., Stern, W., Vitart, F., Wang, B., Wang, W. and
22 Woolnough, S.: MJO simulation diagnostics, J. Clim., 22(11), 3006–3030,
23 doi:10.1175/2008JCLI2731.1, 2009.
- 24 Wallace, J. M. and Gutzler, D. S.: Teleconnections in the Geopotential Height Field
25 during the Northern Hemisphere Winter, Mon. Weather Rev., 109(4), 784–812,
26 doi:10.1175/1520-0493(1981)109<0784:TITGHF>2.0.CO;2, 1981.
- 27 Wang, C., Zhang, L. and Lee, S.: A global perspective on CMIP5 climate model biases,
28 Nat. Clim. Chang., 4(3), 201–205, doi:10.1038/NCLIMATE2118, 2014.

- 1 Wanner, H., Brönnimann, S., Casty, C., Luterbacher, J., Schmutz, C. and David, B.:
2 North Atlantic Oscillation – Concepts and Studies, *Surv. Geophys.*, 22(1984),
3 321–382, doi:10.1023/A:1014217317898, 2001.
- 4 Weaver, A. J., Sedláček, J., Eby, M., Alexander, K., Crespin, E., Fichefet, T.,
5 Philippon-Berthier, G., Joos, F., Kawamiy, M., Matsumoto, K., Steinacher, M.,
6 Tachiiri, K., Tokos, K., Yoshimori, M. and Zickfeld, K.: Stability of the Atlantic
7 meridional overturning circulation: A model intercomparison, *Geophys. Res.*
8 *Lett.*, 39(20), 1–7, doi:10.1029/2012GL053763, 2012.
- 9 Winton, M.: A reformulated three-layer sea ice model, *J. Atmos. Ocean. Technol.*,
10 17(4), 525–531, doi:10.1175/1520-0426(2000)017<0525:ARTLSI>2.0.CO;2,
11 2000.
- 12 Wu, X. and Mao, J.: Interdecadal variability of early summer monsoon rainfall over
13 South China in association with the Pacific Decadal Oscillation, *Int. J. Climatol.*,
14 doi:10.1002/joc.4734, 2016.
- 15 Wu, Z., Li, J., Jiang, Z., He, J. and Zhu, X.: Possible effects of the North Atlantic
16 Oscillation on the strengthening relationship between the East Asian Summer
17 monsoon and ENSO, *Int. J. Climatol.*, 32(5), 794–800, doi:10.1002/joc.2309,
18 2012.
- 19 Xie, S.-P.: A Dynamic Ocean – Atmosphere Model of the Tropical Atlantic Decadal
20 Variability, *J. Clim.*, 12(1), 64–71, 1999.
- 21 Xie, S. -P. and Philander, S. G. H.: A coupled ocean-atmosphere model of relevance to
22 the ITCZ in the eastern Pacific, *Tellus A*, 46(4), 340–350, doi:10.1034/j.1600-
23 0870.1994.t01-1-00001.x, 1994.
- 24 Xie, P., and P.A. Arkin, 1997: Global precipitation: A 17-year monthly analysis based
25 on gauge observations, satellite estimates, and numerical model outputs. *Bull.*
26 *Amer. Meteor. Soc.*, 78, 2539 - 2558.
- 27 Xue, Y., Sellers, P., Kinter, J. and Shukla, J.: A Simplified Biosphere Model for Global

- 1 Climate Studies, *J. Clim.*, 4(3), 345–364, doi:10.1175/1520-
2 0442(1991)004<0345:ASBMFG>2.0.CO;2, 1991.
- 3 Yu, B. and Zwiers, F. W.: The impact of combined ENSO and PDO on the PNA
4 climate: A 1,000-year climate modeling study, *Clim. Dyn.*, 29(7–8), 837–851,
5 doi:10.1007/s00382-007-0267-4, 2007.
- 6 Yu, R. and Zhou, T.: Impacts of winter-NAO on March cooling trends over subtropical
7 Eurasia continent in the recent half century, *Geophys. Res. Lett.*, 31(12), 3–6,
8 doi:10.1029/2004GL019814, 2004.
- 9 Yuan, X. and Yonekura, E.: Decadal variability in the Southern Hemisphere, *J.*
10 *Geophys. Res.*, 116(D19), 1–12, doi:10.1029/2011JD015673, 2011.
- 11 Zebiak, S. E.: Air–Sea Interaction in the Equatorial Atlantic Region, *J. Clim.*, 6(8),
12 1567–1586, doi:10.1175/1520-0442(1993)006<1567:AIITEA>2.0.CO;2, 1993.
- 13 Zhang, C.: Madden-Julian Oscillation, *Rev. Geophys.*, 43(2), 1–36,
14 doi:10.1029/2004RG000158, 2005.
- 15 Zhang, L. and Wang, C.: Multidecadal North Atlantic sea surface temperature and
16 Atlantic meridional overturning circulation variability in CMIP5 historical
17 simulations, *J. Geophys. Res. Ocean.*, 118(10), 5772–5791,
18 doi:10.1002/jgrc.20390, 2013.
- 19 Zhang, L., Ma, H. and Wu, L.: Dynamics and mechanisms of decadal variability of the
20 Pacific-South America mode over the 20th century, *Clim. Dyn.*, 46(11–12),
21 3657–3667, doi:10.1007/s00382-015-2794-8, 2016.
- 22 Zheng, F., Li, J., Clark, R. T. and Nnamchi, H. C.: Simulation and projection of the
23 Southern Hemisphere annular mode in CMIP5 models, *J. Clim.*, 26(24), 9860–
24 9879, doi:10.1175/JCLI-D-13-00204.1, 2013.
- 25

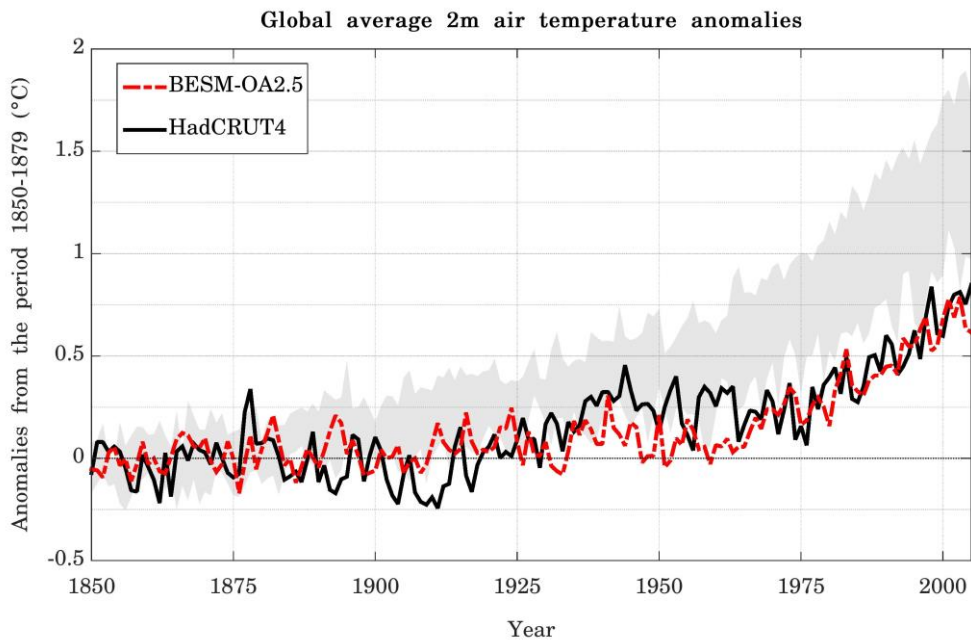
1 List of Figures



2
3
4 Figure 1 – The scheme of principal simulations carried out by BESM-OA2.5 using
5 different forcing conditions according to CMIP5 protocols. The date for the Historical
6 and RCPs simulations are from actual calendar years.

7

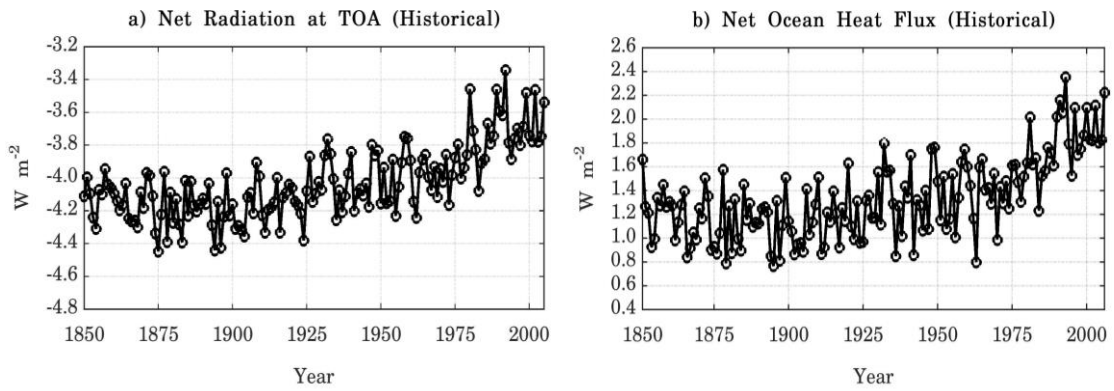
1



2

3 Figure 2 – Global averaged 2-m annual mean air temperature anomalies relative to the
4 period 1850–1879 for BESM-OA2.5 (dashed red line) and observation (solid black
5 line). The grey shadow represents the spread of 11 CMIP5 models (historical GHG
6 simulations). The CMIP5 models anomalies are also computed relative to the period
7 1850–1879, with exception of GFDL-ESM2M and HadGEM2-ES which anomalies are
8 computed relative to the periods 1861–1890 and 1860–1889, respectively. Units are in
9 °C.

10

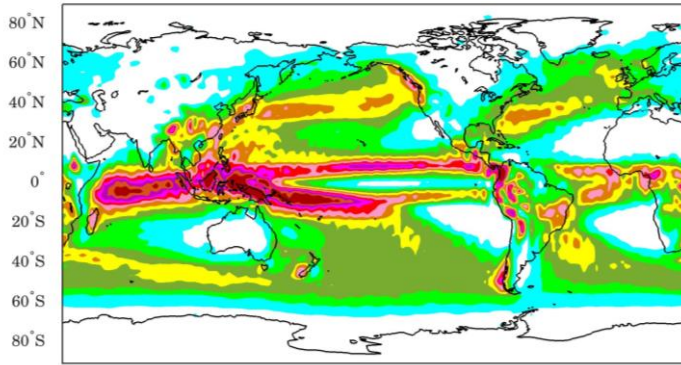


1
 2 Figure 3 – Annual average time series for the global average (a) net of the radiation at
 3 TOA (positive values indicates that the atmosphere is warming) and (b) net of the
 4 ocean/atmosphere heat flux (positive values indicates that the ocean is warming),
 5 simulated by the Historical run over the period 1850-2005 (156 years).

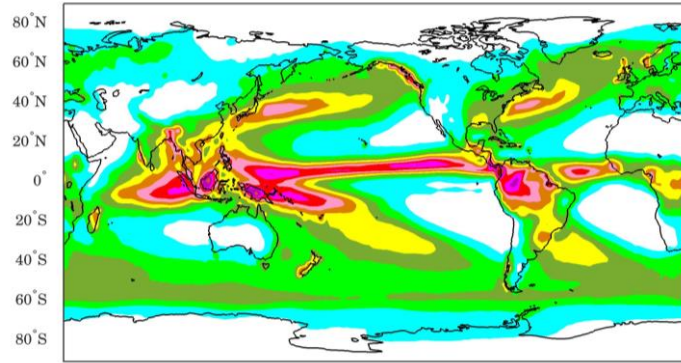
6

7

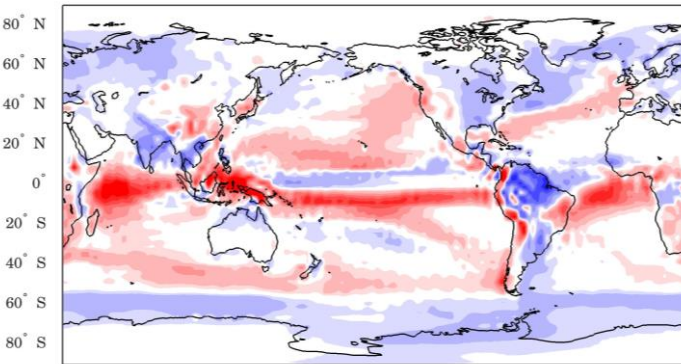
a) Annual mean precipitation (BESM-OA2.5)



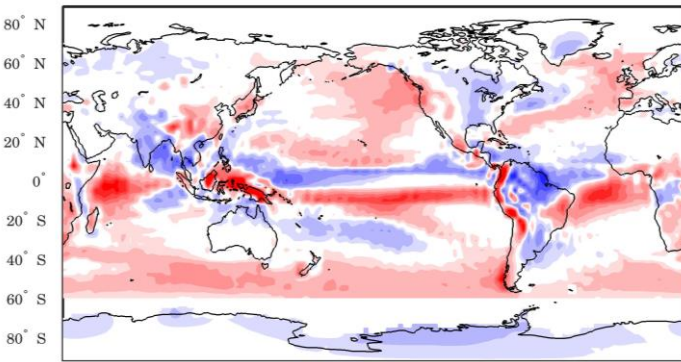
b) Annual mean precipitation (GPCP)



c) BESM-OA2.5 - GPCP mean: 0.3 mm/day rmse: 1.4 mm/day



d) BESM-OA2.5 - CMAP mean: 0.4 mm/day rmse: 1.5 mm/day



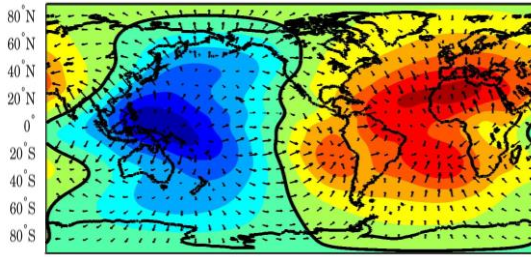
30°E 90°E 150°E 150°W 90°W 30°W 30°E

1 Figure 4 – Spatial map of annual mean precipitation for (a) BESM-OA2.5, for (b)
2 GPCP, (c) the bias of BESM-OA2.5 relative to GPCP and (d) the bias of BESM-OA2.5
3 relative to CMAP. The averages values are computed over the periods 1971–2000 (for
4 BESM-OA2.5) and 1979–2008 (for GPCP and CMAP). Units are in mm day^{-1} .

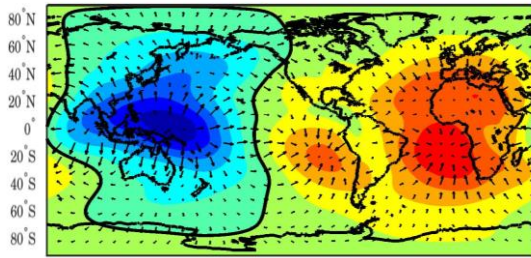
5

6

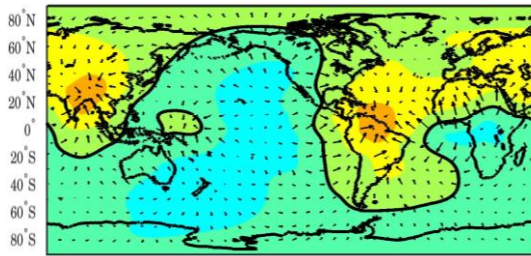
a) BESM-OA2.5 200 hPa Vel. Potential/Div. Wind



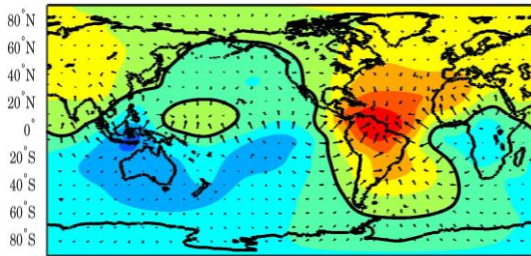
b) 20CRv2 200 hPa Vel. Potential/Div. Wind



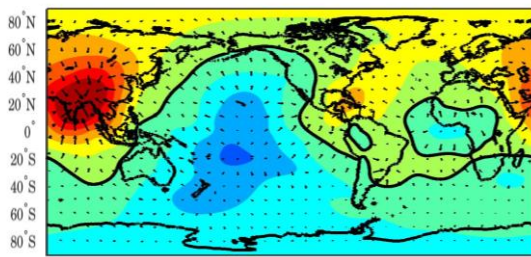
c) BESM-OA2.5 Bias 200 hPa Vel. Potential/Div. Wind



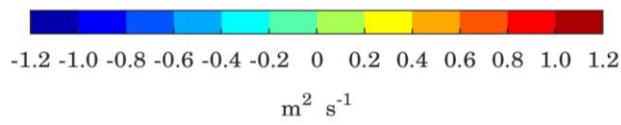
d) BESM-OA2.5 Bias 200 hPa Vel. Potential/Div. Wind MAM



e) BESM-OA2.5 Bias 200 hPa Vel. Potential/Div. Wind JJA



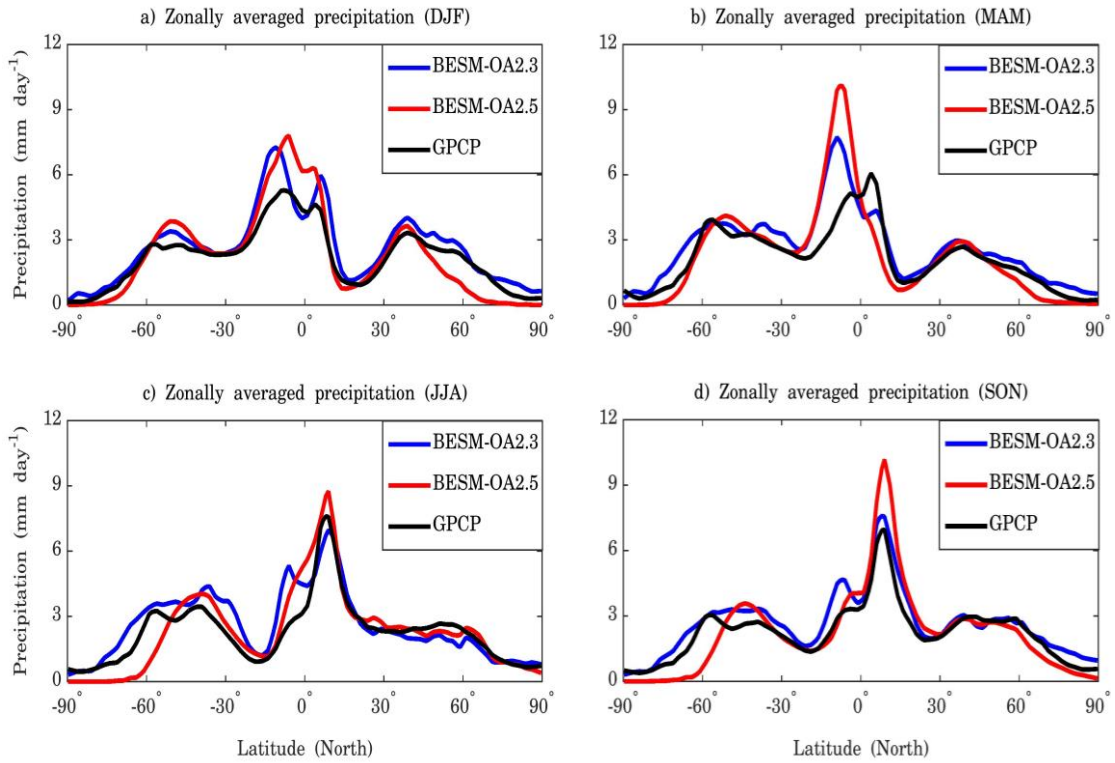
30°E 90°E 150°E 150°W 90°W 30°W 30°E



1 Figure 5 – Spatial maps with averaged global anomalies of velocity potential and wind
2 divergence at 200 hPa pressure level for (a) BESM-OA2.5 and (b) Reanalysis. (c) The
3 bias of the model relative to the Reanalysis, (d) and (e) are the bias for MAM and JJA
4 seasons, respectively. The averages are computed over the period 1950–2005. Units are
5 in m s^{-1} .

6

1



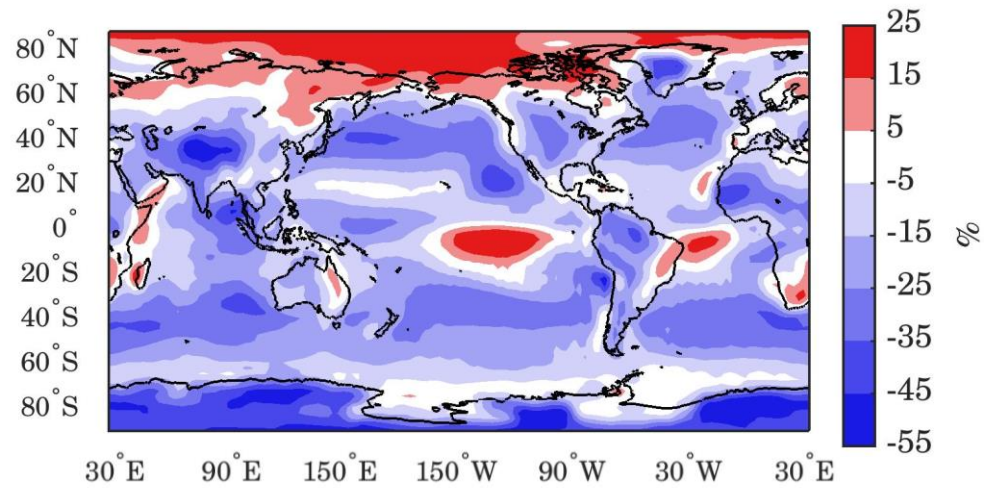
2

3 Figure 6 – Zonally averaged annual mean precipitation for BESM-OA2.5, BESM-
4 OA2.3 and GPCP dataset relative to the seasons DJF, MAM, JJA and SON. The zonally
5 averages values are computed over the periods 1971–2000 and 1979–2008, for BESM-
6 OA2.5 and GPCP, respectively. Units are in mm day⁻¹.

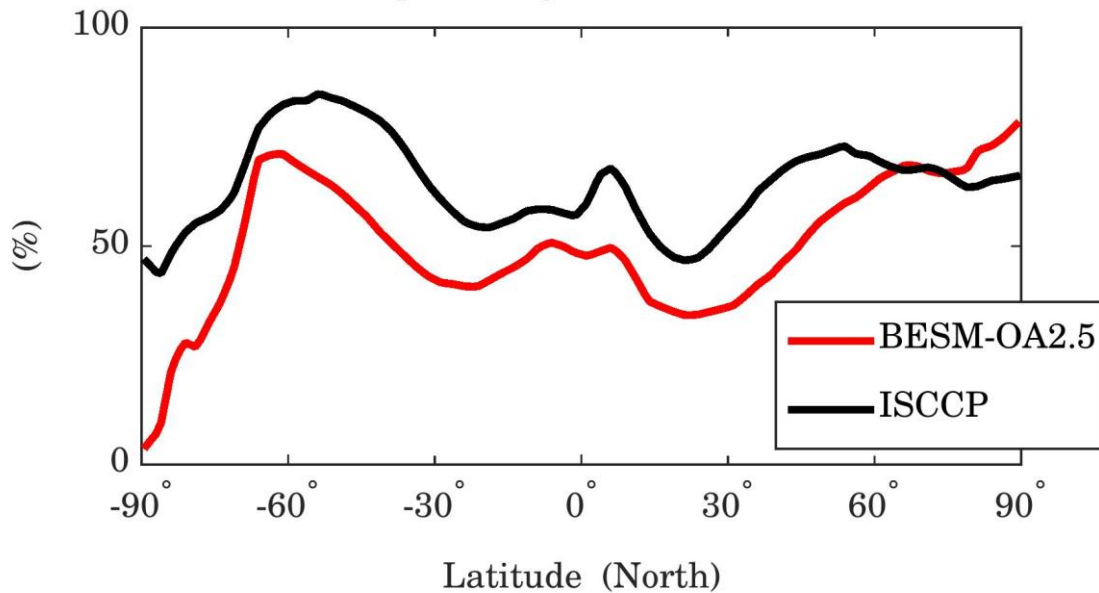
7

8

a) Total cloud fraction (BESM-OA2.5 - ISCCP)



b) Zonally averaged total cloud cover



1

2 Figure 7 – (a) Spatial map of annual mean total cloud fraction bias of BESM-OA2.5

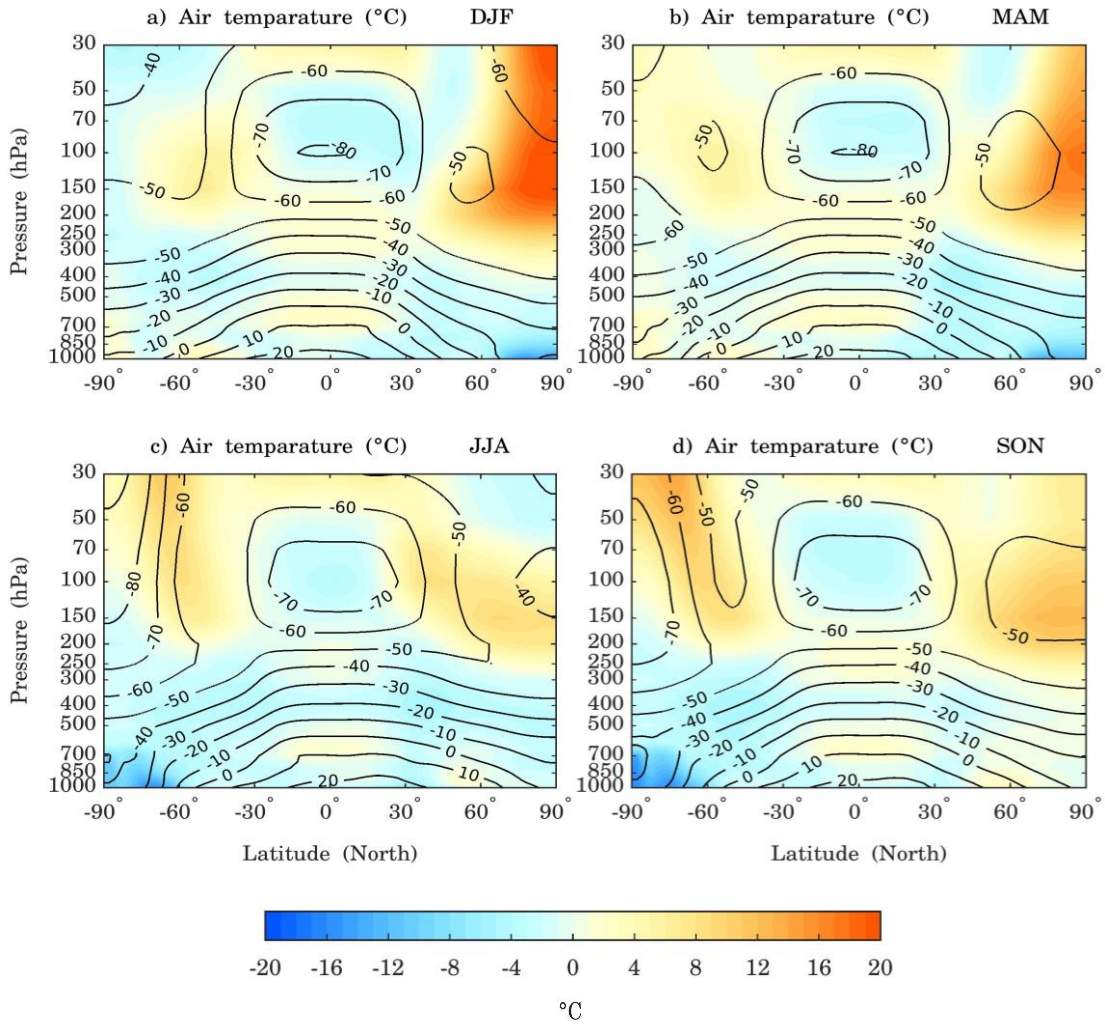
3 relative to ISCCP. (b) Zonally averaged total cloud cover for BESM-OA2.5 and ISCCP

4 dataset. The periods used are 1971–2000 and 1984–2009 for BESM-OA2.5 and ISCCP,

5 respectively. Units are in percentage.

6

1



2

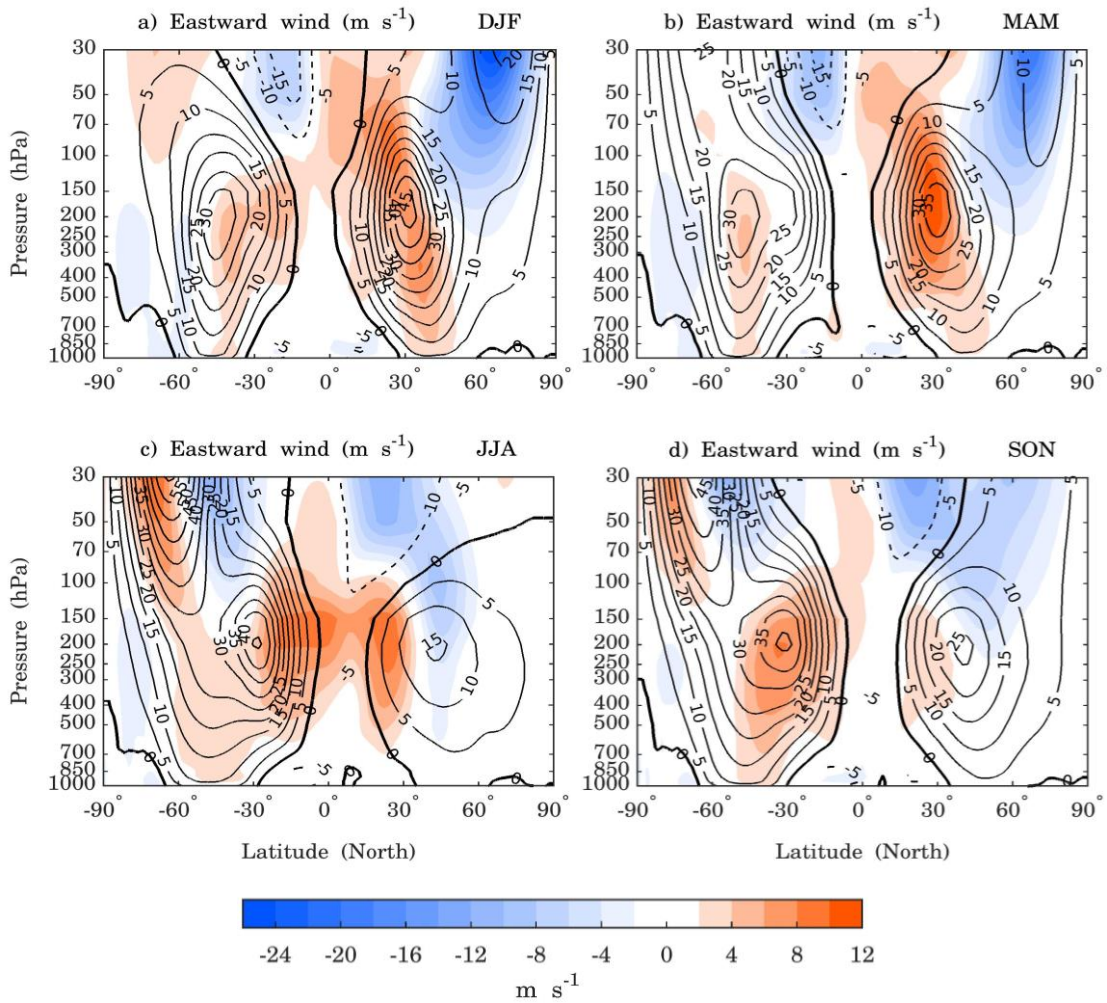
3

4 Figure 8 – Contour lines are the zonally averaged vertical air temperature for BESM-
5 OA2.5 and in shaded are the difference BESM-OA2.5 - 20CRv2 data set. Both are
6 averaged over the period 1971–2000. The units are in °C and the contour interval is 10
7 °C.

8

9

1



2

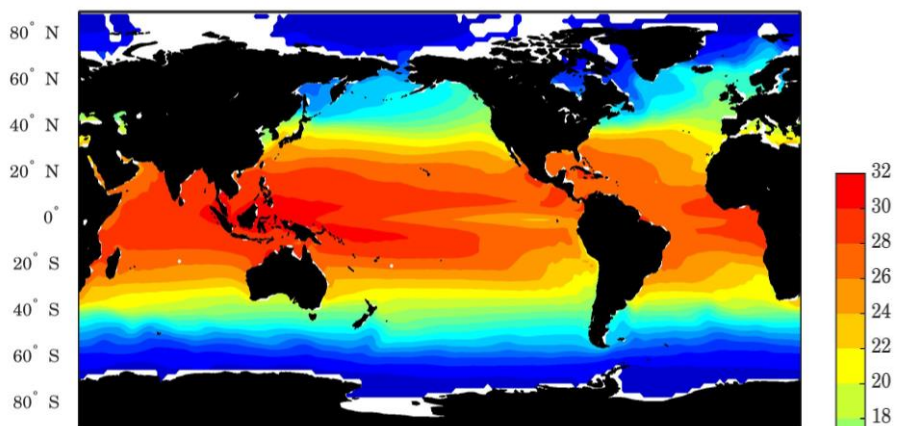
3

4 Figure 9 – Contour lines are the zonally averaged zonal wind for BESM-OA2.5 and in
5 shaded are the difference BESM-OA2.5 - 20CRv2 data set. Both are averaged over the
6 period 1971–2000. The solid contour lines represent eastward zonal wind and the
7 dashed contour lines represents westward zonal wind. The units are in meters per
8 second and the Eastward contour interval is 5 m s^{-1} , with the contour line zero highlighted.

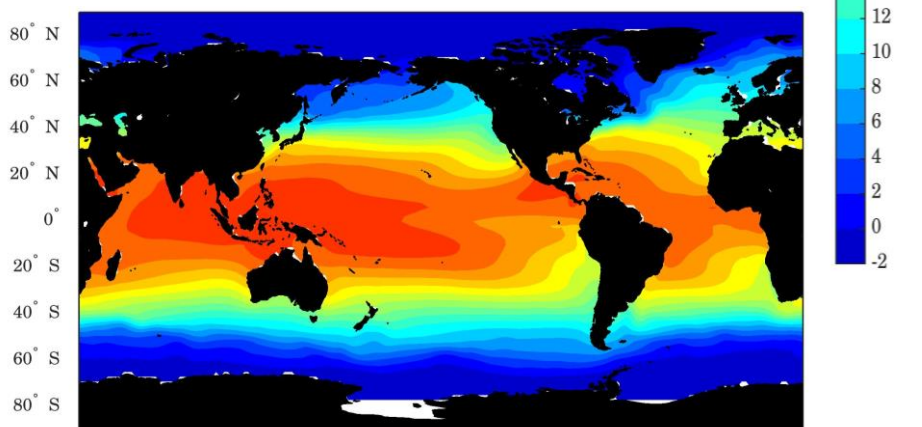
9

10

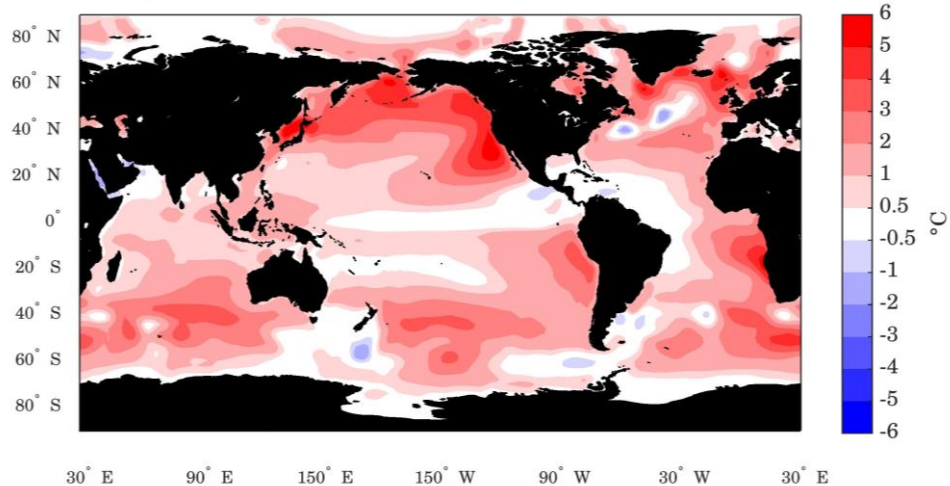
a) Annual mean SST (BESM-OA2.5)



b) Annual mean SST (ERSSTv4)



c) BESM-OA2.5 - ERSSTv4 mean: 1.5°C rmse: 1.9°C



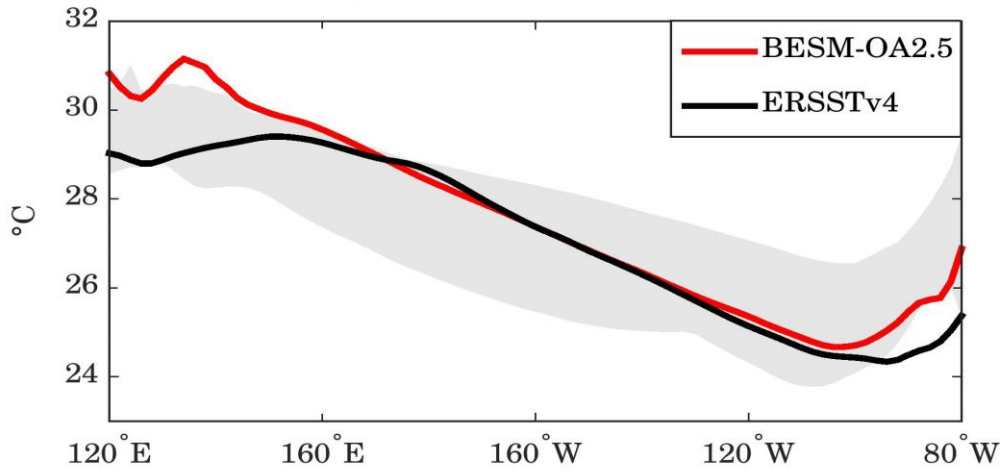
- 1
- 2
- 3

1 Figure 10 – Spatial map of annual mean sea surface temperature for (a) BESM-OA2.5,
2 (b) ERSSTv4 and (c) the bias of BESM-OA2.5 relative to ERSSTv4. The averages are
3 computed over the period 1971–2000. Units are in °C.

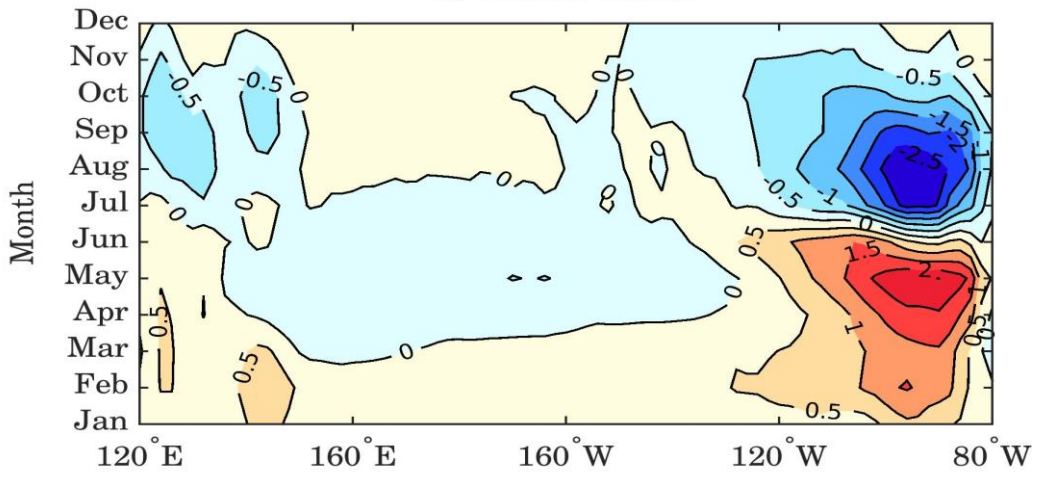
4

5

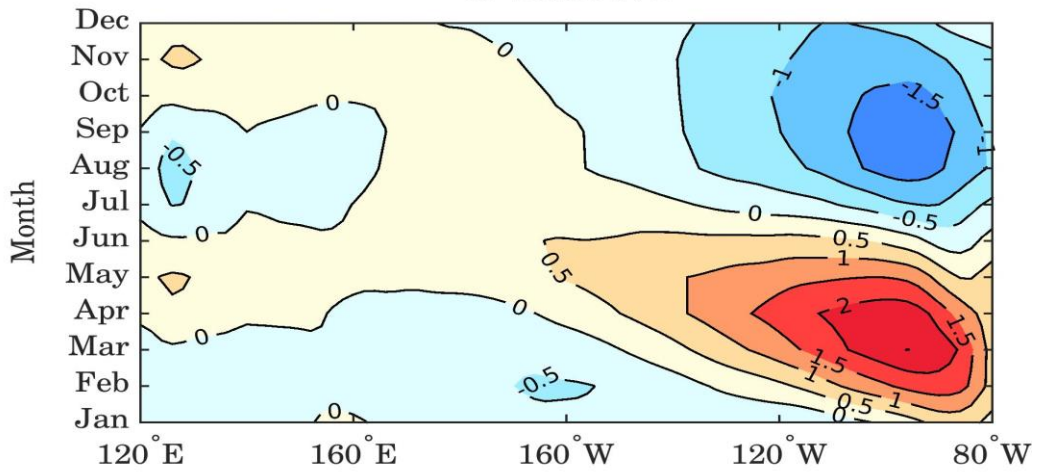
a) Equatorial Pacific Mean SST



b) BESM-OA2.5



c) ERSSTv4



1

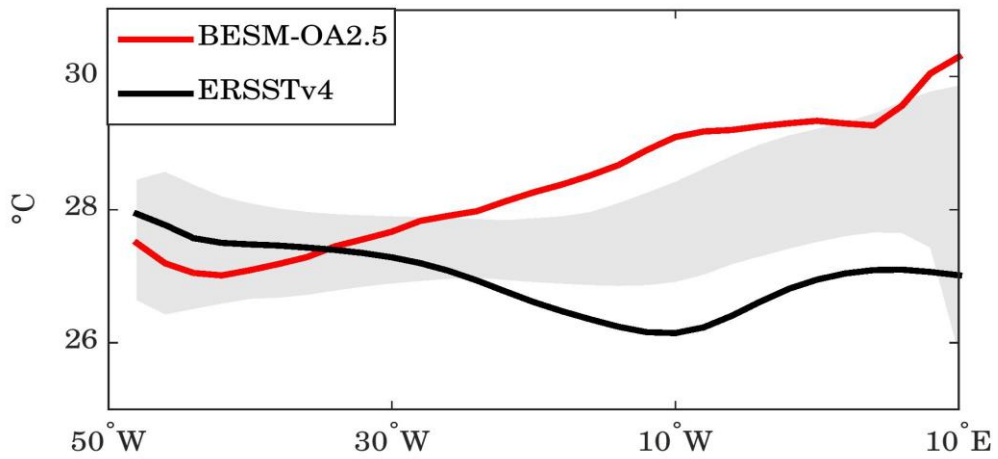
2

1 Figure 11 – (a) Mean SST along the equator in the Pacific Ocean and annual cycle of
2 the equatorial Pacific SST anomalies for (b) BESM-OA2.5 and (c) ERSSTv4.
3 Equatorial region is defined by averaging over 2 °S–2 °N. BESM-OA2.5 and ERSSTv4
4 are averaged over the period 1971–2000. In (a) the grey shadow represents the spread of
5 11 CMIP5 models, which are also averaged over the period 1971–2000. Units are in °C.

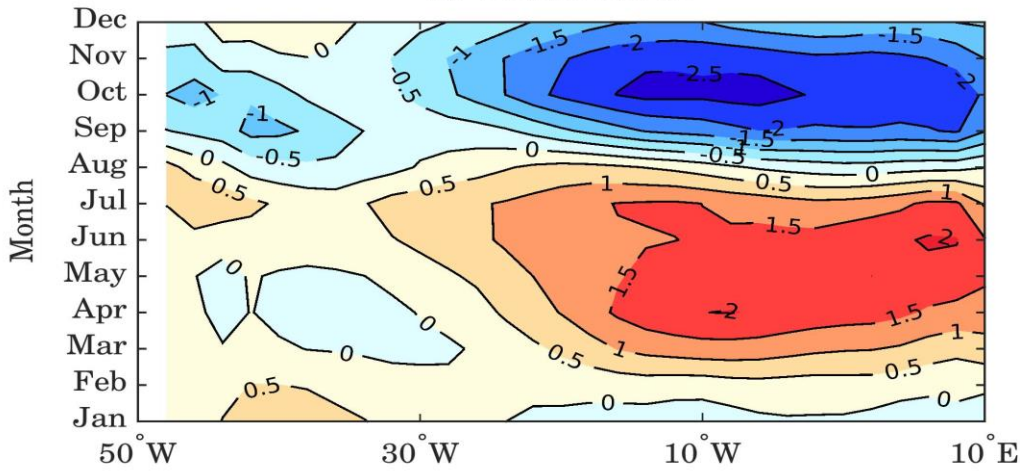
6

7

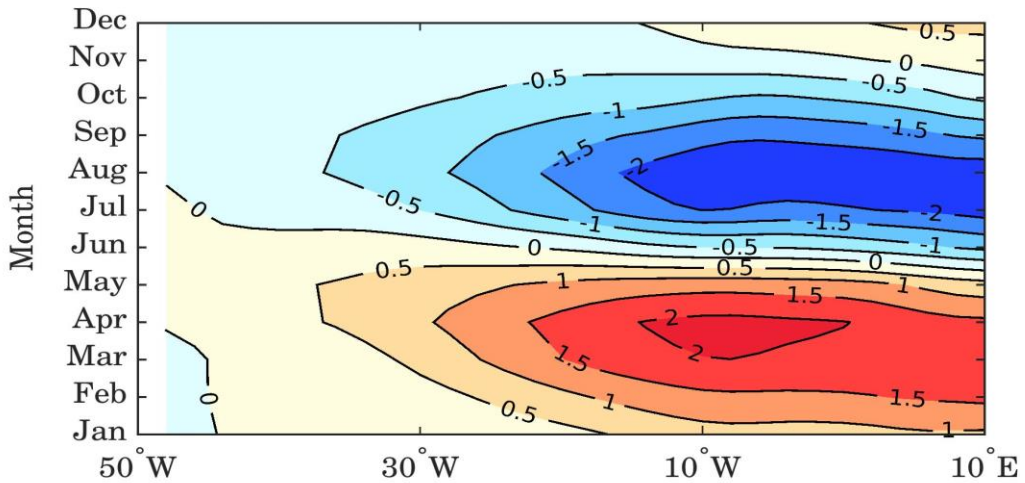
a) Equatorial Atlantic Mean SST



b) BESM-OA2.5

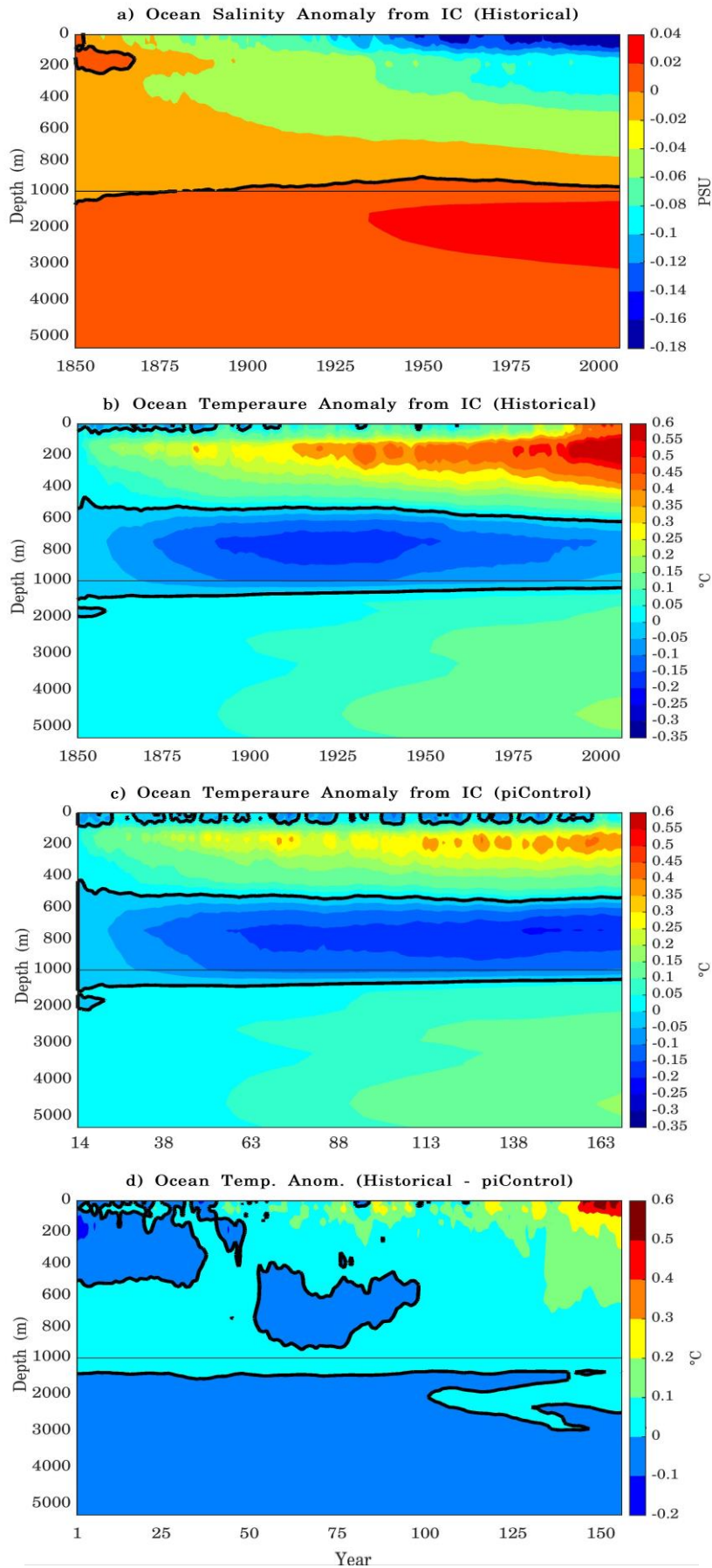


c) ERSSTv4



1

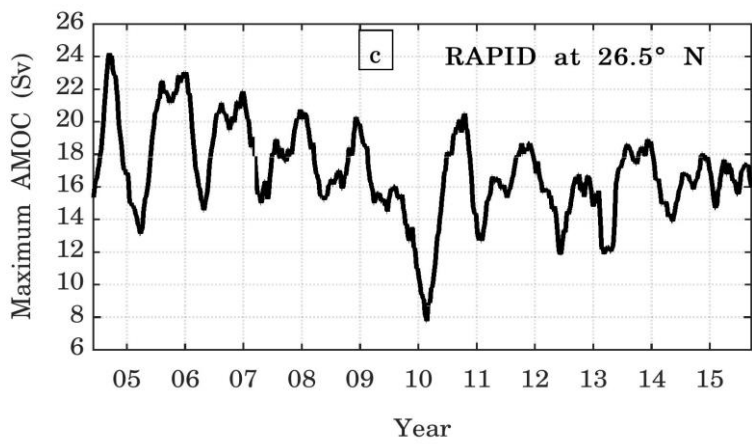
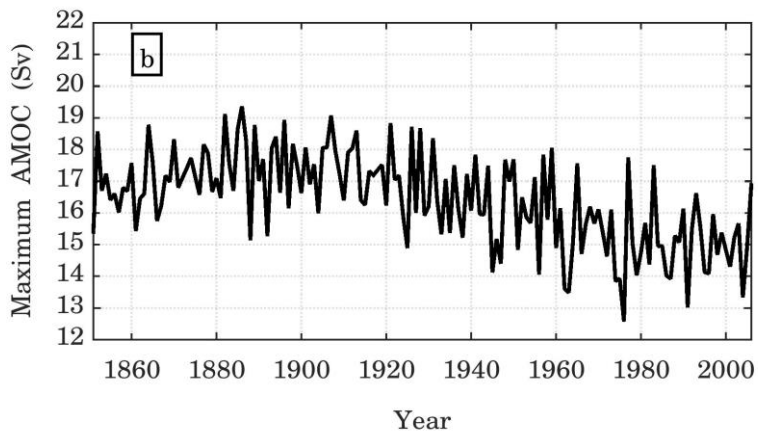
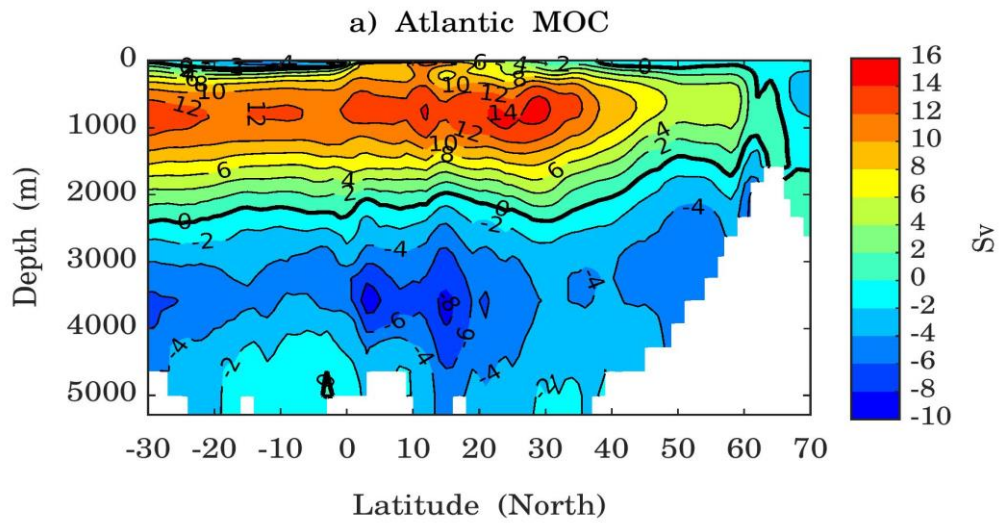
2 Figure 12 – As Fig. 11 but for the Atlantic Ocean.



1 | Figure 13 – Depth-time Hovmöller diagrams of global average ocean (a)temperature
2 | salinity and ~~salinity~~(b) temperature anomalies from the respective initial conditions
3 | (IC). Here the initial conditions are taken from the 1th year for (a, b) Historical
4 | simulation, and 14th year for (c) piControl simulation. (d) presents the difference
5 | between the temperature anomalies of Historical relative to piControl. The diagrams are
6 | based on annual average time series simulated by the Historical simulation over the
7 | period 1850-2005 (156 years) and by piControl simulation over the period 14-169 years
8 | (156 years). The thick black line represents the zero contours. Note that the vertical
9 | scales are different above and below 1000 m.

10

11



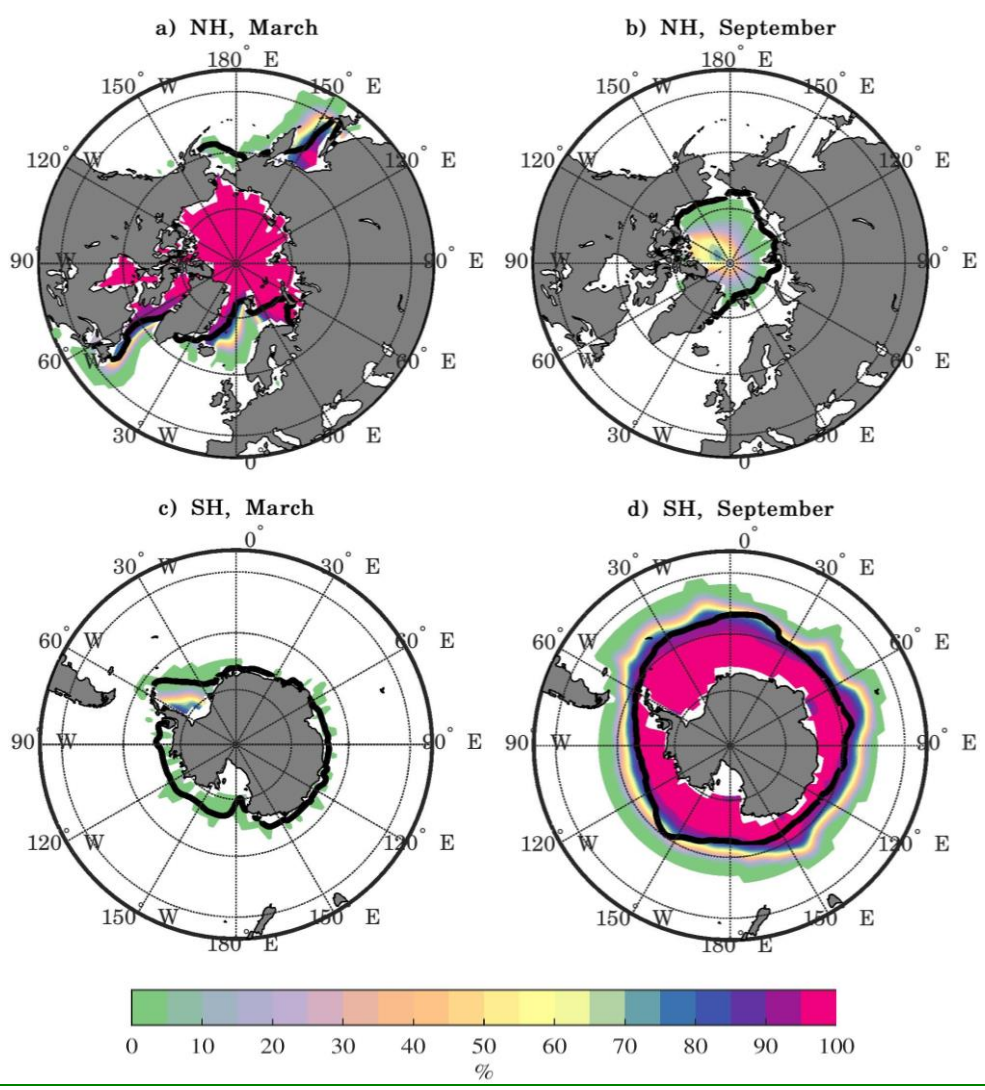
1

2

3

1 Figure 14 – (a) Atlantic Meridional Overturning Circulation averaged for the period
2 1971–2000 and (b) annual mean maximum AMOC strength time series at the latitude
3 30 °N simulated by BESM-OA2.5 for historical simulation over the period 1850–2005.
4 The smaller graph shows the AMOC time series measured by the project RAPID at
5 26.5 ° N over the period April/2004 to October/2015. The RAPID time series is
6 smoothed by a 3-month running average. Units are in Sverdrup.

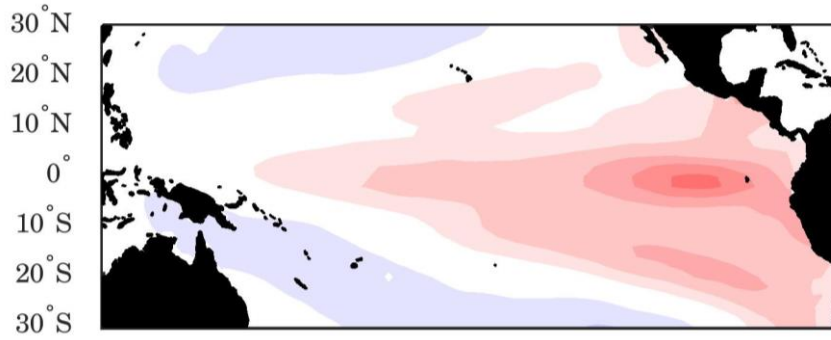
7 |



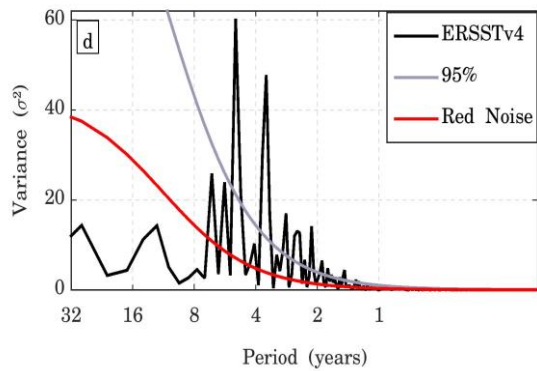
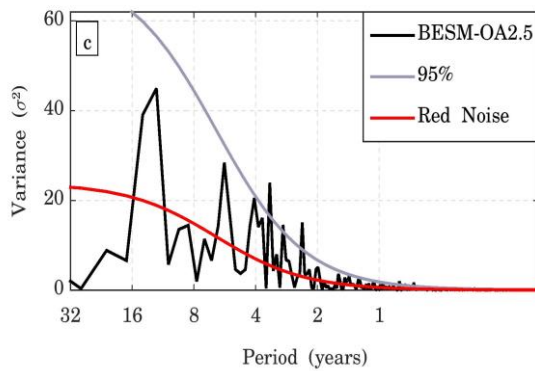
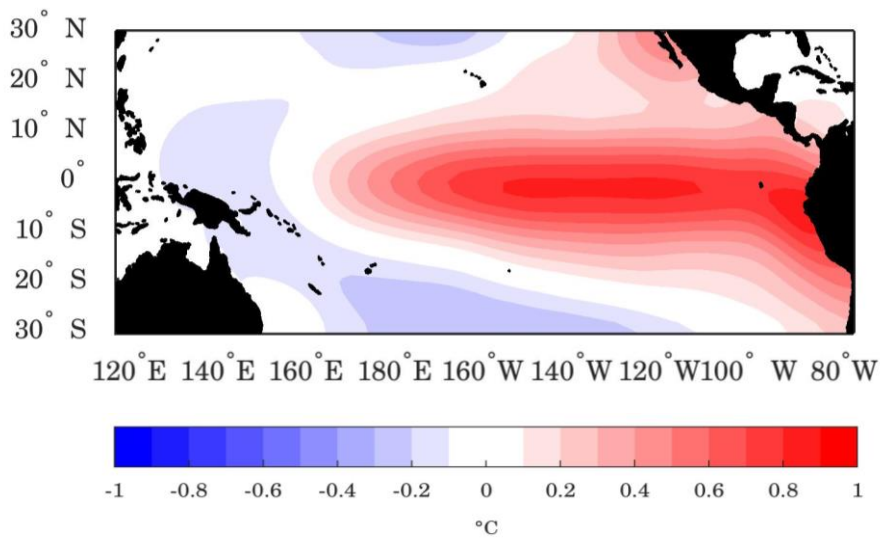
1
2
3
4
5
6
7
8

Figure 15 - BESM-OA2.5 mean sea ice concentration for March (a, c) and September (b, d) for each hemisphere. The solid black lines show the 15 % mean sea ice concentration for 20CRv2 Reanalysis. The averages values are computed over the period 1971–2000 for BESM-OA2.5 and 20CRv2. The concentration is presented in percentage.

a) Pacific SST EOF1 (17.9%) BESM-OA2.5



b) Pacific SST EOF1 (45.0%) ERSSTv4



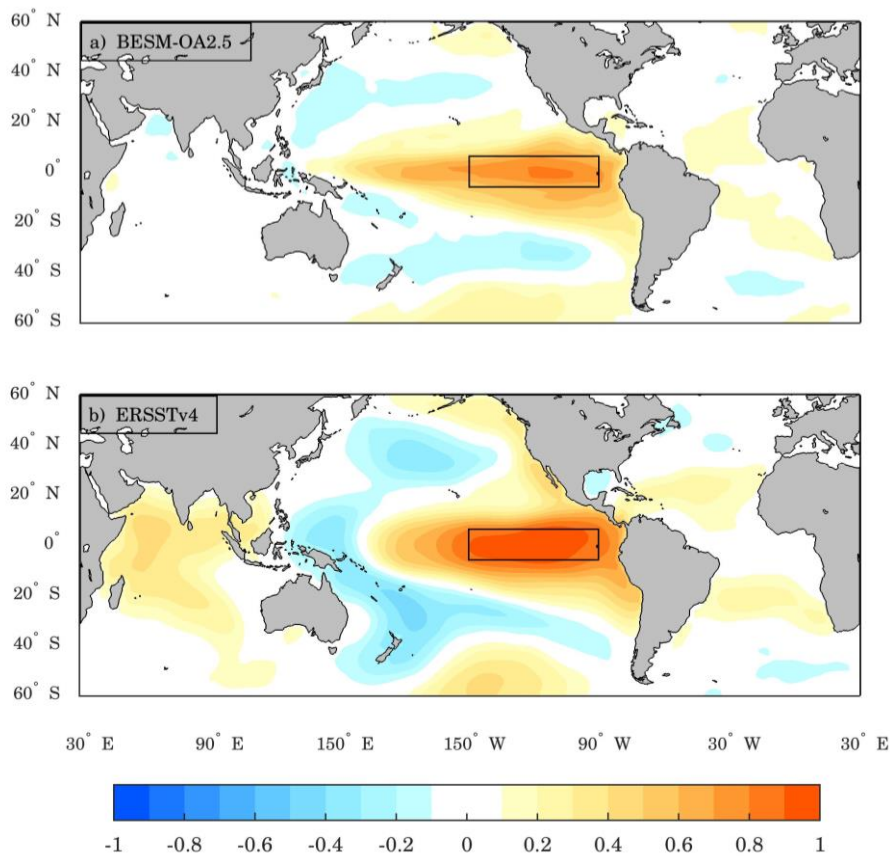
1

2

3 | Figure 165 – The leading EOF modes of the detrended monthly SST anomalies over the

4 | Tropical Pacific region (30° S–30° N; 240°–70° W) for (a) BESM-OA2.5 and (b)

1 ERSSTv4. The results are shown as the SST anomalies regressed onto the
2 corresponding normalized PC time series ($^{\circ}\text{C}$ per standard deviation) over the period
3 1950–2005. The percentage of the variance explained by each EOF is indicated in the
4 title of the figure. The contour interval is 0.1°C . Figures (c) and (d) are the power
5 spectrum of the leading joint PC time series of the pattern for BESM-OA2.5 and
6 ERSSTv4, respectively. The solid red line represents the theoretical red noise spectrum
7 and the gray line represents the 95 % confidence level.
8



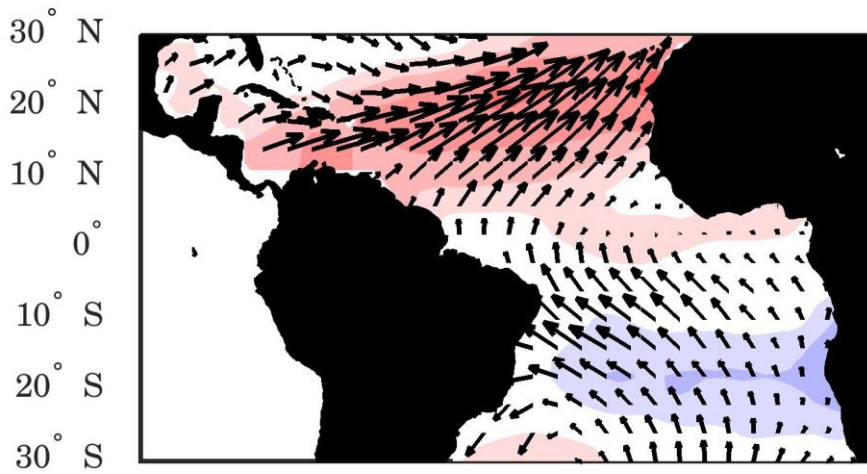
1

2

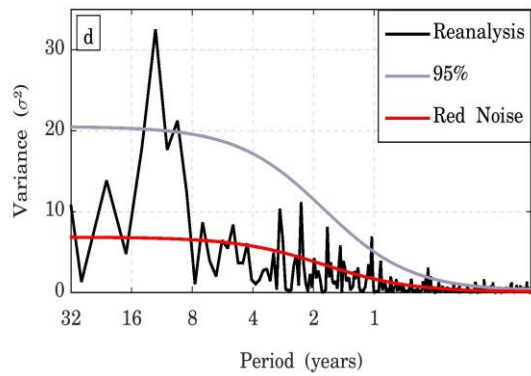
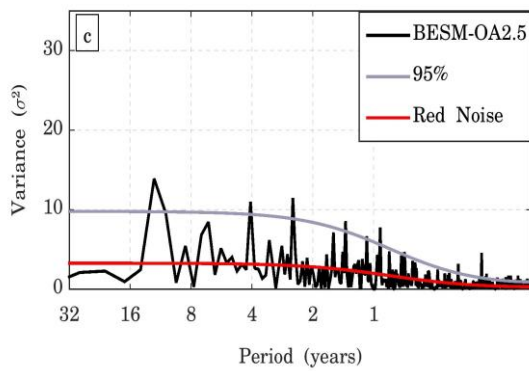
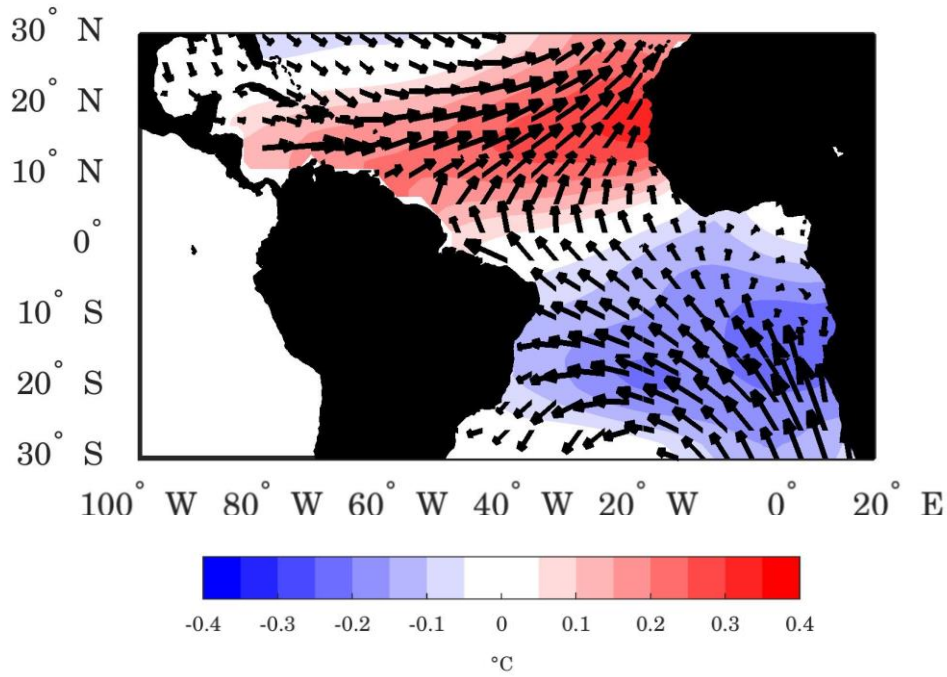
3 | Figure 176 – Spatial maps with the monthly correlation between Niño-3 index and
 4 | global SST anomalies computed for (a) BESM-OA2.5 and (b) ERSSTv4 over the period
 5 | 1900–2005. The anomalies are obtained by subtracting the monthly means for the whole
 6 | detrended time series at each grid point. Black rectangles show the Niño-3 index region.
 7 | Shaded areas are statistically significant at the 95 % confidence level (through two
 8 | tailed t-student test).

9

a) AMM jEOF1 (10.7%) BESM-OA2.5



b) AMM jEOF1 (11.8%) ERSSTv4 (SST), 20CRv2 (Taux,Tauy)

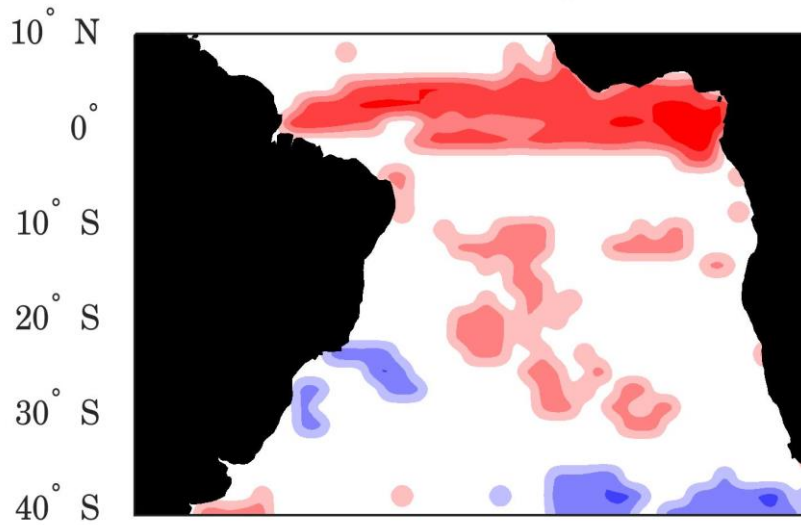


1 | Figure 187 – The leading joint EOF modes of the detrended monthly SST and wind
2 | stress (Taux and Tauy) anomalies for the Tropical Atlantic region (30 °S–30 °N; 100 °
3 | W–20 ° E) for (a) BESM-OA2.5 and (b) for observation (ERSSTv4 and 20CRv2
4 | Reanalysis). The results are shown as the SST anomalies regressed onto the
5 | corresponding normalized PC time series (°C per standard deviation) and wind stress
6 | anomalies regressed onto the corresponding normalized PC time series (ms⁻¹ per
7 | standard deviation) over the period 1950–2005. The percentage of the variance
8 | explained by each EOF is indicated in the title of the figure. The contour interval is 0.05
9 | °C. Figures (c) and (d) are the power spectrum of the leading joint PC time series of the
10 | AMM pattern for BESM-OA2.5 and observation, respectively. The solid red line
11 | represents the theoretical red noise spectrum and the gray line represents the 95 %
12 | confidence level.

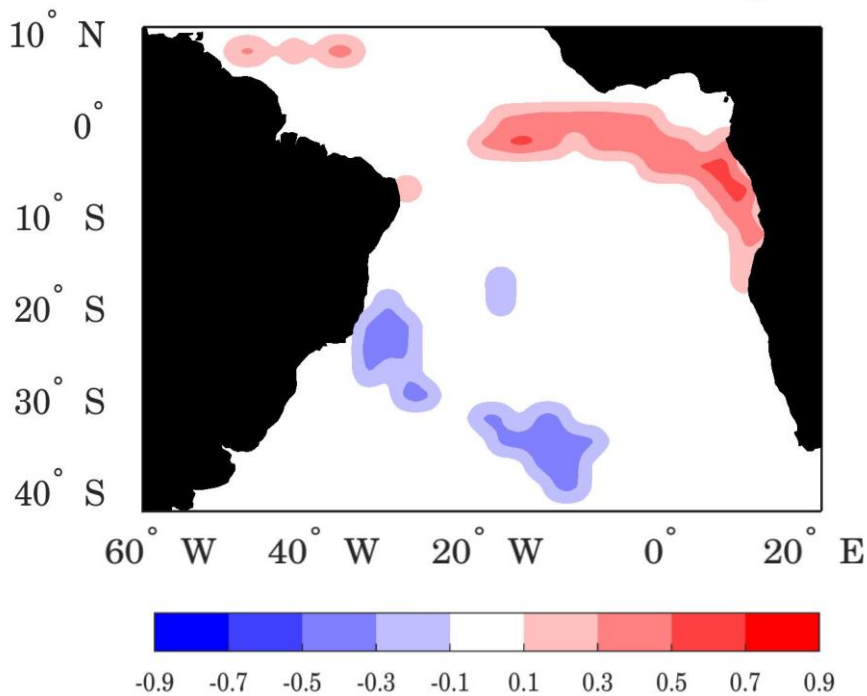
13

14

a) DJF Correlation SST vs Precipitation (BESM-OA2.5)



b) DJF Correlation SST (ERSSTv4) vs Precipitation (GPCP)



1

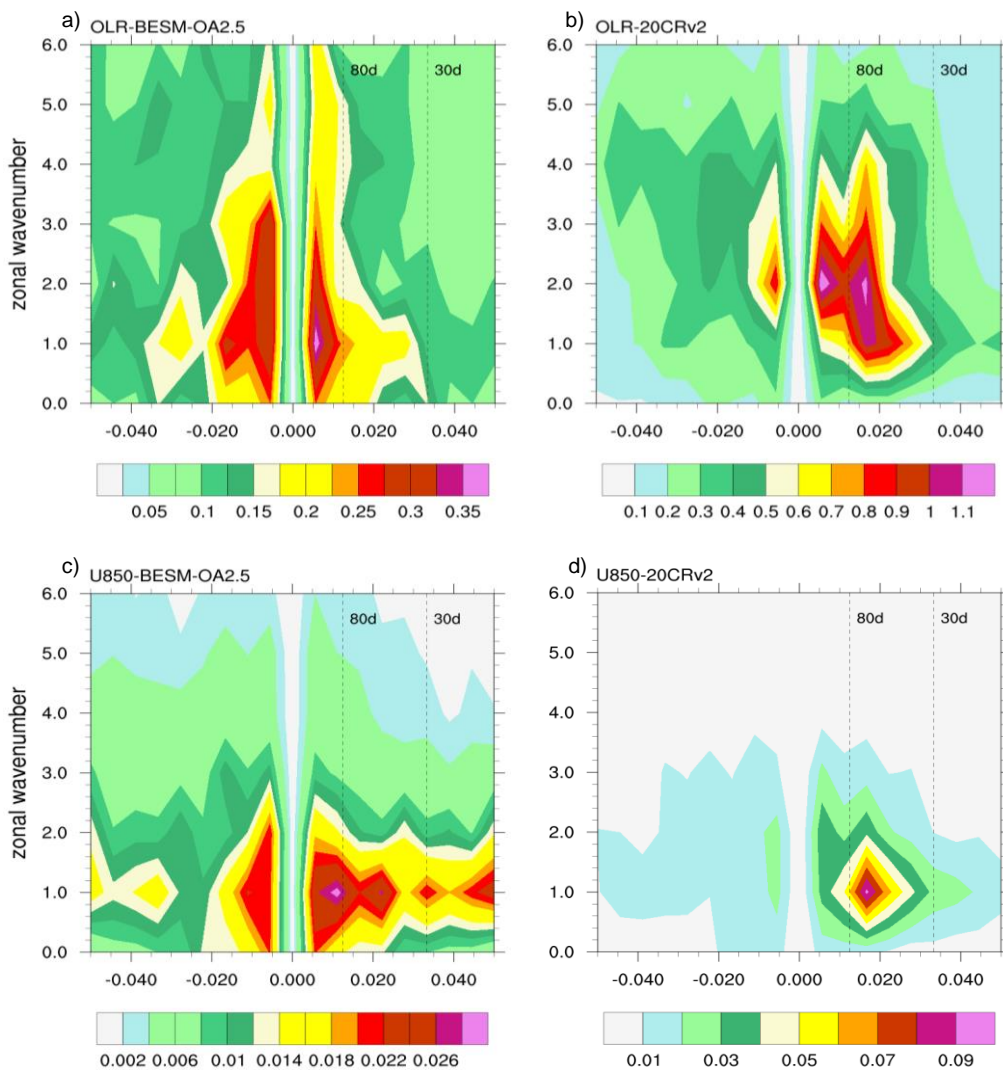
2

3 | Figure 198 – Spatial maps with the correlation between SST and precipitation (seasonal

4 | average DJF) over the South Ocean (40° S–10° N; 70° W–20° E) computed for (a)

5 | BESM-OA2.5 over the period 1971–2002 and (b) observations over the period

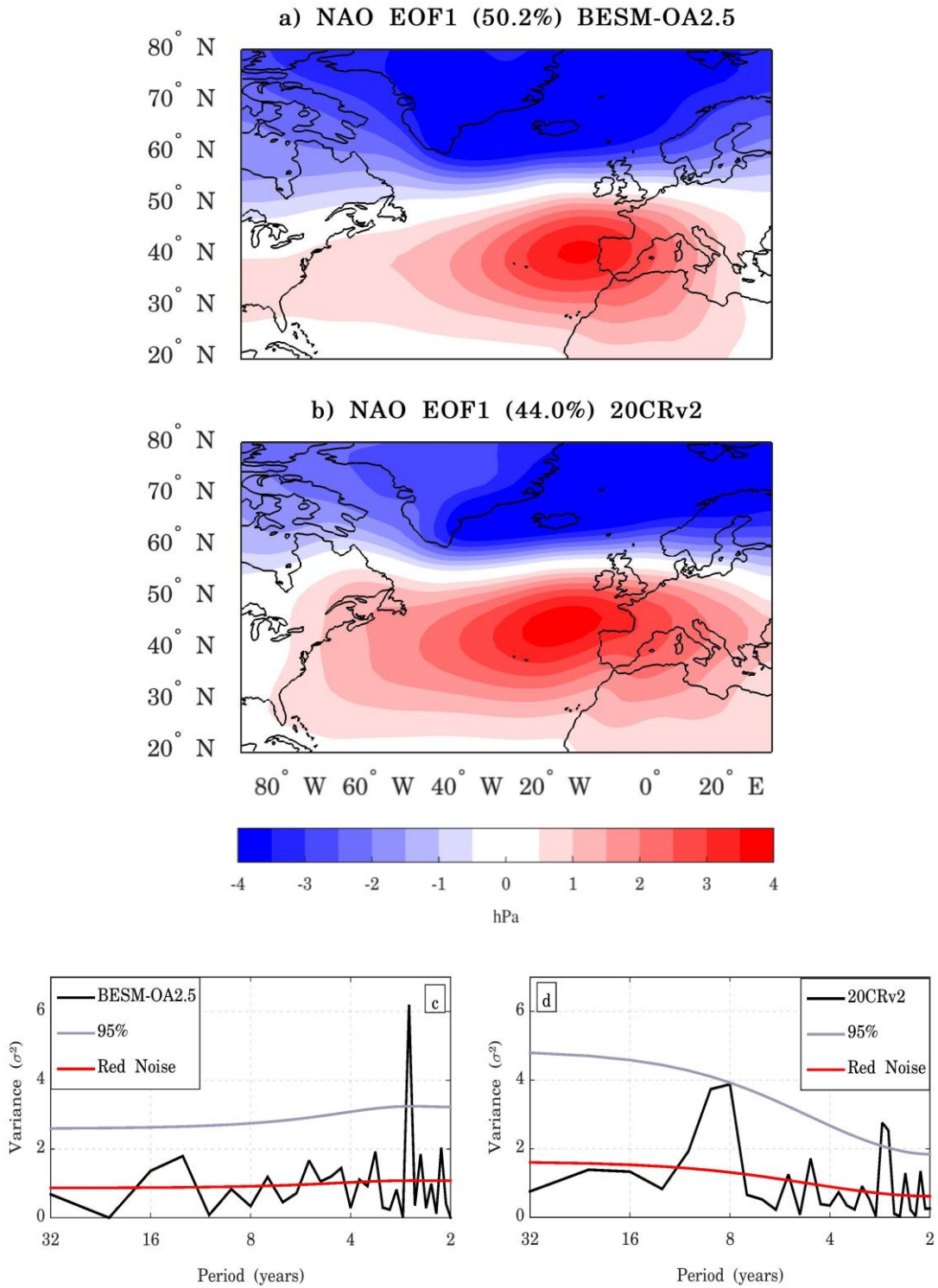
- 1 1979–2010. Shaded areas are statistically significant at the 95 % confidence level
- 2 (through two tailed t-student test).



1
2

3 | Figure 2019 – Wavenumber-frequency power spectrum of tropical (10 S–10 N)
 4 | averaged daily outgoing long-wave radiation (OLR) for (a) BESM-OA2.5 and (b)
 5 | 20CRv2, respectively, and averaged daily zonal wind component at 850 hPa pressure
 6 | level (U850) for (c) BESM-OA2.5 and (d) 20CRv2, respectively. Data used are daily
 7 | anomalies for the boreal winter (Nov–Apr) over the period 1971–2000. Daily anomalies
 8 | are obtained by subtracting the climatological daily mean calculated over the period
 9 | 1971–2000. Individual spectra were calculated for each boreal winter and then averaged

- 1 over the time period used. Units for the zonal wind (OLR) are $\text{m}^{-2} \text{s}^{-2} (\text{W m}^2 \text{s}^{-1})$ per
- 2 frequency interval per wavenumber interval.



1

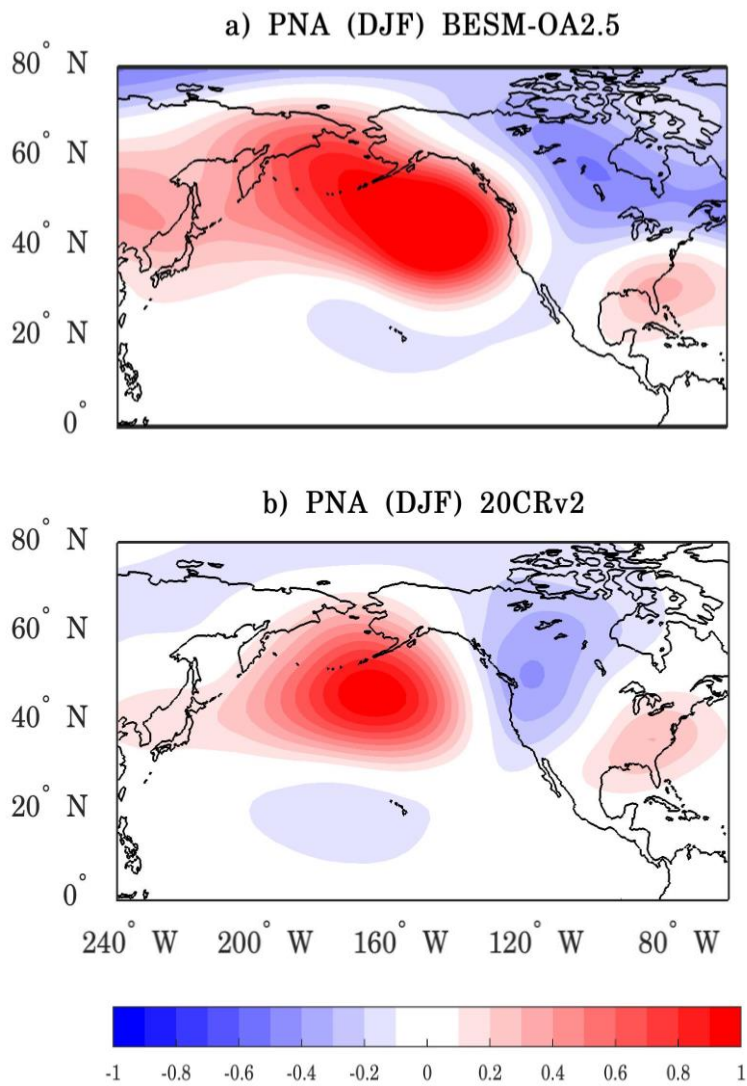
2

3 | Figure 210 – The leading EOF modes of the boreal winter (DJF) seasonal averaged SLP
 4 | anomalies for the Euro-Atlantic region (20°–80° N; 100° W–30° E) for (a) BESM-

1 OA2.5 and (b) 20CRv2. The results are shown as the SLP anomalies regressed onto the
2 corresponding normalized PC time series (hPa per standard deviation) for the period
3 1950–2005. The percentage of the variance explained by each EOF is indicated at the
4 title of the figure. The contour interval is 0.5 hPa. Figures (c) and (d) are the power
5 spectrum of the leading PC time series of the NAO pattern for BESM-OA2.5 and
6 20CRv2, respectively. The solid red line represents the theoretical red noise spectrum
7 and the gray line represents the 95 % confidence level.

8

9



1

2

3 | Figure 22+ – One-point correlation map for (a) BESM-OA2.5 and (b) 20CRv2

4 | Reanalysis showing the correlation coefficient of 500 hPa geopotential level based at

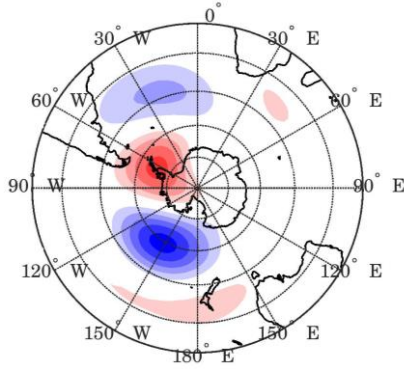
5 | 45 °N, 165 °W and the other grid points. The time series used are boreal winter seasonal

6 | (DJF) averaged dataset for the period 1950–2005.

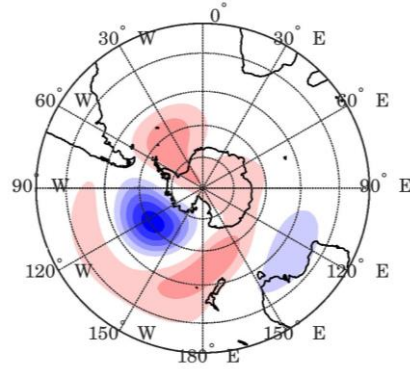
7

8

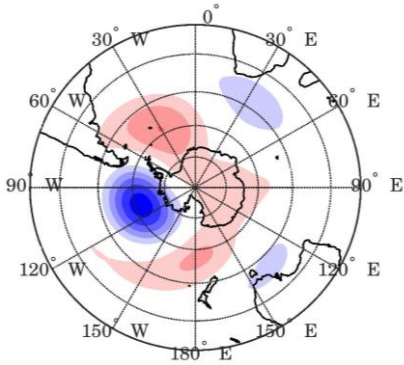
a) PSA EOF2 (9.3%) BESM-OA2.5



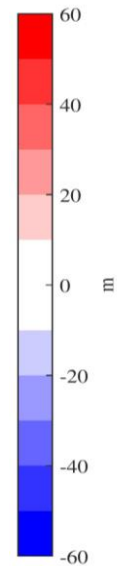
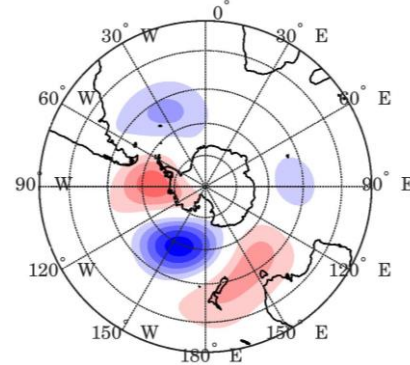
b) PSA EOF2 (11.0%) 20CRv2



c) PSA EOF3 (8.4%) BESM-OA2.5



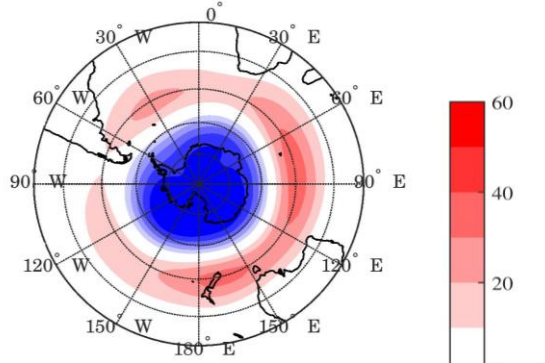
d) PSA EOF3 (10.3%) 20CRv2



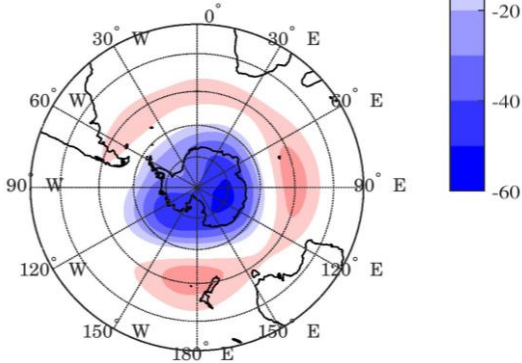
1
2
3
4
5
6
7
8
9
10

Figure 232 – (a) The second and third EOF modes of the monthly mean 500 hPa geopotential height field for the Southern Hemisphere (20°–90° S) for BESM-OA2.5 (b) and for 20CRv2 Reanalysis. The results are shown as the 500 hPa geopotential height regressed onto the corresponding normalized PC time series (meters per standard deviation) over the period 1950–2005. The percentage of the variance explained by each EOF is indicated at the title of the figure. The contour interval is 10 m.

a) SAM EOF1 (34.1%) BESM-OA2.5

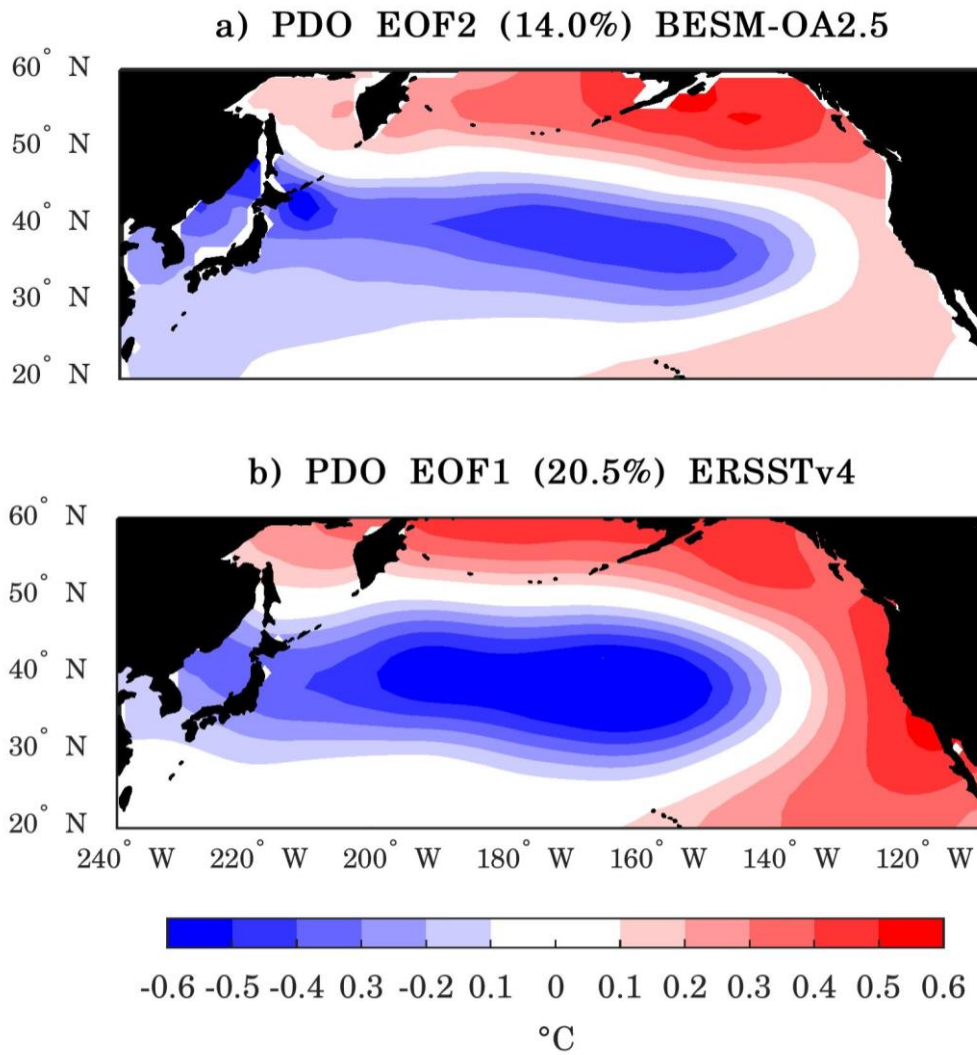


b) SAM EOF1 (21.0%) 20CRv2



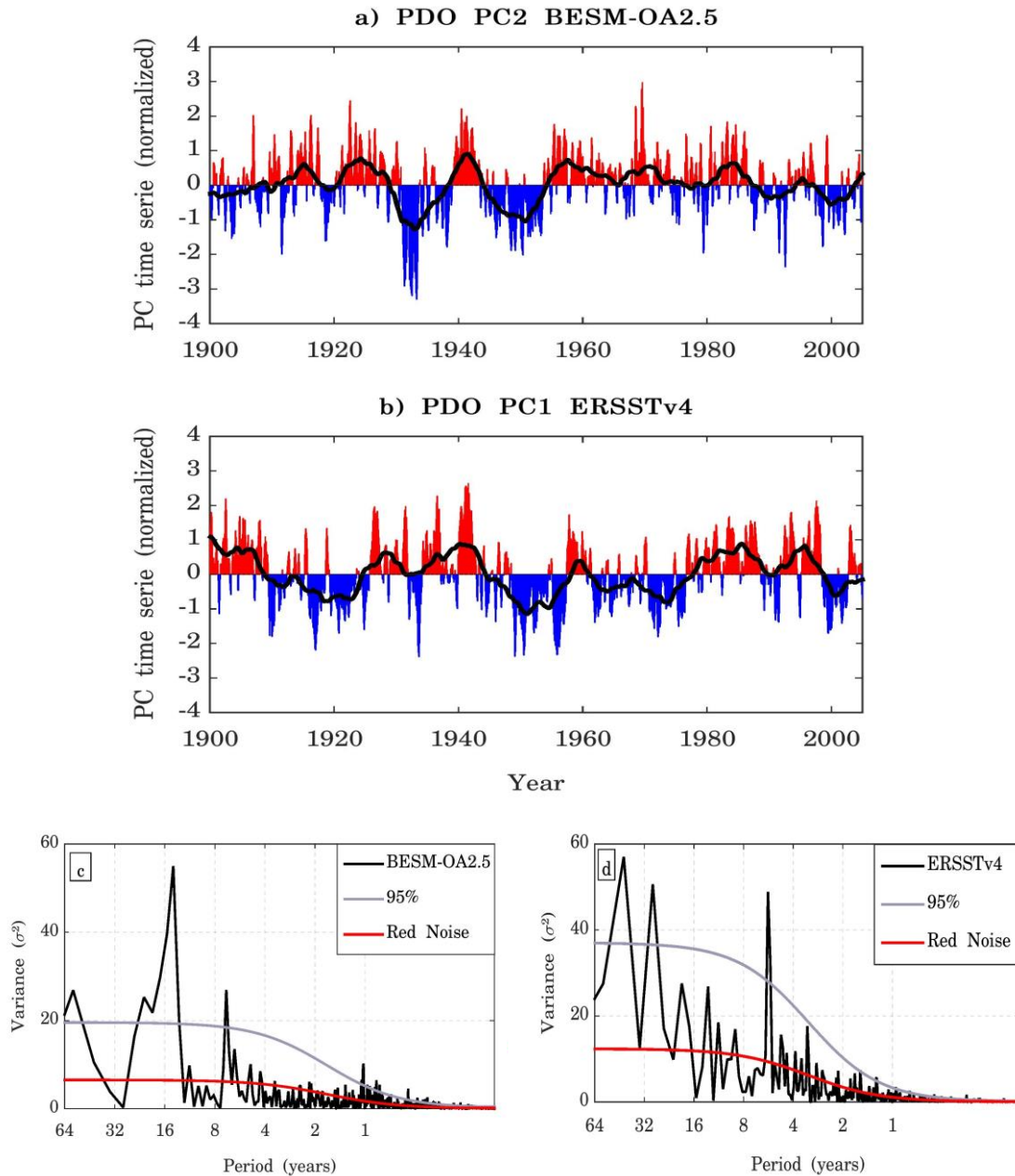
1
2
3
4
5
6
7
8
9
10

Figure 243 – The leading EOF modes of the monthly mean 500 hPa geopotential height field for the Southern Hemisphere (20°–90° S) for (a) BESM-OA2.5 and (b) for 20CRv2 Reanalysis. The results are shown as the 500 hPa geopotential height regressed onto the corresponding normalized PC time series (meters per standard deviation) over the period 1950–2005. The percentage of the variance explained by each EOF is indicated at the title of the figure. The contour interval is 10 m.



1
2
3
4
5
6
7
8
9
10

Figure 254 – (a) The second EOF mode of monthly SST anomalies of BESM-OA2.5 and (b) the leading EOF mode of monthly SST anomalies of ERSSTv4, both over North Pacific Ocean (20°–60° N; 240°–110° W). The results are shown as the monthly SST anomalies regressed onto the corresponding normalized PC time series (°C per standard deviation) over the period 1900–2005. The percentage of the variance explained by each EOF is indicated at the title of the figure. The contour interval is 0.1 °C.



1

2 | Figure 256 – Normalized second PC time series for (a) BESM-OA2.5 and normalized
 3 | leading PC time series for (b) ERSSTv4 over the period 1900–2005. The solid black
 4 | lines are the 5-year running average. Figures (c) and (d) are the power spectrum of the
 5 | second PC time series for BESM-OA2.5 and for the leading PC time series for 20CRv2,
 6 | respectively. The solid red line represents the theoretical red noise spectrum and the
 7 | gray line represents the 95 % confidence level.

Institute	Model	Simulation	horizontal resolution (lat × lon)	
			Atmosphere	Ocean
Commonwealth Scientific and Industrial Research Organisation/Bureau of Meteorology (Australia)	ACCESS1.3	Historical GHG r3i1p1	1.25 ° × 1.875 °	300 × 360 (tripolar)
Canadian Centre for Climate Modelling and Analysis (Canada)	CanESM2	Historical GHG r1i1p1	2.7906 ° × 2.8125 °	0.9303 ° ; 1.1407 ° × 1.40625 °
National Center for Atmospheric Research (USA)	CCSM4	Historical GHG r1i1p1	0.9424 ° × 1.25 °	384 × 320 (tripolar)
Centre National de Recherches Météorologiques/Centre Européen de Recherche et de Formation Avancé en Calcul Scientifique (France)	CNRM-CM5	Historical GHG r1i1p1	1.4008 ° × 1.40625 °	292 × 362 (tripolar)
Geophysical Fluid Dynamics Laboratory (USA)	GFDL-ESM2M	Historical GHG r3i1p1	2.0225 ° × 2.5 °	0.3344 ° ; 1 ° × 1 °
Goddard Institute for Space Studies (USA)	GISS-E2-H	Historical GHG r1i1p1	2 ° × 2.5 °	1 ° × 1 °
Met Office Hadley Centre (UK)	HadGEM2-ES	Historical GHG r1i1p1	1.25 ° × 1.875 °	0.3396 ° ; 1 ° × 1 °
L'Institut Pierre-Simon Laplace (France)	IPSL-CM5A-MR	Historical GHG r1i1p2	1.2676 ° × 2.5 °	149 × 182 (tripolar)
Japan Agency for Marine-Earth Science and Technology, Atmosphere and Ocean Research Institute (The University of Tokyo), and National Institute for Environmental Studies (Japan)	MIROC-ESM	Historical GHG r1i1p1	2.7906 ° × 2.8125 °	0.5582 ° ; 1.7111 ° × 1.40625 °
Meteorological Research Institute (Japan)	MRI-CGCM3	Historical GHG r1i1p1	1.12148 ° × 1.125 °	0.5 ° ; 0.5 ° × 1 °
Bjerknes Centre for Climate Research and Norwegian Meteorological Institute (Norway)	NorESM1-M	Historical GHG r1i1p1	1.8947 ° × 2.5 °	384 × 320 (tripolar)

1

2 Table 1 - List of models from CMIP5 with historical GHG simulations used to compare
3 with BESM-OA2.5. Models with higher resolution in the tropical region and a

- 1 decreasing resolution towards the poles have two values for latitude in their respective
- 2 oceanic resolution column. Models with oceanic tripolar grid, the number of grid points
- 3 in each coordinate are presented.
- 4
- 5